Einar Stiansen

Criticality in Quantum Dissipative Systems

Thesis for the degree of Philosophiae Doctor

Trondheim, July 2012

Norwegian University of Science and Technology
Faculty of Natural Sciences and Technology
Department of Physics

NTNU – Trondheim
Norwegian University of
Science and Technology

NTNU
Norwegian University of Science and Technology

Thesis for the degree of Philosophiae Doctor

Faculty of Natural Sciences and Technology
Department of Physics

ISBN 978-82-471-3679-9 (printed ver.)
ISBN 978-82-471-3680-5 (electronic ver.)
ISSN 1503-8181

Doctoral theses at NTNU, 2012:192

Printed by NTNU-trykk

Abstract

This thesis consists of five scientific papers in the field of condensed matter physics. In all papers we employ large scale Monte Carlo simulations to investigate quantum critical behavior in systems coupled to an environment. Special attention is paid to possible anisotropies between spatial fluctuations and fluctuations in imaginary time. Implications of the results to the loop current theory of cuprates are discussed.

Preface

This thesis is submitted by the author as part of the requirements for the degree Philosophiae Doctor at the Norwegian University of Science and Technology (NTNU). It is the conclusion of three years of work, in which the equivalent of half a year of full-time study is devoted to coursework.

All papers are co-authored by Iver Bakken Sperstad and Asle Sudbø. The work has been performed at the Norwegian University of Science and Technology. My supervisor has been Professor Asle Sudbø. All papers have required many CPU hours at the supercomputing facilities at University of Tromsø (`Stallo`).

The thesis is organized as follows: In Chapter 1 I give a brief introduction to the research field and motivate the study of dissipative quantum phase transitions. Chapter 2 provides some important theoretical concepts related to both classical and quantum phase transitions. In Chapter 3 a selection of "simple" models are introduced. These models enter as "building blocks" in the more involved models considered in the research papers. Chapter 4 covers Monte Carlo techniques including several algorithms and some post processing techniques. Chapter 5 touches upon some the results of the papers. The topics presented here are chosen to answer some of the questions raised in Chapter 1 as well as simply reflecting the author's subjective idea of what is the most interesting physics. In Chapter 6 we make a few concluding remarks.

The introductory chapters are not intended to be self-contained or in any sense a substitute for textbooks. They should rather be viewed as a brief recapitulation for the already experienced theoretical physicist. As a consequence, many quantities and concepts are used and referred to without introduction or explanation.

Natural units are used when suitable.

Acknowledgments

Professor Asle Sudbø has been my supervisor both in the undergraduate and graduate studies. His extraordinary, and very contagious, enthusiasm for physics has been sincerely valued. At times when progress –if any at all– was slow and motivation was suffering his inspirational supervision was invaluable. I also thank him for, even when functioning as Head of Department, always being available for discussion and questions.

During my PhD work I have collaborated closely with fellow graduate student Iver Bakken Sperstad. I have benefited enormously from his programming skills, insight into physics and work capacity in general. Also, it has been pleasurable to have someone to bounce ideas off! –It has been a true pleasure working with you.

Great credit is given to the academic staff at the department of physics for teaching me the trade and sharing their knowledge and insight with me. Some of my fellow PhD-students also deserve to be mentioned: Egil Herland, Arne Stormo, Andrè Kapelrud, Gard Spreeman, and Marianne Rypestøl, thank you for keeping me sane. In particular, I would like to thank Henrik Enoksen with whom I shared office the last two years. I have enjoyed all the discussions we have had on everything from hiking routes to beer.
Thanks also to my flatmates Rannveig, Frøydis og Lars Olav. Thank you for providing such a nice atmosphere in Fridtjof Nansens vei.

Department of Physics at University of Oslo is acknowledged for kind hospitality during my many stays in Oslo during the last year.

The Hole/Haukvik family deserves special mentioning for their unparalleled hospitality and kindness. Your support, especially during the last year, has been deeply appreciated.

I would also like to thank my family for love and support through my entire life. Petter, Heidi, and Kjetil, you deserve my deepest gratitude.

A PhD study involves a lot of frustration and disappointment. Anne, you have managed to endure my many downhearted periods during the last few years and have enlivened me with your comforting smile countless times. Thank you for your love and patience. –Nå flytter jeg endelig hjem til deg!

List of Articles

Article I

Iver Bakken Sperstad, Einar B. Stiansen and Asle Sudbø

Monte Carlo simulations of dissipative quantum Ising models
Phys. Rev. B **81**, 104302 (2010)

The dynamical critical exponent z is a fundamental quantity in characterizing quantum criticality, and it is well known that the presence of dissipation in a quantum model has significant impact on the value of z. Studying quantum Ising spin models using Monte Carlo methods, we estimate the dynamical critical exponent z and the correlation length exponent ν for different forms of dissipation. For a two-dimensional Ising model with Ohmic site dissipation, we find $z \approx 2$ as for the corresponding one-dimensional case, whereas for a one-dimensional Ising model with Ohmic bond dissipation we obtain the estimate $z \approx 1$.

Article II

Einar B. Stiansen, Iver Bakken Sperstad and Asle Sudbø

Criticality of compact and noncompact quantum dissipative Z_4 models in $(1+1)$ *dimensions*
Phys. Rev. B **83**, 115134 (2011)

Using large-scale Monte Carlo computations, we study two versions of a $(1+1)$D Z_4-symmetric model with ohmic bond dissipation. In one of these versions, the variables are restricted to the interval $[0, 2\pi\rangle$, while the domain is unrestricted in the other version. The compact model features a completely ordered phase with a broken Z_4 symmetry and a disordered phase, separated by a critical line. The noncompact model features three phases. In addition to the two phases exhibited by the compact model, there is also an intermediate phase with isotropic quasi-long-range order. We calculate the dynamical critical exponent z along the critical lines of both models to see if the compactness of the variable is relevant to the critical scaling between space and imaginary time. There appears to be no difference between the two models in that respect, and we find

$z \approx 1$ for the single phase transition in the compact model as well as for both transitions in the noncompact model.

Article III

Iver Bakken Sperstad, Einar B. Stiansen and Asle Sudbø

Quantum criticality in a dissipative (2+1)-dimensional XY model of circulating currents in high-T_c cuprates
Phys. Rev. B **84**, 180503 (2011)

We present large-scale Monte Carlo results for the dynamical critical exponent z and the spatio-temporal two-point correlation function of a (2+1)-dimensional quantum XY model with bond dissipation. The phase variables of the model, originating with a parametrization of circulating currents within the CuO_2 unit cells in high-T_c cuprates, are compact, $\{\theta_{\mathbf{r},\tau}\} \in [-\pi, \pi\rangle$. The dynamical critical exponent is found to be $z \approx 1$, and the spatio-temporal correlation functions are explicitly demonstrated to be isotropic in space-imaginary time. In the fluctuation spectrum of the model, momentum and frequency enter on equal footing.

Article IV

Einar B. Stiansen, Iver Bakken Sperstad and Asle Sudbø

Three distinct types of quantum phase transitions in a (2+1)-dimensional array of dissipative Josephson junctions
Submitted to Phys. Rev. B

We have performed large-scale Monte Carlo simulations on a model describing a (2+1)-dimensional array of dissipative Josephson junctions. We find three distinct stable quantum phases of the system. The most ordered state features long-range spatial ordering in the phase θ of the superconducting order parameter, but temporal ordering only in spatial gradients $\Delta\theta$, not in θ. Significantly, the most ordered state therefore does not have 3D XY ordering. Rather, it features 2D spin waves coexisting with temporally disordered phases θ. There is also an intermediate phase featuring quasi-long-range spatial order in θ coexisting with a gas of instantons in $\Delta\theta$. We briefly discuss possible experimental signatures of such a state, which may be viewed as a local metal and a global superconductor. The most disordered state has phase disorder in all spatio-temporal directions, and may be characterized as a gas of proliferated vortices coexisting with a gas of $\Delta\theta$-instantons. The phase transitions between these phases are discussed. The transition from the most ordered state to the intermediate state is driven by proliferation of instantons in $\Delta\theta$. The transition from the intermediate state to the most disordered state is driven by the proliferation of spatial point vortices in the background of a proliferated

$\Delta\theta$-instanton gas, and constitutes a Berezinskii-Kosterlitz-Thouless phase transition. The model also features a direct phase transition from the most ordered state to the most disordered state, and this transition is neither in the 2D XY nor in the 3D XY universality class. It comes about via a simultaneous proliferation of point vortices in two spatial dimensions and $\Delta\theta$-instantons, with a complicated interplay between them. The results are compared to, and differ in a fundamental way from, the results that are found in dissipative quantum rotor systems. The difference originates with the difference in the values that the fundamental degrees of freedom can take in the latter systems compared to dissipative Josephson junction arrays.

Article V

Iver Bakken Sperstad, Einar B. Stiansen and Asle Sudbø

Quantum criticality in spin chains with non-ohmic dissipation
Submitted to Phys. Rev. B

We investigate the critical behavior of a spin chain coupled to bosonic baths characterized by a spectral density proportional to ω^s, with $s > 1$. Varying s changes the effective dimension $d_{\text{eff}} = d + z$ of the system, where z is the dynamical critical exponent and the number of spatial dimensions d is set to one. We consider two extreme cases of clock models, namely Ising-like and $U(1)$-symmetric ones, and find the critical exponents using Monte Carlo methods. The dynamical critical exponent and the anomalous scaling dimension η are independent of the order parameter symmetry for all values of s. The dynamical critical exponent varies continuously from $z \approx 2$ for $s = 1$ to $z = 1$ for $s = 2$, and the anomalous scaling dimension evolves correspondingly from $\eta \gtrsim 0$ to $\eta = 1/4$. The latter exponent values are readily understood from the effective dimensionality of the system being $d_{\text{eff}} \approx 3$ for $s = 1$, while for $s = 2$ the anomalous dimension takes the well-known exact value for the 2D Ising and XY models, since then $d_{\text{eff}} = 2$. A noteworthy feature is, however, that z approaches unity and η approaches $1/4$ for values of $s < 2$, while naive scaling would predict the dissipation to become irrelevant for $s = 2$. Instead, we find that $z = 1, \eta = 1/4$ for $s \approx 1.75$ for both Ising-like and $U(1)$ order parameter symmetry. These results lead us to conjecture that for all site-dissipative Z_q chains, these two exponents are related by the scaling relation $z = \max\{(2 - \eta)/s, 1\}$. We also connect our results to quantum criticality in nondissipative spin chains with long-range spatial interactions.

My contribution to the papers

In those papers where I am listed as the first author, namely Paper II and Paper IV, I have made significant contributions to all parts of the papers. That is, I wrote simulation code, carried out the majority of the simulations or calculations, performed post processing of the data and generated figures. I was also

involved in interpreting the results, and contributed to all parts of the text.

I am listed as the second author in the remaining papers Paper I, Paper III and, Paper V. In these papers I wrote parts of the simulation code and contributed to the Monte Carlo studies. I was also involved in interpreting the results and writing the papers.

Contents

Chapter 1

Introduction

> Sane sicut lux se ipsam et tenebras manifestat, sic veritas norma sui et falsi est.[1]
>
> Spinoza, Ethics (1677), Proposition 43

Superconductivity, the ability of a material to sustain a dissipationless current, was first discovered by Heike Kammerlingh-Onnes in 1911[1] as a new startling phase of ultracold mercury. In 1957, Bardeen, Cooper and Schrieffer (BCS)[2] succeeded in formulating a theory for the underlaying mechanisms of this new phase of matter. The microscopic theory explains superconductivity in terms of pairing of itinerant electrons into so-called Cooper pairs. The pairing comes from an effective attractive force between electrons mediated by phonons.
Until 1986, the highest superconductor transition temperature was 23.2K for Nb_3Ge[3]. Then Bednorz and Müller found a ceramic compound that became superconducting at approximately 30 K[4]. For this work they were awarded the Nobel prize already the following year. The relatively high T_c made it clear that the standard BCS theory might have serious shortcomings when it comes to explaining this new class of materials. Still now, almost thirty years after the discovery of high-temperature superconductivity, the underlying mechanisms of the phenomenon remain elusive. In contrast to the BCS theory which adequately explains the conventional superconductors, an overall theory for high-T_c materials is still missing. An important clue to understand the properties and mechanisms of high-T_c superconductivity is believed to lie in the structural similarities between different materials and the generic phase diagram they present.

1.1 The Cuprate Phase Diagram

It appears that high-T_c superconductors are almost exclusively doped ceramic compounds with properties very different from normal metals. The compounds

[1] Indeed, just as light defines itself and darkness, so truth sets the standard for itself and falsity.

consist of a layered structure of copper-oxygen planes with different "charge-reservoirs" sandwiched between them[5, 6]. The electronic operative element

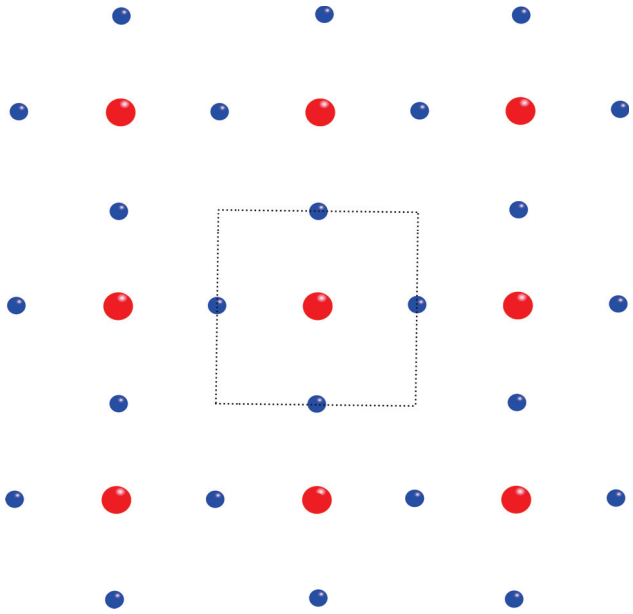

Figure 1.1: The crystal structure of the CuO_2 sheets in cuprate superconductors. Copper and oxygen are indicated by red and blue dots, respectively. The dotted box indicates a specific choice of unit cell.

in the compounds is believed to be the copper-oxygen planes[7, 8], which may be described as doped Mott-insulators. The doping is controlled by chemical substitution in the charge reservoirs, thereby one is capable of controlling the number of free charge carriers in each unit cell. This kind of doping leads to superconductivity and many other effects. Fig. 1.1 shows the crystal structure of the CuO_2-planes.

In Fig. 1.2 we present a sketch of the phase-diagram which shows the basic generic features of hole-doped cuprates. On the x-axis we find doping level as deviation from half-filling and on the y-axis we find the temperature. At perfect stoichiometry ($x = 0$) the cuprates are antiferromagnetic (AFM) insulators up to a Néel-temperature of $\sim 300K$[8]. When holes are introduced into the cuprate plane the Néel-temperature decreases rapidly and the long-range AFM order is destroyed completely at $x \sim 0.02$. A superconducting (SC) state sets in at $x \sim 0.05$ and lasts up to $x \sim 0.25$[5]. The doping level that corresponds to the highest critical temperature T_c is called *optimal doping*, whereas doping levels under or above this are called *underdoped* and *overdoped*, respectively. As a generic term, the area outside the superconducting dome is called the *normal state*.

The underdoped region at non-zero temperature (the region indicated by II in Fig. 1.2) is called the *pseudogap* region. This region holds several unusual properties that will be discussed in Section 1.3. Above the superconducting

dome we find the *strange metal* region. This region (region I in Fig. 1.2) will be discussed in Section 1.2. At even higher doping levels we find a phase that can be described by the Fermi liquid formalism (region III). The line separating the strange metal region and the Fermi liquid region is believed to be a cross-over line, thus the physical properties changes gradually between these two regions.

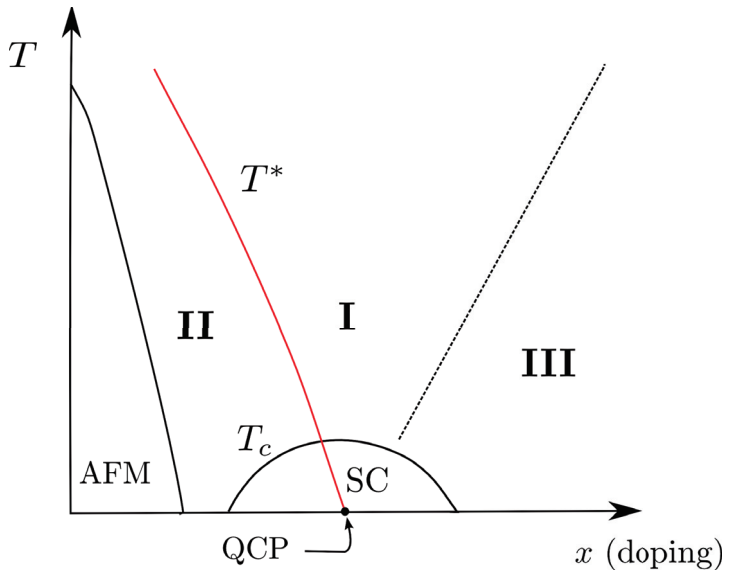

Figure 1.2: Schematic phase-diagram of the cuprates showing only the hole doping side ($x > 0$). The level of doping x, away from half-filled conduction band, is given on the abscissa and the temperature on the ordinate. The pseudogap line T^* (shown in red) is conjectured to continue into the superconducting (SC) state and terminate at $T = 0$ somewhere near optimal doping.

1.2 Marginal Fermi Liquid

At intermediate doping, at temperatures above the superconducting dome, one finds a non-Fermi-liquid region commonly referred to as the strange metal region because of its unusual properties. The transport properties in this peculiar region differ from what is predicted from standard Fermi liquid theory (FLT). One of the most prominent anomalies is the linear resistivity ρ above T_c, signaling a deviant scattering of the charge carriers (FLT predicts $\rho \propto T^2$). For an optimally doped sample this behavior is seen over a temperature range of several hundred degrees above the transition to superconductivity[9].
The anomalous normal state properties led to the proposition of the marginal Fermi liquid hypothesis[10]. The basic assumption is that the electrons are scattering off a particular kind of bosonic fluctuation spectrum where the only

energy scale is set by the temperature [2]

$$\mathrm{Im}\chi(\mathbf{q},\omega,T) \propto \begin{cases} \omega/T\ , & \omega \ll T \\ \text{const.}\ , & T \ll \omega \ll \omega_c. \end{cases} . \tag{1.1}$$

Here ω_c is a cut-off frequency to be specified by experiments, T is temperature, $\mathbf{q}$ is momentum and ω is the frequency. The quasiparticle weight following from these fluctuations is given by[10] $z(\omega) = (1 - \partial\Sigma_R/\partial\omega)^{-1} \propto \ln|\omega_c/\omega|^{-1}$, where Σ_R is the real part of the electron self-energy. The proposed fluctuation spectrum causes $z(\omega)$ to vanish logarithmically at the Fermi surface. Consequently, the momentum distribution function, $n(k)$, does not have the step discontinuity at the Fermi level as expected from FLT. Notably the fluctuation spectrum is momentum independent, implying spatial locality of the fluctuations.
C. M. Varma and collaborators showed in Ref. [10] that this kind of fluctuation spectrum suffices to explain all anomalous transport properties of the strange metal region.

1.3 Pseudogap

In the underdoped region there is a large body of evidence for an unconventional normal state[11, 12, 13] characterized by the opening of a highly anisotropic excitation gap. That is, below the temperature T^* and above the onset of superconductivity T_c there are regions in momentum space where gapless excitations exist and other regions where the excitations are gapped. The regions with gapless excitations are centered around the four nodal directions $k_x = \pm k_y$ and the extent of these *Fermi arcs* is diminishing with decreasing temperature. This four-fold symmetry closely resembles the d-wave gap of the superconducting phase, only in this phase the regions with gapless excitations are confined to the four nodal points on the Fermi surface.[3]
The origin of the pseudogap remains elusive and is considered to be one of the most fundamental problems in contemporary condensed matter physics. Crudely speaking, two major classes of theoretical models have evolved in order to explain the phenomenon. The first describes a precursor to the superconducting phase through the notion of preformed Cooper pairs below the temperature T^*. This means that there must be some pairing mechanism tending to give the local pair correlations needed to give rise to superconductivity, but the system lacks long-range phase coherence. In this way the temperature T^* marks the onset of Cooper pairing and T_c marks the onset of phase coherence. The similar symmetries of the superconducting gap and the pseudogap makes the preformed pair scenario a very attractive theory. However, there are objections raised to this theory, see Ref. [15] for a discussion regarding this. Also, recent angle-resolved photoemission spectroscopy (ARPES) experiments have indicated that the pseudogap may be originating with a phenomenon not directly related to superconductivity[13, 16].

[2] χ is the Fourier transform of a correlation function of the bosonic field.
[3] It should be noted that recent experiments have shown that in the underdoped phase the momentum dependence of the energy gap deviates from d-wave form[14, 13].

The second class explains the pseudogap by some sort of ordered phase competing with (or possibly facilitating) the superconducting state.[4] This thesis is motivated by this point of view. Like Varma[22, 18, 21], we will acknowledge that the topology of the phase diagram is that which is expected around a quantum critical point (QCP)[23]. The temperature T^* is known to decrease with increasing doping level, and T^* supposedly reaches zero at a QCP at $x = x_c$ hidden within the superconducting dome. In this way the QCP is the source of the scale-invariant fluctuations of the marginal Fermi liquid theory (1.1). At low temperatures a region of Fermi liquid behavior is consequently expected at $x > x_c$ and a region of broken symmetry is expected for $x < x_c$[21].

1.4 The loop current model

In a portfolio of papers Varma and collaborators propose that the pseudogap region represents a phase which breaks time-reversal symmetry by a spontaneous ordering of loop-currents without changing the translational symmetry of the cuprate lattice[21, 18, 24, 25]. In this way, T^* represents a true phase transition separating the pseudogap region, where the current loops are ordered into a specific pattern, from the strange metal phase where these loops are fluctuating. In Fig. 1.3 we show the four possible orientations of the current pattern within each unit cell.
Experimental signatures conforming with the ordering of circulating currents below T^* have been found by several experimental techniques[17, 26, 27, 28, 29, 30]. However, it should immediately be emphasized that others argue that these signatures may have a quite different origin[31, 32, 33, 34].
The orientations of the current orbitals come about by the four possible permutations of the directions of the horizontal and the vertical currents crossing the unit cell. It has been derived from a microscopic theory[35] that the Hamiltonian describing the finite temperature behavior of such a system is given by a generalized Ashkin-Teller model[36]. It turned out that the derived Hamiltonian was a generalization of a model already proposed[24, 18] to describe the loop currents. In a range of parameters this model may undergo a phase transition with suppressed specific heat divergence. Since no specific heat singularity has been observed when crossing T^* in any cuprate[11, 15], this is a very important achievement for a theory describing the pseudogap line as an onset of a hidden order.
Previous numerical work[37] on the loop current model has been restricted to finite temperatures where thermal fluctuations dominate the critical behavior. In this thesis we attempt to study the quantum critical point directly by performing path integral Monte Carlo simulations on the effective action conjectured (see below) to describe fluctuating loop currents in the quantum regime. It has been shown[24] that this action exhibits exactly the form of *local quantum*

[4] There are numerous theories for what the nature of this ordered state might be, but no consensus has been established. Some of the conjectured orders are: Various types of density waves (*d*-density-wave, charge- or spin-density-wave) or circulating currents (staggered flux phases)[17, 18, 19, 20, 21].

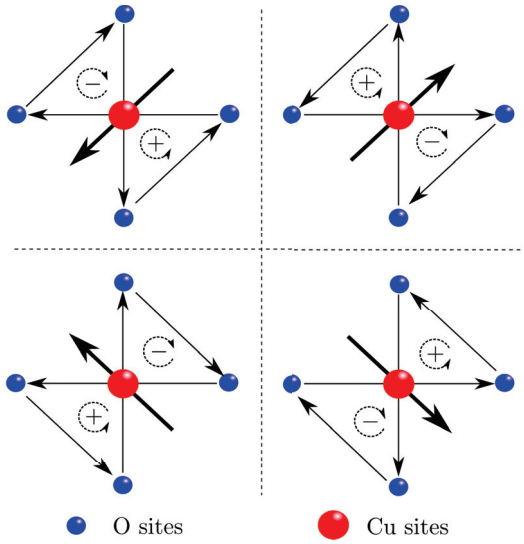

Figure 1.3: A sketch of the proposed orbital current pattern that forms spontaneously at T^* in the cuprate planes. The loops are generated by horizontal and vertical currents running through the copper sites and closing by direct hopping between the oxygen sites. The magnetic moments induced by the loop currents are shown as $+/-$. The large arrow centered at the copper site illustrates the pseudospin abstraction the current patterns.

criticality that Eq. (1.1) represents. This calculation hinges on a decoupling of the partition function into two families of topological defects; spatial vortices and a novel variant of topological defects, namely, *warp* defects in the imaginary time[25, 38]. Arguably, the dissipation induced phase transition is driven solely by warps while the vortices may be considered "inert". The correlations at criticality are therefore local in space and power law in time. Defining the dynamical critical exponent z from the scaling of momentum and frequency at the quantum critical point, we get $\omega \sim q^z$. Formally, this means that $z = \infty$. These results would imply that the phenomenological marginal Fermi liquid hypothesis, Eq. (1.1), has been derived from a microscopic theory. However, since the analytical derivation of the fluctuation spectrum from the microscopic theory is highly nontrivial, it is important to carry out an unbiased numerical investigation. We now go on to describe the proposed form of the action and some of its fundamental assumptions.

Each of the four distinct orientations of the circulating currents in Fig. 1.3 may be associated with a pseudospin which is restricted to the four angular directions $\theta \in \{\pi/4, 3\pi/4, 5\pi/4, 7\pi/4\}$. In order to formulate a quantum version of the theory, a quantum kinetic term and a dissipation term is included to the classical action[24]. At this point the Ashkin-Teller term, which was essential to generate a nondivergent specific heat at finite temperature, is neglected because it is no longer important at $T = 0$[24]. Also, the restriction on the direction of the pseudospin is relaxed in such a way that the spin may vary continuously[24, 25].

The effective action takes the form[24]

$$S = S_{\text{kin}} + S_J + S_{\text{diss}}, \tag{1.2}$$

where

$$S_{\text{kin}} = \frac{K_\tau}{2} \sum_{\mathbf{x}} \int_0^\beta \mathrm{d}\tau \left(\frac{\partial \theta_{\mathbf{x}}(\tau)}{\partial \tau} \right)^2, \tag{1.3}$$

$$S_J = -K \sum_{\langle \mathbf{x},\mathbf{x}' \rangle} \int_0^\beta \mathrm{d}\tau \cos(\Delta\theta_{\mathbf{x},\mathbf{x}'}(\tau)), \tag{1.4}$$

and

$$S_{\text{diss}} = \frac{\alpha}{2} \sum_{\langle \mathbf{x},\mathbf{x}' \rangle} \int_0^\beta \mathrm{d}\tau \int_0^\beta \mathrm{d}\tau' \left(\frac{\pi}{\beta} \right)^2 \frac{(\Delta\theta_{\mathbf{x},\mathbf{x}'}(\tau) - \Delta\theta_{\mathbf{x},\mathbf{x}'}(\tau'))^2}{\sin^2(\pi/\beta|\tau - \tau'|)}. \tag{1.5}$$

The summation over $\mathbf{x}$ goes over all spatial coordinates, and the angular brackets indicate nearest neighbor summation. $\Delta\theta_{\mathbf{x},\mathbf{x}'}(\tau) = \theta_{\mathbf{x},\tau} - \theta_{\mathbf{x}',\tau}$ is the lattice gradient, defined on the bonds of the numerical lattice. K_τ and K sets the scale of the quantum kinetic energy and the spatial interactions, respectively. α quantifies the strength of the dissipation.

The dissipation term reportedly originates with a coupling between the bosonic currents and fermionic degrees of freedom near the Fermi surface[24]. The form of the dissipation term is identical to the result of coupling the bond variables $\Delta\theta$ to infinite oscillator baths, often referred to as the Caldeira-Leggett[39] model. In Sec. 3.1 we introduce the basic ideas of this model.

The functional form of Eq. (1.2) coincides with the action describing a two-dimensional array of resistively shunted Josephson junctions[40, 41, 42, 43, 44, 38]. We return to an interpretation of the system in terms of Josephson junctions in Sec. 5.3 and discuss the implications for the loop current scenario in Sec. 5.3.1.

Additionally, since it is unclear how local quantum criticality in the sense $z \to \infty$ may occur in an extended system, we have studied variants of Eq. (1.2) featuring different dimensionalities and order parameter symmetries.

Chapter 2

Phase Transitions

The current chapter aims to provide a brief introduction to the concepts of critical phenomena. We start by introducing phase transitions occurring at finite temperature before moving on to discuss quantum phase transitions, i.e. transitions at zero temperature.

2.1 Classical statistical mechanics and phase transitions

Statistical mechanics provides a link between the microscopic constituents of a system, like for instance the molecules in a container of gas, and the observable macroscopic properties. Instead of solving the equations of motion for the enormous number of particles in the container, statistical mechanics treats the particles probabilistically in such a way that the number of relevant parameters necessary to describe the system is reduced to only a handful, *e.g.* temperature, pressure, and density. In classical statistical mechanics the probability distribution of the microscopical configurations $\{\Psi\}$ is given by the Boltzmann weight

$$p_\Psi = \frac{1}{\mathcal{Z}} \mathrm{e}^{-\beta H[\Psi]}, \tag{2.1}$$

where H is the Hamiltonian of the system and $\beta \equiv 1/(k_B T)$. Superficially, the quantity $\mathcal{Z}$, called *the partition function*,

$$\mathcal{Z} = \sum_{\{\Psi\}} \mathrm{e}^{-\beta H[\Psi]}, \tag{2.2}$$

enters only as a normalization constant for the Boltzmann distribution. However, this function plays a central role in statistical mechanics: All information about thermodynamic properties of the system may be dug out from $\mathcal{Z}$ by various manipulations. Examples of such quantities are the heat capacity $C_V = -k_B \beta^2 \partial^2 \ln Z / \partial \beta^2$ and the Helmholtz free energy $F = -(1/\beta) \ln Z$. Consequently, one can argue that the problem of understanding phase transitions is a question of calculating partition functions.
In preparation for a discussion of quantum statistical mechanics, we note two important features of the classical partition function. In a classical system

the kinetic and potential part of H commute, enabling a factorization of the partition function[45]. The kinetic factor does not drive any critical behavior since it derives from a product of Gaussian integrals. As a consequence, classical critical behavior may be formulated as a time-independent theory. The other point the reader should note at this stage is that the temperature, through the parameter β, sets the overall energy scale and that each term in the Hamiltonian is weighted equally.

When the temperature is tuned through a phase transition the system abruptly changes its behavior. The quantity F provides a simple conceptual picture of why phase transitions occur in nature. The Helmholtz free energy may be formulated as

$$F = U - TS, \tag{2.3}$$

where U is the internal energy and T and S are temperature and entropy, respectively. A system will organize itself in such a way as to minimize its free energy. This minimalization can be done in two ways: When T is small the second term in Eq. (2.3) have little impact on F, therefore the free energy is minimized by lowering U. At higher temperature, free energy is minimized by disordering the system in order to gain entropy. Because it is not possible to achieve high entropy and low internal energy at the same time, a phase transition will emerge out of competition between the two quantities.

Broadly speaking, there are basically two ways a phase transition may occur.[1] The first kind involves co-existence of two phases which means that the free energy associated with the phases coincide at the transition point. Phase transitions of this kind is referred to as *discontinuous-* or *first order* phase transitions. Everyday examples are freezing and boiling of water. *Second order* phase transitions do not involve co-existence, instead there is a continuous evolution from one phase to the next. Precisely at the transition point the two phases become indistinguishable. In the following we will limit the discussion to continuous transitions.

A second order phase transition can usually be described by the continuous onset of an *order parameter*. An order parameter is a quantity that is zero in the disordered state and non-zero in the ordered phase. The choice of order parameter is sometimes obvious, like total magnetization in systems undergoing a phase transition between a paramagnetic and a ferromagnetic state. However, there are also cases where the choice of order parameter is complicated.[2]

Due to thermal noise the order parameter will fluctuate around its equilibrium value. As the critical point is approached the typical spatial length scale ξ, at which the local order parameter field is correlated, diverges. The divergence is described by

$$\xi \propto |t|^{-\nu}, \tag{2.4}$$

[1] A noteworthy example of a third kind is the Berezinskii-Kosterlitz-Thouless transition which we return to in Sec. 3.3.

[2] In Paper IV, we encounter a peculiar case where there are essential differences between fluctuations in different directions. The result is that we are unable to construct an order parameter describing all fluctuations adequately.

where ν is the *critical exponent*, and t is the reduced temperature, $|t| = |T - T_c|/T_c$, a dimensionless measure of the distance from the critical point. This divergence is a defining property of critical phenomena and indicates that fluctuations of the order parameter occur on all length scales.[3] Consequently, all observables must exhibit scale invariant power law dependence on external parameters in the critical regime. The exponents of these power laws enable a complete characterization of the phase transition.
In Tab. 2.1 we show the various critical exponents needed to fully describe a system undergoing a second order phase transition. To simplify the discussion we consider an unspecified order parameter m. In addition to the exponent ν describing the divergence of the correlation length upon approaching the critical point, there are several other exponents in use. In total they describe the dependence of the order parameter and its correlations on the distance from the critical point and on an external field h conjugate to m.

Table 2.1: The critical exponents describing the behavior of various observables near a second order phase transition.

Observable	Exponent	Definition	Conditions
Heat capacity	α	$C_V \propto \lvert t\rvert^{-\alpha}$	$t \to 0, h = 0$
Susceptibility	γ	$\chi \propto \lvert t\rvert^{-\gamma}$	$t \to 0, h = 0$
Order parameter	β	$m \propto \lvert t\rvert^{\beta}$	$t \to 0^-, h = 0$
Order parameter	δ	$m \propto \lvert h\rvert^{1/\delta}$	$t = 0, h \to 0$
Correlation length	ν	$\xi \propto \lvert t\rvert^{-\nu}$	$t \to 0, h = 0$
Correlation function	η	$G(r) \propto \lvert r\rvert^{-(d-2+\eta)}$	$t = 0, h = 0$

In the mid-1960's Widom[47, 48] amongst others suggested that close to critical temperature the free energy would consist of an analytical part and a singular part. The singular part, f_s can be approximated by the homogeneity relation[4]

$$f_s(|t|, h) = b^{-d} f_s(|t| b^{1/\nu}, h b^{y_h}). \tag{2.5}$$

Here, b is an arbitrary scaling factor and y_h is the scaling exponent of the external field h. This homogeneity relation is a formal expression reflecting the scale invariance of the critical regime. Close to the critical point, the only relevant length scale in the system is the correlation length. Thus, rescaling all lengths in the system with a common factor b, and at the same time readjusting external parameters in such a way that the correlation length retains its original value, should not affect physical properties.
The exponents α, γ, δ and β may all be extracted from the singular free energy by taking appropriate differentiations. Since the free energy only contains two independent scaling exponents, the other critical exponents must be interconnected. The resulting relations between the exponents are called *scaling laws* and are given by

$$\alpha + 2\beta + \gamma = 2, \tag{2.6}$$

[3] It is necessary to include a microscopic cutoff on the length scale of the fluctuations in order to explain the *anomalous dimension* η[46].

[4] This can be shown to be valid through the framework of the renormalization group.

and

$$\alpha + \beta(\delta + 1) = 2. \tag{2.7}$$

These laws are called Rushbrooke's and Griffiths' laws, respectively. In addition, there are relations involving the exponents of the correlation length and the correlation function:

$$2 - \alpha = d\nu, \tag{2.8}$$

and,

$$(2 - \eta)\nu = \gamma. \tag{2.9}$$

These two relations are called the hyperscaling relation[5] and Fisher's law, respectively. The hyperscaling relation is the only scaling relation in which the dimension of the system enters explicitly. This relation is known to be violated in certain systems[46].
A cornerstone in the theory of critical phenomena is the concept of *universality classes*. Very different physical systems may present the same set of critical exponents at the phase transition. Broadly speaking the classes are characterized, not by microscopic details, but by global properties like the dimensionality of the system and the symmetries of the order parameter.
In addition to the critical exponents introduced above we have deliberately chosen to omit an additional exponent describing the *critical slowing down* of a system near a critical point. This exponent is called the dynamical critical exponent z, and is defined by

$$\xi_\tau \propto \xi^z. \tag{2.10}$$

At a finite temperature critical point, this exponent describes the diverging relaxation time towards thermodynamic equilibrium. Since the partition function separates into a kinetic part and a potential part which may be considered separately, the dynamical critical exponent does not enter the scaling relations and may be considered separated from the other exponents.

2.2 Quantum statistical mechanics and quantum phase transitions

Quantum mechanics will start to affect the system when the energy scale associated with thermal fluctuations, $k_B T$, is comparable to the typical quantum energy scale $\hbar\omega_c$. When $k_B T$ drops below $\hbar\omega_c$ the character of the fluctuations driving the phase transition changes from classical to quantum mechanical. Conversely, thermal fluctuations are dominant if $\hbar\omega_c < k_B T$. The divergent time scale briefly mentioned in the last section implies that the relevant frequency of the fluctuations goes to zero like $\hbar\omega_c \propto |t|^{\nu z}$ at a continuous phase

[5] The hyperscaling relation is sometimes referred to as Josephson's law.

transition. For a transition occurring at T_c, this means that quantum mechanics will be unimportant if the distance from the critical point is smaller than $|t| \propto T_c^{1/\nu z}$. As long as $T_c > 0$ the behavior of the system arbitrarily close to the critical point is therefore always dominated by thermal fluctuations. This does not mean that quantum mechanics is unimportant at the phase transition. The very existence of the order parameter may be fundamentally quantum mechanical. Indeed, this is the case for the transition involving liquidification of ^{4}He, where the order parameter is the macroscopic wavefunction of the Bose-Einstein condensate. If the critical point occurs *at zero temperature* as a function of some other non-thermal external parameter, the regime in which thermal fluctuations dominates has vanished. Therefore, the behavior is dominated by quantum fluctuations and is referred to as a *quantum critical point*.
Similarly to the classical case, all relevant observables can be derived from the partition function. However, the function is modified from (2.2) to

$$\mathcal{Z} = \sum_{\Psi} \langle \Psi | \mathrm{e}^{-\beta \hat{H}} | \Psi \rangle = \mathrm{Tr} \left\{ \mathrm{e}^{-\beta \hat{H}} \right\}. \tag{2.11}$$

The Hamiltonian $\hat{H}$ is now treated as an operator, operating on the wavefunctions $|\Psi\rangle$ describing the states of the system. Expectation values of operators are evaluated in the standard fashion

$$\langle \mathcal{O} \rangle = \frac{1}{\mathcal{Z}} \mathrm{Tr} \left\{ \mathcal{O} \mathrm{e}^{-\beta \hat{H}} \right\}. \tag{2.12}$$

In contrast to the classical formulation, the kinetic and potential terms of a quantum Hamiltonian generally do not commute. In effect, we are forced to solve statics and dynamics at the same in order to describe a quantum system. It is therefore natural that a quantum system requires an order parameter field that varies in both space and time. The way to proceed further from this observation is to notice that the density matrix $\mathrm{e}^{-\beta \hat{H}}$ looks exactly like the quantum mechanical time evolution operator $\mathrm{e}^{-\mathrm{i}\hat{H}t/\hbar}$ if one assigns an imaginary time, $\tau = -\mathrm{i}\hbar\beta$. With this reinterpretation $\mathcal{Z}$ takes the form of a sum of probabilities for the system to evolve from an initial state $|\Psi\rangle$, and then return to the same state after a finite time interval $-\mathrm{i}\hbar\beta$. The Feynman path integral formalism prescribes a practical way of calculating this net transition probability through a sum over all possible intermediate states between the initial and final state. We will not spend much time discussing the construction of the path integral formalism, instead the reader is referred to more extensive literature. The textbooks [49] and [50] are recommended in that respect.
The starting point of the procedure is to divide the imaginary time interval into a large number of intermediate time steps called *Trotter slices*. Formally,

$$\mathrm{e}^{-\beta \hat{H}} = (\mathrm{e}^{-\delta\tau \hat{H}/\hbar})^{N_\tau}, \tag{2.13}$$

where N_τ is an integer indicating the total number of Trotter slices. Thus, $N_\tau \delta\tau = \hbar\beta$. At each time step a sum over a complete set of states is inserted

so that $\mathcal{Z}$ is given by[6]

$$\mathcal{Z} = \sum_n \sum_{m_1, m_2, \ldots, m_{N_\tau}} \langle n|\mathrm{e}^{-\mathrm{i}\delta\tau\hat{H}}|m_1\rangle\langle m_1|\ldots|m_{N_\tau}\rangle\langle m_{N_\tau}|\mathrm{e}^{-\mathrm{i}\delta\tau\hat{H}}|n\rangle \tag{2.14}$$

The quantum partition function now takes the form of a classical partition function in one higher dimension compared to the original system. However, the extent of the extra dimension is finite for finite temperatures, $\beta \propto 1/T < \infty$. In this case the system is a "slab" with infinite spatial extent, but finite temporal "thickness". Due to the divergent length scale in the imaginary time direction, the correlation length ξ_τ will out-scale the extent of the imaginary time if the system is tuned sufficiently close to the phase transition. Thus, at any finite temperature the extra dimension will not affect the critical behavior. The extent of the imaginary time direction diverges as $T \to 0$, such that the correlation length, ξ_τ, is no longer limited by $\hbar\beta$. In this case the effective dimensionality of the system is increased. The crossover from classical criticality to quantum criticality may therefore be regarded as a dimensional crossover.
From the definition of the divergent length scale in imaginary time, Eq. (2.10), it is clear that the imaginary time scales as length raised to a power z. The critical dynamical exponent z is completely decoupled from the other exponents in classical critical systems, but enters the homogeneity relation and thereby hyperscaling in quantum systems. As we have seen this originates with the intertwining of thermodynamics and dynamics for a quantum system. For simple systems, i.e. systems lacking disorder, dissipation or other auxiliary effects the imaginary time scales just like an additional spatial dimension. In this case $z = 1$, which is an indication of space-time isotropy. However, as was first pointed out by Hertz[51] quantum critical points may in general feature values of z deviating from unity.
The homogeneity postulate should be augmented from the classical case to take the extra dimension(s) into account. For the generic case of power law relation between the divergent lengths in space and time the quantum generalization reads

$$f_s(t, T, h) = b^{-(d+z)} f_s(|t|b^{1/\nu}, Tb^z, hb^{y_h}). \tag{2.15}$$

Now, $|t| = |g - g_c|/g_c$ indicates a dimensionless *non-thermal* control parameter in the system. Compared to the classical case, Eq. (2.5), the present homogeneity relation shows that the number of effective dimensions have increased from d to $d + z$. The critical exponents may be extracted from (2.15) in the same way as discussed in the context of classical criticality.[7]
In the context of classical criticality temperature sets the energy scale through the factor β that couples to the whole Hamiltonian. In a quantum system the transition occurs as an abrupt alteration of the ground state as a consequence of competition between different terms in the Hamiltonian. In experiments, this would correspond to the competition between, *e.g.* Josephson potential

[6] For clarity, we let $\hbar = 1$
[7] Strictly speaking, the heat capacity exponent α is not well-defined when $T = 0$.

and charging energy in Josephson junctions or the exchange potential and the transverse field in a quantum spin system.
As a last comment on this introduction to quantum criticality, it should be mentioned that the last pages have discussed conventional quantum criticality. In this case the correlation lengths in space and time both diverge as power laws as a function of the distance from the quantum critical point. We have

$$\xi \propto |t|^{-\nu} \quad \text{and} \quad \xi_\tau \propto |t|^{-\nu z}. \tag{2.16}$$

More complicated critical behaviors have been conjectured, for example, there are systems where the order parameter fluctuations are in some sense *local*. Recent theoretical research have studied such systems in the context of heavy fermion compounds[52, 53]. Another variant of locality is described by *activated dynamical scaling*. In this scenario the power law relation between ξ and ξ_τ is replaced by $\ln \xi_\tau \propto \xi^\psi$[54]. Eq. (1.1) also describes a variant of local quantum fluctuations. The loop current theory therefore prescribes a quantum critical point which in some sense violates Eq. (2.16).

Chapter 3

Relevant Models

This chapter gives a short introduction to some basic models that are central in the subsequent discussion.

3.1 The Caldeira-Leggett model

The Caldeira-Leggett model[39] describes the effect of coupling a quantum system to an environment. Although originally introduced to study the effect of an environment on tunneling rates, it has found widespread applications. The environment is modeled as a reservoir, or bath, of harmonic oscillators that couples linearly to some degree freedom of the quantum system. Because of the interaction between the two subsystems, energy is transferred irreversibly from the system to the bath, causing dissipation in the system. In general, dissipation weaken quantum fluctuations and may facilitate states of broken symmetry.
The Hamiltonian describing such a system may be formulated as[1]

$$\hat{H} = \hat{H}_S + \hat{H}_{SB} + \hat{H}_B. \tag{3.1}$$

The three terms describe the system, the coupling between the system and the bath, and the bath itself, respectively. Below we present a simple introduction to the Caldeira-Leggett formalism in the context of a single particle moving in a position dependent potential.
The Hamiltonian describing only the system, i.e. a particle with coordinate operator $\hat{q}$ and mass M moving in a potential $V(\hat{q})$ is given by

$$\hat{H}_S = \frac{\hat{P}^2}{2M} + V(\hat{q}), \tag{3.2}$$

where $\hat{P}$ is the momentum operator conjugated to position $\hat{q}$. The bath of harmonic oscillators is described by

$$\hat{H}_B = \sum_n \left(\frac{\hat{p}_n^2}{2m_n} + \frac{1}{2} m_n \omega_n^2 \hat{x}_n^2 \right), \tag{3.3}$$

[1]The introduction of the Caldeira-Leggett framework is based on Refs. [55] and [56].

where m_n, ω_n and $\hat{x}_n$ represent the oscillator mass, frequency and position operator, respectively. The coupling between the two subsystems is given by

$$\hat{H}_{SB} = -\hat{q}\sum_n c_n\hat{x}_n + \hat{q}^2\sum_n \frac{c_n^2}{2m_n\omega_n^2}. \tag{3.4}$$

The first term of $\hat{H}_{SB}$ gives a bilinear coupling between the position operator of the system $\hat{q}$ and the position operators of the bath $\hat{x}_n$. The second term compensates for the renormalization of the potential minimum introduced by the coupling term[39].
The partition function of the complete system can be obtained using the path integral formalism

$$\mathcal{Z} = \int \mathrm{d}q \int_{\substack{q'(\beta)=q\\ q'(0)=q}} \mathcal{D}q' \int \mathrm{d}\mathbf{x} \int_{\substack{\mathbf{x}'(\beta)=\mathbf{x}\\ \mathbf{x}'(0)=\mathbf{x}}} \mathcal{D}\mathbf{x}' \mathrm{e}^{-S[q',\mathbf{x}']}, \tag{3.5}$$

where $\mathbf{x} = \{x_1, \ldots, x_n\}$. From the construction of the path integral it follows that periodic boundary conditions must be imposed in the imaginary time direction. $S[q,\mathbf{x}]$ is called the *Euclidean action* and is defined by an integral over imaginary time τ of the Euclidean Lagrangian L^E:

$$S[q,\mathbf{x}] = \int_0^\beta \mathrm{d}\tau L^E[q,\mathbf{x}] = \int_0^\beta \mathrm{d}\tau \left(L_S^E[q] + L_B^E[\mathbf{x}] + L_{SB}^E[q,\mathbf{x}]\right). \tag{3.6}$$

The three terms in the Euclidean Lagrangian corresponding to the Hamiltonian Eq. (3.1) read

$$L_S^E[\mathbf{x}] = \frac{M}{2}(\partial_\tau q)^2 + V(q), \tag{3.7}$$

$$L_B^E[\mathbf{x}] = \sum_n \left(\frac{m_n}{2}(\partial_\tau x_n)^2 + \frac{1}{2}m_n\omega_n^2 x_n^2\right), \tag{3.8}$$

$$L_{SB}^E[q,\mathbf{x}] = -q\sum_n c_n x_n + q^2\sum_n \frac{c_n^2}{2m_n\omega_n^2}. \tag{3.9}$$

Since the action (3.6) only contains terms that are linear or quadratic in the oscillator coordinates it is possible to integrate out the bath degrees of freedom on closed form. After a somewhat lengthy calculation[2] one ends up with an effective action where the influence of the oscillator bath is contained in a non-local interaction term in imaginary time:

$$\begin{aligned} S_{\mathrm{eff}[q]} = &\int_0^\beta \mathrm{d}\tau \left(\frac{M}{2}(\partial_\tau q(\tau))^2 + V(q(\tau))\right) \\ &+ \frac{\eta}{4\pi}\int_0^\beta \mathrm{d}\tau \int_0^\beta \mathrm{d}\tau' \left(\frac{\pi}{\beta}\right)^2 \frac{(q(\tau)-q(\tau'))^2}{\sin^2(\frac{\pi}{\beta}|\tau-\tau'|)}. \end{aligned} \tag{3.10}$$

By exchanging fluctuations with the oscillator bath the particle can self-interact through a retarded interaction in imaginary time.

[2] The complete calculation may be found elsewhere[55, 56].

Central to the resulting mathematical form of the long-ranged temporal interaction is the spectral density of the bath oscillators. This quantity is defined by

$$J(\omega) = \frac{\pi}{2} \sum_n \frac{c_n^2}{m_n \omega_n} \delta(\omega - \omega_n). \tag{3.11}$$

The particular form of the spectral function may be given by direct knowledge of the bath and its interaction with the system. Often, however, one studies the classical equations of motion and deduce phenomenologically the required form of the spectral function needed to invoke a certain variant of dissipative effects. The above mentioned result (3.10) comes about by using a spectral function linear in the oscillator frequencies, $J(\omega) = \eta\omega$, which is referred to as *ohmic* dissipation. An obvious generalization is to employ a non-linear spectral density function, i.e. $J(\omega) = \eta\omega^s$. Depending on the value of the exponent s, the dissipation that the spectral density leads to is referred to as *sub-ohmic* for $0 < s < 1$, ohmic for $s = 1$ and *super-ohmic* for $s > 1$. Most of the work considered in this thesis is related to ohmic dissipation, however, in Paper V we consider a model describing a chain of quantum spins with a spectral exponent s in the super-ohmic regime.

3.2 Ising model

A ferromagnet with only one easy axis of orientation can be modeled by the Ising model[57]. The Hamiltonian describing this model in the presence of an external, axially directed magnetic field h is given by

$$H = -J \sum_{\langle \mathbf{x}, \mathbf{x}' \rangle} \sigma_{\mathbf{x}} \sigma_{\mathbf{x}'} - h \sum_{\mathbf{x}} \sigma_{\mathbf{x}}. \tag{3.12}$$

Here, J sets the interaction strength and the angular brackets indicate summation over nearest neighbor spins at position $\mathbf{x}$ and $\mathbf{x}'$. The spins can take the values $\sigma = \pm 1$ and are placed on the vertices of a regular cubic lattice. The Hamiltonian is invariant under the inversion of every spin in the system, $\sigma \to -\sigma$. This discrete symmetry is referred to as a Z_2 symmetry.
In $d = 1$ and with $h = 0$ the model does not present any phase transition at finite temperatures. However, in $d = 2$ Onsager[58] showed that the model undergoes a second order phase transition at a critical temperature given by $T_c = 2J/\ln(\sqrt{2} + 1)$. When $T > T_c$ there is no net magnetization

$$m = \frac{1}{V} \sum_{\mathbf{x}} \sigma_{\mathbf{x}} = 0, \tag{3.13}$$

because the available thermal energy is sufficient to disorder the system. V is the normalization volume of the system. At the critical temperature the system starts to organize the spins in such a way that the majority is pointing in the same direction. Thus, for $T < T_c$ the Z_2 symmetry of the Hamiltonian is spontaneously broken.

3.3 Two-dimensional XY-model

The XY-model allows the spin introduced in the last section to rotate in the xy-plane. For spins of unit length ($|\boldsymbol{\sigma}| = 1$) the Hamiltonian is given by

$$H = -K \sum_{\langle \mathbf{x},\mathbf{x}' \rangle} \boldsymbol{\sigma}_{\mathbf{x}} \cdot \boldsymbol{\sigma}_{\mathbf{x}'} = -K \sum_{\langle \mathbf{x},\mathbf{x}' \rangle} \cos(\theta_{\mathbf{x}} - \theta_{\mathbf{x}'}). \tag{3.14}$$

Where θ is the angular direction of spin $\boldsymbol{\sigma}$ relative to some arbitrary reference angle. The Hamiltonian is invariant with respect to rotating all spins an arbitrary angle ϕ,

$$\theta_{\mathbf{x}} \to \theta_{\mathbf{x}} + \phi, \tag{3.15}$$

which is referred to as a global $U(1)$ symmetry. The Hohenberg-Mermin-Wagner theorem[59] states that a system at finite temperatures with a continuous symmetry can never exhibit long-range order if the dimensionality is less than or equal to two. Specifically, the two-dimensional XY-model is unable to establish long-range order at low temperatures because of energetically cheap excitations above the ground state. These excitations are referred to as spin-waves and effectively destroy the spins tendency to point in the same direction. Consequently, the total magnetization is zero for all temperatures. Even so, the model features a phase transition at a critical temperature where the correlation function changes from power-law decay in the low temperature regime to exponential decay in the high temperature regime.
The transition separating the discorded phase from the quasi-ordered phase is the Berezinskii-Kosterlitz-Thouless transition[60]. It involves proliferation of a certain topological defect called *vortices*. The vortices originate with the periodic nature of the variables θ and may be identified by performing a loop integral on the phase gradient surrounding the vortex core,

$$\oint \nabla\theta \cdot \mathrm{d}\mathbf{l} = 2\pi q. \tag{3.16}$$

The sign of the vortex charge, or vorticity, q provides information about the direction of the curl of the phase field around the vortex core. In Fig. 3.1 we show a two-dimensional spin configuration with a vortex and an anti-vortex. The rotation of the phase field is oppositely directed around the two vortex cores, hence, the total vorticity of the configuration is zero.
The transition separating the two phases may be identified by calculating the helicity modulus. This quantity is the second derivative of the free energy with respect to an infinitesimal twist, δ, of the phases in the μ direction. For the classical model (3.14) the helicity modulus is given by

$$\Upsilon_\mu = \left.\frac{\partial^2 F}{\partial \delta^2}\right|_{\delta=0} = \frac{1}{V}\left\langle \sum_{\langle \mathbf{x},\mathbf{x}' \rangle} \cos(\Delta_\mu \theta_{\mathbf{x},\mathbf{x}'}) \right\rangle - \frac{K\beta}{V}\left\langle \left[\sum_{\langle \mathbf{x},\mathbf{x}' \rangle} \sin(\Delta_\mu \theta_{\mathbf{x},\mathbf{x}'}) \right]^2 \right\rangle. \tag{3.17}$$

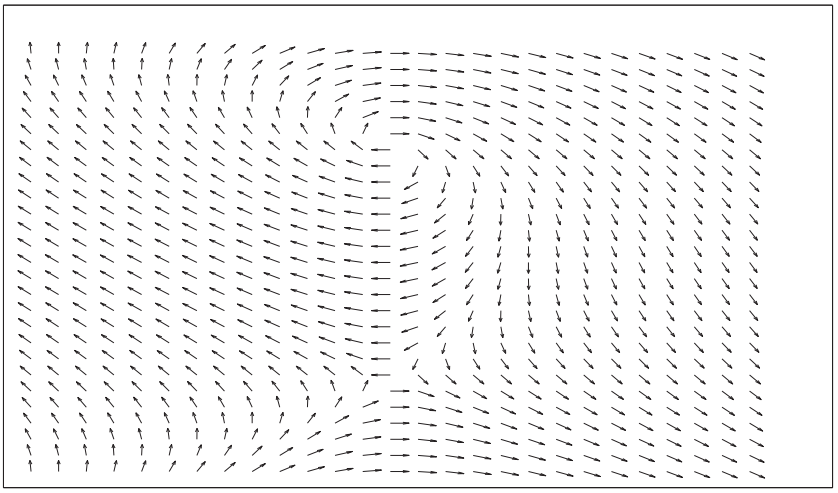

Figure 3.1: A configuration of two-dimensional spins including two vortices of opposite vorticity.

In the two-dimensional XY model $\Upsilon_\mu = 0$ defines the disordered state where vortices are proliferated. $\Upsilon_\mu \neq 0$ on the other hand reflects the finite rigidity of the quasi-ordered state where vortices are bound.
In higher dimensional generalizations of the model the helicity modulus scales with the spatial system size L as $\Upsilon \propto L^{2\beta/\nu-\eta}$ at the critical point where the $U(1)$ symmetry is broken. For a two-dimensional XY model the exponent combination $2\beta/\nu - \eta = 0$ at the critical end-point of the quasi-ordered phase. In this case the finite size scaling is given by the logarithmic corrections[61],

$$\Upsilon(L) = \Upsilon(\infty)\left(1 + \frac{1}{2}\frac{1}{\ln L + C}\right). \tag{3.18}$$

Here, $\Upsilon(\infty)$ is the value of the helicity modulus when $L \to \infty$, and C is an undetermined constant.

3.4 Clock models

Clock models are models for interacting spins in the same way as the Ising model and the XY model. The Hamiltonian describing a classical clock model is often given as

$$H_p = -J \sum_{\langle \mathbf{x},\mathbf{x}' \rangle} \cos(\theta_{\mathbf{x}} - \theta_{\mathbf{x}'}) - h \sum_{\mathbf{x}} \cos(p\theta_{\mathbf{x}}), \tag{3.19}$$

where θ is a continuous variable in the primary interval $\theta \in [-\pi, \pi\rangle$. J sets the energy scale for the interactions between nearest neighbor spins. The anisotropy parameter h quantifies the tendency of the spin to point in certain directions. At $h = \infty$ each spin can only point in p discrete angles $\theta = 2\pi m/p$, where

$m \in \{1, \ldots, p\}$. In this case the Hamiltonian is invariant under the discrete transformations $\theta \to \theta + 2\pi m/p$ (cyclic Z_p symmetry). The opposite limit, $h = 0$, reproduces the XY model (3.14). Considering a classical two-dimensional clock model with $h = \infty$, both $p = 2$ and $p = 4$ are in the Ising universality class. The intermediate $p = 3$ corresponds to the three-states Potts model[62]. In both these cases the model can be solved exactly, and is found to present a phase transition separating a low-temperature phase with broken Z_p symmetry and a high-temperature phase in which this symmetry is restored. For values of $p > p^*$, where p^* is some threshold number of states, the model features three phases. In addition to the two already mentioned there is an intermediate *quasiliquid* phase[63, 64]. The intermediate phase is characterized by power-law decaying two-point correlation functions and an *emergent* $U(1)$ symmetry. The phrase "emergent" refers to the somewhat unusual situation that the symmetry of the order parameter is not present in the Hamiltonian. We will return to a variant of this phenomena in Sec. 5.2, where we discuss a quantum dissipative Z_4 clock model.

Chapter 4

Numerical considerations

In Sec. 2.1 we noted that all observables of a statistical mechanical model were encoded in the partition function. An exact calculation of this function is normally not feasible due to the enormous number of terms in the summation. Hence, one is generally forced to resort to approximation schemes. The Monte Carlo method is likely one of the most widespread and important numerical tools to study physical systems in all variants and shapes. Instead of performing the entire sum that makes up the partition function, the basic idea behind Monte Carlo simulations is to use random numbers to evolve the system from one configuration to a new state statistically independent from the first. In this way the random numbers introduces the randomness needed to mimic thermal noise in thermodynamics or quantum fluctuations in quantum statistical mechanics. In Sec. 4.1 we consider the celebrated Metropolis algorithm which has been a central workhorse in statistical physics since its development at the end of the Second World War. In Sec. 4.2 we consider two related variants of cluster algorithms. These algorithms enable a simultaneous update of an extended part of the system, thus reducing the ergodicity time and critical slowing down[65]. Typically, cluster algorithms are tailored to the specific problem at hand. Models with bond dissipation considered in several variants in Paper I, Paper II, Paper III and Paper IV may at the present time not be simulated by a cluster algorithm because no such algorithms have been constructed yet. Thus, we are confined to utilize local update schemes like the Metropolis algorithm. In Sec. 4.3 we present the parallel tempering algorithm which enables a reduction of large autocorrelation times often associated with rugged energy landscapes. We find this algorithm to be very useful even when restricted to local update algorithms.

4.1 The Metropolis Algorithm

What we really want when doing computer simulations on a statistical mechanical model is to investigate how the system behaves when some external parameter varies. Each possible configuration of the system is realized according to the Boltzmann distribution $p_\psi = (1/\mathcal{Z})\mathrm{e}^{-S[\psi]}$. The peaked functional form of this distribution means that only a few important states are dominant

in the calculation of physically observables. Thus, the strategy of the Metropolis algorithm is to introduce the concept of *importance sampling* which helps realizing the few important states more frequently instead of spending time generating unimportant states.
The basic steps of the algorithm involve creating a sequence of states where each state evolves into the next according to some transition criteria. Usually the dynamics is chosen so that the corresponding series of states is a Markov chain. That is, every state depends solely on the preceding state and no further history. Two important conditions must be fulfilled by the transition rules. The first condition is the *detailed balance* which requires

$$p_\psi P(\psi \to \psi') = p_{\psi'} P(\psi' \to \psi), \tag{4.1}$$

where $P(\psi \to \psi')$ is the probability for the system to transition from state ψ to ψ'. This requirement makes the system come to an equilibrium after a finite number of Markov steps. Additionally, the *accessibility assumption* must be fulfilled. The latter requirement demands that any given configuration must be reachable in a finite number of steps. In this way we assure that we are sampling from the entire phase space.
We know that a classical thermodynamic system evolves according to the Boltzmann probability distribution in which a state ψ appears with probability

$$p_\psi = \frac{\mathrm{e}^{-\beta H_\psi}}{\mathcal{Z}}. \tag{4.2}$$

If we could mimic this behavior, expectation values of observables could be approximated by

$$\langle \mathcal{O} \rangle = \frac{1}{N} \sum_i \mathcal{O}_i, \tag{4.3}$$

where $\mathcal{O}_i$ are independent measurements of some observable calculated from a system evolving according to p_ψ. A major drawback to this procedure is our lack of knowledge of the partition function which is needed to normalize the probability distribution function. The Metropolis algorithm handles this in a very elegant way: It only makes use of the ratio between probability distributions instead of the distribution itself. In this way the knowledge of $\mathcal{Z}$ is no longer needed.
The Metropolis algorithm, in the language of a classical Ising spin system, can be summarized as follows

1. When in configuration ψ_{old}, choose a spin site $\mathbf{x}$ at random. Propose a spin flip of the variable, $\sigma_{\mathbf{x}} \to -\sigma_{\mathbf{x}}$, to generate a new configuration ψ_{new}.
2. Calculate the energy change associated with the spin flip. $\Delta H = H_{\text{new}} - H_{\text{old}}$.
3. Accept the new state with probability $P(\psi_{\text{old}} - \psi_{\text{new}}) = \min[1, \mathrm{e}^{-\beta \Delta H}]$.
4. Go to 1.

In practice we often traverse the lattice sequentially and propose an update on each lattice point. After going through all points on the grid, we say we have performed a Monte Carlo *sweep*. Observables are calculated at regular intervals throughout the simulation. The simulation is typically programmed to terminate after a specific number of sweeps on each temperature.

4.2 Cluster algorithms

The degree to which subsequent measurements are correlated with each other may be quantified through the autocorrelation function

$$\phi(t) = \frac{\langle \mathcal{O}(t)\mathcal{O}(0)\rangle - \langle \mathcal{O}\rangle^2}{\langle \mathcal{O}^2\rangle - \langle \mathcal{O}\rangle^2}. \tag{4.4}$$

In a Markov chain the autocorrelation decays like $\phi(t) \propto \mathrm{e}^{-t/\tilde{t}}$ with a characteristic timescale $\tilde{t}$ for the decorrelation. The Metropolis algorithm suffers from an autocorrelation time $\tilde{t}$ diverging as a power of the system size in the critical regime. Upon approaching a critical point, the sizes of ordered regions grow to include a vast number of spins. Considering a single site update algorithm it is clear that in order to flip an entire region a large number of intermediate, energetically unfavorable, states must be realized. This means that states that are close in energy, and thereby should be realized with roughly the same probability, are separated from each other by a "barrier of states" that are much less likely. To remedy this *critical slowing down*, one may instead employ cluster algorithms.
The strength of the cluster algorithms lies in its nonlocal character. A *Wolff* cluster algorithm builds up clusters of spins and flip these simultaneously. Because most updates take place in large regions of aligned spins, the algorithm is particularly advantageous in the critical regime where fluctuating regions of order exist on all scales. Below, we present the basic steps of this algorithm[66] applied on a Ising variant model.

4.2.1 Wolff algorithm

The central point of the Wollf algorithm is the identification of the clusters. For an Ising model with short-ranged ferromagnetic coupling J the procedure can be outlined as[66]

1. Randomly choose a random spin site as a cluster seed.

2. Consider all spins that interact with the seed and add them to the cluster with probability $p = 1 - \mathrm{e}^{-2J}$ if they have the same sign as the seed.

3. Now consider all the spins that were added to the cluster and accept their neighbors with the same probability and sign requirement. This is iterated until all neighbors of all spins in the cluster have been considered.

4. Flip the cluster.

When these steps have been completed, a new seed is randomly chosen to start the generation of a new cluster. Measurements are performed at regular intervals in the program. The whole process is repeated until the required accuracy is obtained. A thorough discussion of the Wolff algorithm and its performance in various coupling limits may be found in Ref. [67].
The Wolff-algorithm may also be extended to the case where the variables are planar spins that are free to rotate in the xy-plane[68, 66]. In this case a direction in the plane, $\hat{\mathbf{n}}$, is chosen at random and all spins are projected onto this. In effect one ends up with an Ising like system and the algorithm outlined above may be utilized. In this case, flipping the cluster means inverting the projected component of the spins according to[1]

$$\boldsymbol{\sigma} \to \boldsymbol{\sigma} - 2(\boldsymbol{\sigma} \cdot \hat{\mathbf{n}})\hat{\mathbf{n}}. \tag{4.5}$$

The bold letters indicate the vector nature of the variables.

4.2.2 Luijten-Blöte algorithm

We discovered in Sec. 3.1 that introducing dissipation to a system by coupling some degree of freedom in a system to a bath of harmonic oscillators generated a $1/\tau^2$-interaction in imaginary time. This means that each spin in the system interacts with a large number of replicas of itself along the imaginary time direction. Straightforwardly generalizing the Wolff-algorithm outlined in the previous section to take long-ranged interactions into account may be accomplished by exchanging the probability to add a spin with

$$p(|n-m|) = 1 - \mathrm{e}^{-2J(|n-m|)}. \tag{4.6}$$

Here, $J(|n-m|)$ is the distance dependent coupling strength between spins at positions n and m. In general, interactions (like the dissipation term) decay more or less rapidly with distance. This means that the coupling strength between far separated spins is small, implying that the probability of adding a spin to the cluster is also small. Consequently, a large number of operations must be performed for each spin that is actually included into the cluster. To remedy this Luijten and Blöte[69] reformulated the cluster construction by optimizing the process of identifying the spins that are included. Below, we go through the basic steps of the *Luijten-Blöte* algorithm for long-range interacting systems. The presentation will follow Ref. [70] closely. To simplify the discussion, we introduce the algorithm in the context of a one-dimensional Ising spin chain with distance dependent interaction. This is equivalent to a $(0+1)$-dimensional quantum system with long range interaction in imaginary time. Later, we return to a short discussion of the generalizations necessary to take other variable symmetries into account.
Each cluster construction is initiated by randomly selecting a seed spin in the system. All other spins are included into the cluster with probability given by Eq. (4.6) if their spins are parallel to the seed spin. If a spin is included into

[1] This procedure is also valid if the variables are not rotational symmetric, but are of some Z_n symmetry.

the cluster an address is associated with it and it is placed on a *stack*. The next spin to be included in the cluster is found by considering a cumulative probability distribution defined by

$$C(j) = \sum_{n=1}^{j} P(n) \tag{4.7}$$

where,

$$P(n) = \left\{ \prod_{m=1}^{m=n-1} (1 - p_m) \right\} p_n. \tag{4.8}$$

We have defined origin at the seed spin such that p_m denotes the probability $p(|m|)$. In this way, $P(n)$ is the probability that the first $n-1$ spins are skipped and the n'th spin is added to the cluster. From this cumulative probability distribution we can find the next spin to be added using a random number $r \in [0, 1\rangle$. If $C(j-1) < r < C(j)$, $j-1$ spins are skipped and the j'th spin is added to the cluster if it has the same sign as the seed spin. The next spin to be included is found in a similar manner, but the requirement that the new spin, at distance k, must be found at a larger distance ($k > j$) than the previous means that the cumulative probability, Eq. (4.7), should be shifted according to

$$C_j(k) = \sum_{n=j+1}^{k} P_j(n). \tag{4.9}$$

Here,

$$P_j(k) = \left\{ \prod_{m=j+1}^{k-1} (1 - p_m) \right\} p_k. \tag{4.10}$$

By inserting the specific form of the probability p_k and expanding, it is straightforward to show that this expression simplifies to

$$C_j(k) = 1 - \exp\left[-2 \sum_{n=j+1}^{k} J(n) \right]. \tag{4.11}$$

This means that the next spin is added in the range $[j+1, k]$ with a probability that is given by the same expression as the original probability distribution function, except the coupling value is traded for the sum over all the coupling values in the specific range. All spins that are actually added to the cluster also have their address added to the stack. When all spins interacting with the seed spin have been evaluated, a new spin is read from the stack, and the process is continued as long as there are spins left on the stack. When the stack is empty all spins in the cluster are flipped and a new seed spin is chosen to grow the new cluster.

The shifted cumulative probability distribution may be constructed from $C(j)$

$$C_j(k) = \frac{C(k) - C(j)}{1 - C(j)}. \tag{4.12}$$

In this way, $C_j(k)$ may be tabulated during the initialization of the program. Hence, finding the distance to the next spin amounts to looking up in a table rather than repeatedly calculating cumulative probabilities.
The generalization to non-Ising like symmetries is based on a similar projection as discussed in Sec. 4.2.1. The distances to the next proposed spin is determined in exactly the same way as for Ising spins. However, the demand that the spins must point in the same direction must be refined. The projections of the spins onto a random direction $\hat{\mathbf{n}}$ determine if the proposed spin is included or not. Also, it must be taken into account that the interactions between the spins are weaker than assumed in the cumulative probabilities. In practice, a random number r is generated and the proposed spin is included in the cluster if[68]

$$r < \frac{1 - \mathrm{e}^{-2J(|n-m|)(\boldsymbol{\sigma}_n \cdot \hat{\mathbf{n}})(\boldsymbol{\sigma}_m \cdot \hat{\mathbf{n}})}}{1 - \mathrm{e}^{-2J(|n-m|)}}. \tag{4.13}$$

After having completed the generation of the cluster, all spins in the cluster are mirrored according to (4.5).

4.3 Parallel Tempering

The versatility of the Wolff- and Luijten-Blöte algorithms is seriously limited by the requirement that there can not be competing interactions in the system. That is, all couplings in the system must be of the same sign (either ferromagnetic or antiferromagnetic). In the presence of interactions combining antiferromagnetic and ferromagnetic coupling values the algorithm will generate clusters of roughly the size of the entire system and flip them as a whole. The effect is extremely large autocorrelation times, although eventually yielding the correct results. The problem of a combination of coupling types is inherent in the models we have considered with bond dissipation. Also, the noncompact variables considered in some parts of this thesis makes it difficult to define projections, a necessary point for the Wolff algorithm and its Luijten-Blöte extension. Consequently, we are restricted to employ local update algorithms whenever we consider a bond dissipative model.
The energy-landscape generated by bond dissipation is generally characterized by high entropic barriers. Simulations using a local update algorithm are therefore likely to be seriously slowed down because of the low probability to tunnel through these barriers. The *parallel tempering* algorithm (also called *replica-exchange method*) is widely employed in this thesis to cope with the presence of such a dissipation term. Below we explain the algorithm and show why it is beneficiary to use it.
The parallel tempering algorithm is parallel in the sense that N replicas of the same system is simulated simultaneously at different coupling strengths. After a certain number of standard Metropolis sweeps a swap of two systems at two

neighboring coupling values is proposed and accepted with a certain probability. In this way, every replica will perform a random walk in coupling space in order to effectively explore the complex energy landscape: If a copy is to some degree confined to a metastable state, the algorithm enables the system to escape the local minimum by wandering to lower coupling values.
The basic steps of the algorithm is outlined in the following. Each of the N copies is simulated on its own processor at an individual coupling strength κ. After a specified number of sweeps[2] a swap of coupling values is proposed between two copies operating at neighboring coupling values.
The exchange of coupling values between two realizations of the system is accepted with a probability that may be found from a simple argument closely resembling the argument given for transition probabilities in Sec. 4.1, see for example Ref. [71]. The transition probability between can be expressed as

$$\Xi_{PT} = \begin{cases} 1 & \text{if } \Delta < 0 \ , \\ \mathrm{e}^{-\Delta} & \text{if } \Delta \leq 0. \end{cases} \tag{4.14}$$

Where, $\Delta = \kappa' \left(\overline{S}[\mathbf{X};\kappa'] - \overline{S}[\mathbf{X}';\kappa']\right) - \kappa \left(\overline{S}[\mathbf{X};\kappa] - \overline{S}[\mathbf{X}';\kappa]\right)$. κ is the coupling parameter varied in the simulations and $\overline{S}$ is the part of the action that couples linearly to κ. The state of the ensemble is characterized by the set of configurations $\mathbf{X} \in \{\mathbf{X}_1, \ldots, \mathbf{X}_N\}$.

4.3.1 Selecting coupling values

The performance of the PT algorithm is very sensitive to the distribution of coupling values. The acceptance ratio of the coupling swaps decreases exponentially with the difference $|\kappa - \kappa'|$. Consequently, the coupling values must be placed in such a way as to assure a fair overlap between the histogram describing the distribution of $\overline{S}$ at coupling κ and the corresponding distribution at coupling κ'. Otherwise few swaps will be accepted and the performance of the algorithm will be roughly the same as for the Metropolis algorithm. If the system undergoes a second order phase transition with divergent heat capacity further considerations are necessary. It can be shown that the acceptance rate of the proposed swaps is related to the functional behavior of the inverse of the heat capacity per spin[71]. Thus, if the heat capacity diverges, the swap acceptance rate will be forced to zero at the transition coupling. This will in turn mean that configurations are not free to wander around in coupling space as the phase transition acts as an effective barrier, separating the weak coupling from the strong coupling regime. This scenario seriously limits the effectiveness of the algorithm because metastable configurations can not take advantage of disordering in the weak coupling regime.
These difficulties can be avoided if the coupling values are assigned with care. Following Ref. [72] we remedy the vanishing acceptance rate in the critical regime by demanding a constant acceptance rate across the phase transition. The weakest coupling is set low enough to effectively disorder the system, and

[2]Here, we refer to a number of Metropolis sweeps, but the algorithm may be straightforwardly reformulated to *e.g.* cluster updates.

similarly, the strongest coupling should be well inside the ordered phase. All other coupling values are subject to the iteration scheme outlined below.
The starting point is to demand that the transition probability from a coupling κ_n to both its nearest neighbors should be equal

$$\begin{aligned}(\kappa_{n-1}-\kappa_n)\{\overline{S}(\kappa_{n-1})-\overline{S}(\kappa_n)\}&=A,\\(\kappa_n-\kappa_{n+1})\{\overline{S}(\kappa_n)-\overline{S}(\kappa_{n+1})\}&=A,\end{aligned}\tag{4.15}$$

where A is an unknown constant. The next step in the iteration procedure is given by $\kappa_n(t+1)=1/2[\kappa_n(t)+R(\kappa_n(t))]$, where the function R is given by

$$\begin{aligned}\kappa_n &= R(\kappa_n) \\ &= \frac{1}{\overline{S}(\kappa_{n-1})-\overline{S}(\kappa_{n+1})}\left\{\kappa_{n-1}\overline{S}(\kappa_{n-1})-\kappa_{n+1}\overline{S}(\kappa_{n+1})-\overline{S}(\kappa_n)(\kappa_{n-1}-\kappa_{n+1})\right\}\end{aligned}\tag{4.16}$$

In simulations a pilot simulation is performed in order to distribute the coupling values in an optimal manner before the production sweeps are initiated.

4.4 Error estimates

To estimate the accuracy of the simulation results we have used the *jackknife method*. This error estimation procedure takes the autocorrelation, Eq. (4.4), between measurements into account by restructuring the data into bins that may be considered independently[73, 74, 75]. The method is widely used in this thesis and is therefore schematically introduced here.
The Jackknife method is a way of calculating the standard deviation in a set of stochastic, though correlated, measurements in a systematic way. Let the quantity $\mathcal{O}$ be measured in a Monte Carlo simulation. Then the Jackknife error may be calculated by:

- Calculate the expectation value $\langle\mathcal{O}\rangle$ from the entire dataset, $\{\mathcal{O}_i\}$ where $i\in[1,\ldots,N]$. N is the total number of measurements.
- Divide the full dataset into M bins. (The size of the bin must be much larger than the autocorrelation time.)
- Calculate the average $\langle\mathcal{O}\rangle_m$ using data from all bins except bin m.
- The error estimate may be calculated by

$$\delta\langle\mathcal{O}\rangle=\sqrt{\frac{M-1}{M}\sum_{m=1}^{M}[\langle\mathcal{O}\rangle_m-\langle\mathcal{O}\rangle]^2}.\tag{4.17}$$

4.5 Reweighting

When performing a Monte Carlo simulation we apply one of the discussed algorithms on the system at different coupling values. The raw data from such simulations can tell us a great deal more than just the behavior of the system

at the simulated coupling values. Through the concept of *reweighting* we can expand the results calculated at a certain coupling value to other nearby values, and thus extract information about the system at coupling strengths not simulated.
To illustrate the principle, lets first look at a simple case where we have performed a simulation at a single coupling value κ_1. The index i labels the N measurements of the observable $\mathcal{O}_i$ and the action S_i.[3] The expectation value of the observable is given by

$$\langle \mathcal{O} \rangle_{\kappa_1} \equiv \frac{1}{\mathcal{Z}_{\kappa_1}} \sum_{\{\psi\}} \mathcal{O}_\psi \mathrm{e}^{-\kappa_1 S(\psi)} \approx \frac{1}{N} \sum_i \mathcal{O}_i. \tag{4.18}$$

Consider the observables $\mathcal{O}\mathrm{e}^{-(\kappa-\kappa_1)S}$ and $\mathrm{e}^{-(\kappa-\kappa_1)S}$, these have expectation values

$$\left\langle \mathcal{O}\mathrm{e}^{-(\kappa-\kappa_1)S} \right\rangle_{\kappa_1} = \frac{\sum_{\{\psi\}} \mathcal{O}_\psi \mathrm{e}^{-(\kappa-\kappa_1)S(\psi)} \mathrm{e}^{-\kappa_1 S(\psi)}}{\mathcal{Z}_{\kappa_1}} \approx \frac{1}{N} \sum_i \mathcal{O}_i \mathrm{e}^{-(\kappa-\kappa_1)S_i} \tag{4.19}$$

and

$$\left\langle \mathrm{e}^{-(\kappa-\kappa_1)S} \right\rangle_{\kappa_1} = \frac{\sum_{\{\psi\}} \mathrm{e}^{-(\kappa-\kappa_1)S(\psi)} \mathrm{e}^{-\kappa_1 S(\psi)}}{\mathcal{Z}_{\kappa_1}} \approx \frac{1}{N} \sum_i \mathrm{e}^{-(\kappa-\kappa_1)S_i}. \tag{4.20}$$

When inspecting the last equality we see that this is nothing else than $\mathcal{Z}_\kappa / \mathcal{Z}_{\kappa_1}$. Now, combining Equations (4.19) and (4.20) we see that we get an estimate for $\mathcal{O}$ at $\kappa \neq \kappa_1$,

$$\langle \mathcal{O} \rangle_\kappa = \frac{\sum_{\{\psi\}} \mathcal{O}_\psi \mathrm{e}^{-\kappa S(\psi)}}{\mathcal{Z}_\kappa} \approx \frac{\sum_i \mathcal{O}_i \mathrm{e}^{-(\kappa-\kappa_1)S_i}}{\sum_i \mathrm{e}^{-(\kappa-\kappa_1)S_i}} \tag{4.21}$$

In other words, we can estimate the quantity $\mathcal{O}$ at a coupling $\kappa \neq \kappa_1$, based on measurements taken at κ_1, given that the difference $|\kappa - \kappa_1|$ is sufficiently small.
In this work we have used a more complicated form of reweighting, the Ferrenberg-Swendsen *multiple histogram reweighting*[76]. Although the underlying principles are the same as demonstrated above, the algorithm drastically improves the quality of estimates by combining data from simulations at *several* different coupling values. The method is quite involved, but fortunately we have been provided a software package implemented by Kari Rummukainen which has been used throughout the thesis.

4.6 Finite size scaling and Binder analysis

Sharp phase transitions only take place in the thermodynamic limit, i.e. in infinitely large systems. It goes without saying that this cannot possibly be

[3] We are considering only the term of the action which couples linearly to the coupling parameter varied in the simulations.

simulated on a computer where there are limitations such as storage capacity etc. Thereby, we are restricted to work with systems of finite sizes.
Approaching a classical second order phase transition, the correlation length diverges according to $\xi \propto |t|^{-\nu}$, but this divergence is halted if the system size is finite. This means that $\xi \to L$ as $t \to 0$. The result is that divergences of observables appear rounded, discontinuities are smeared out and critical coupling strengths are shifted. Even though the behavior of the system is severely altered in the critical regime by these *finite size effects*, a systematic investigation of observables as a function of L enables us to extract important information from the system. By inserting $L \propto |t|^{-\nu}$ in the definitions of the critical exponents found in Tab. 2.1, we obtain explicit size dependence in the scaling relations. Specifically, for a finite temperature phase transition we obtain

$$C_V \propto L^{\alpha/\nu}, \tag{4.22}$$

and similarly for the order parameter and its susceptibility

$$\begin{aligned} m &\propto L^{-\beta/\nu}, \\ \chi &\propto L^{\gamma/\nu}. \end{aligned} \tag{4.23}$$

Finite size scaling relations like Eqs. (4.22) and 4.23 are of limited use if we do not know the critical temperature. Because the correlation length is limited by the system size near T_c the system appears to be ordered at a "pseudocritical" point $\tilde{T}$. We have, $|\tilde{T}-T_c|^{-\nu} \propto \xi = L$. This implies that the system is effectively ordered at $\tilde{T} = T_c + \text{const.} \times L^{-1/\nu}$. This makes it complicated even to locate the transition if we do not know the exponent ν in advance.
A well known method to determine the value of the critical coupling is to calculate the Binder ratio

$$Q = \frac{\langle m^4 \rangle}{\langle m^2 \rangle^2}, \tag{4.24}$$

and use this to plot the Binder cumulant $g \equiv 1 - Q/3$. The Binder cumulant at criticality is independent of system size (to leading order in L). The crossing point of $g(T)$ for different system sizes thus defines the (pseudo)critical point.
So far, we have glossed over the fact that in order to study a $T = 0$ problem, we should also take into account the correlation length divergence in imaginary time. Just like ξ is restricted by the spatial system size L, ξ_τ is restricted by the size of the system in the imaginary time direction. Assuming correlation lengths scaling according to $\xi_\tau \propto \xi^z$, the scaling of the Binder cumulant now includes two independent scaling variables instead of just one,

$$Q(L, L_\tau) = \mathcal{G}\left(\frac{L}{\xi}, \frac{L_\tau}{\xi_\tau}\right). \tag{4.25}$$

Eq. (4.25) has an important characteristic: There is an optimal choice of temporal size, L_τ^* for each spatial system size. For this particular aspect ratio, the system size reflects the anisotropy of the divergent correlation lengths, $L/L_\tau^* \sim \xi/\xi_\tau$, and the system appears as isotropic as it possibly can be, the anisotropic interactions taken into account.

In Fig. 4.1 we illustrate the necessity that the system sizes must reflect the anisotropy of the correlation lengths. In the topmost panel, the typical size of a correlated area (shown in purple) does not have the same aspect ratio as the system (shown in gray). Consequently, the system may be decomposed into independently fluctuating "chunks" which decreases the total degree of order. The lowermost panel shows the case where we have adjusted the system aspect ratio to fit the shape of the correlated area. In this case, ξ will diverge and be limited by L simultaneously as ξ_τ is limited by L_τ. Physically, this means that the thermodynamic limit ($L \to \infty$) coincides with the quantum limit ($T \to 0$).
A strategy we have employed extensively is to simulate the system at coupling values surrounding the putative critical coupling for a number of different temporal sizes L_τ for each individual spatial size L.[4] L_τ^* is extracted by plotting the Binder cumulant g as a function of L_τ (semi logarithmically) for fixed L and coupling. L_τ^* corresponds to the maximum of the resulting curve, as decreasing or increasing the L_τ will make the system appear less ordered. Having localized the points (L_τ^*, g^*) we may plot the optimal values of the Binder cumulant, g^*, as a function of coupling (See panel (b) of Fig. 2 in Paper I). From the scaling ansatz (4.25) it follows that the value of Q is independent of its arguments at the critical point. Therefore, an estimate of the critical coupling can be found from the value to which the crossing point for two subsequent values of L converges for $1/L \to 0$. Alternative ways of extrapolating to the thermodynamic limit is mentioned in Paper I and Paper V.
Having found the characteristic L_τ at criticality for each L, the dynamical critical exponent may be extracted by considering the slope of the $\ln L_\tau^*$ versus $\ln L$ plot. An example of this is shown explicitly in panel (c) of Fig. 2 in Paper I. Lastly, one may check the self-consistency of the obtained values for the critical coupling and z by plotting the putative data collapse of the Binder cumulant as a function of L_τ/L^z.
In the two topmost panels of Fig. 4.2 we show the coupling dependence of the Binder cumulant g for various system sizes. The data shown are taken from the finite size analysis of Paper V. The various curves correspond various spatial system sizes that are increasing from left to right. The left panel corresponds to a subcritical value of the coupling, while the right panel corresponds to a supercritical value. In the lowermost left panel the coupling has been adjusted to the critical value, consequently, there is a vertical alignment of the curves. In the remaining panel the curves are scaled with L^z in order to align them horizontally. The net result is a complete collapse of the Binder cumulant curves onto a universal function.

[4] In practice, pilot simulations is necessary to obtain a rough estimate of the critical coupling and to make sure the distribution of L_τ includes the optimal L_τ^*.

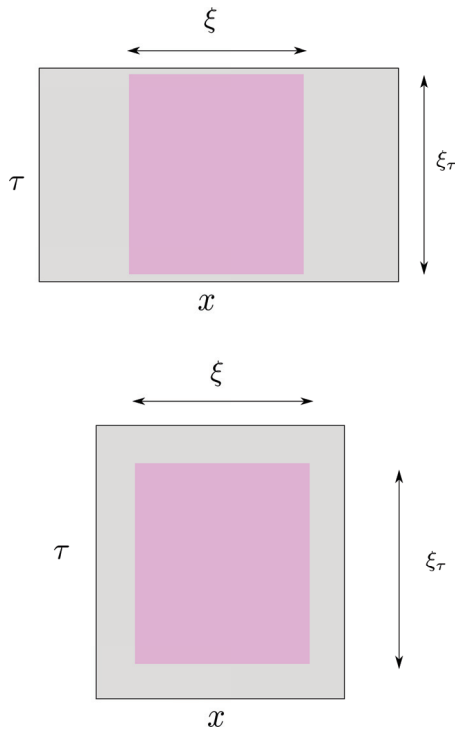

Figure 4.1: In the topmost panel the aspect ratio, or shape, of typical correlated regions (shown in purple) is not similar to the numerical grid(indicated by the gray region). The system may therefore be decomposed into independently fluctuating parts. The lowermost panel corresponds to a scenario where the aspect ratio of the numerical grid reflects the aspect ratio of typical correlated regions.

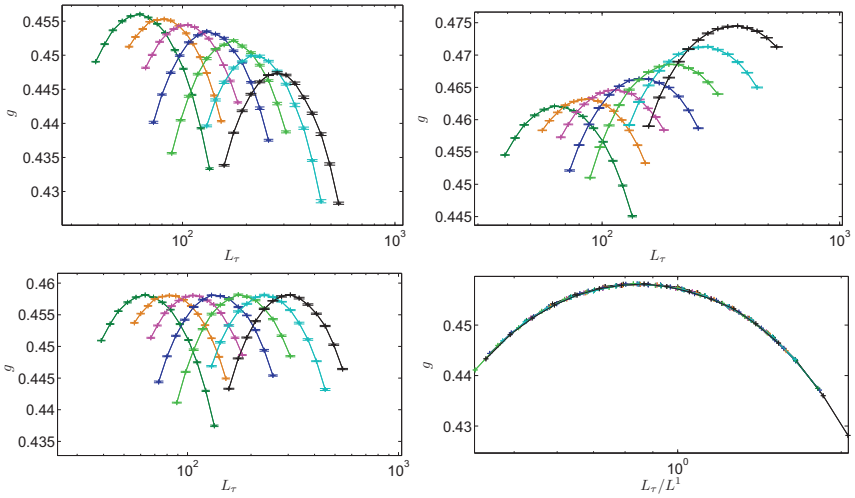

Figure 4.2: The Binder cumulant g calculated for several system sizes at a specific parameter set of the model considered in Paper V. In the left panel in the topmost row the cumulants are calculated at a subcritical coupling strength and there is consequently a considerable size dependence. In the right panel in the same row the cumulants are shown at a supercritical coupling value. The cumulants are vertically aligned at criticality in the leftmost panel in the bottom row. The collapse of the cumulants in the right panel in this row validates the scaling ansatz (4.25). For this particular model we obtain an optimal collapse with a dynamical critical exponent $z = 1$.

Chapter 5

Central results

5.1 The dissipative transverse field Ising model

In Paper I we consider two variants of dissipative transverse field Ising models at zero temperature. In the absence of dissipative effects the Hamiltonian for this model reads

$$\hat{H} = -J \sum_{\langle \mathbf{x},\mathbf{x}' \rangle} \hat{\sigma}^z_{\mathbf{x}} \hat{\sigma}^z_{\mathbf{x}'} - \Gamma \sum_{\mathbf{x}} \hat{\sigma}^x_{\mathbf{x}} \tag{5.1}$$

The first summation runs over all nearest neighbors on a regular d-dimensional cubic lattice, the second summation simply traverses all gridpoints. $\hat{\sigma}^z_{\mathbf{x}}$ and $\hat{\sigma}^x_{\mathbf{x}}$ are Pauli matrices which represent the quantum mechanical degrees of freedom. The first term in this Hamiltonian describes the magnetic exchange interaction, when $J > 0$ this term facilitates global alignment of the spins along the z-direction. If this term dominates there are two possible ground states of the system, either all spins are pointing upwards or all are pointing downwards. The second term tend to align the spins in the direction of the transverse field Γ. Hence, this term disturbs the alignment even at zero temperature. If Γ dominates it enforces a new ground state where the spins are aligned to the applied field in the x-direction.

At this point we mention an important conceptual difference in the interpretation of the thermally disordered state of a classical system and the quantum disordered state. The classical (finite temperature) case is disordered due to spins being randomly perturbed by thermal noise. The quantum disordered state is a ground state dominated by the traverse field, projected onto the basis where $\hat{\sigma}^z$ is diagonal, this "looks" like a disordered state (zero magnetization), but is actually a coherent superposition of the eigenstates $\sigma^z = \pm 1$[77].

As was discussed in the Sec. 3.1, one may introduce dissipation to a quantum system by coupling some degree of freedom to a bath of harmonic oscillators. The case of a single two-state system coupled to a bath has been well investigated[78, 79, 80, 50]. In comparison, the spatially extended version of a dissipative two-state system has, until recently, received relatively little attention. Werner *et al.* considered a $(1+1)$-dimensional system with bosonic baths coupling locally to each individual spin in Ref. [81]. This amounts to adding

the term[81],

$$\hat{H}_{\text{diss}} = \sum_{\mathbf{x},n} \left\{ c_n \hat{\sigma}^z_{\mathbf{x}} (a^\dagger_{\mathbf{x},n} + a_{\mathbf{x},n}) + \omega_{\mathbf{x},n} a^\dagger_{\mathbf{x},n} a_{\mathbf{x},n} \right\}, \tag{5.2}$$

to (5.1). Here, $a^\dagger_{\mathbf{x},n}$ ($a_{\mathbf{x},n}$) are creation (annihilation) operators of the harmonic oscillator n which couples to the Pauli operator at position $\mathbf{x}$. $\omega_{\mathbf{x},n}$ and c_n are chosen such that the spectral function is linear (ohmic damping): $J(\omega) = 4\pi \sum_n c_n^2 \delta(\omega - \omega_{\mathbf{x},n}) = 2\pi\alpha\omega$ for all ω less than some cutoff frequency. After formulating the problem on a path integral form and having integrated out the bosonic degrees of freedom, one ends up with an effective action $S = S_0 + S_{\text{diss}}$, where[1]

$$S_0 = -K \sum_{\langle \mathbf{x},\mathbf{x}' \rangle} \sum_{\tau}^{N_\tau} \sigma_{\mathbf{x},\tau} \sigma_{\mathbf{x}',\tau} - K_\tau \sum_{\mathbf{x}} \sum_{\tau}^{N_\tau} \sigma_{\mathbf{x}\tau} \sigma_{\mathbf{x},\tau+1} \tag{5.3}$$

and

$$S_{\text{diss}} = \frac{\alpha}{4} \sum_{\mathbf{x}} \sum_{\tau \neq \tau'} \left(\frac{\pi}{N_\tau} \right)^2 \frac{(\sigma_{\mathbf{x},\tau} - \sigma_{\mathbf{x},\tau'})^2}{\sin^2(\pi/N_\tau |\tau - \tau'|)}. \tag{5.4}$$

The σ's now indicate the classical Ising variables $\{\sigma = \pm 1\}$. The coupling parameters K and K_τ are related to the exchange interaction J and transverse field Γ, respectively[82]. N_τ indicates the number of Trotter slices used to discretize imaginary time.

Werner *et al.* found[81] that the critical behavior of the system was neither that of a single dissipative two-state system nor that of a dissipationless system. To be specific, they found critical behavior involving anisotropy between the divergence of the correlation lengths in space and imaginary time. In Paper I we expand on these results by investigating the model in (2+1) dimensions in order to test the robustness of the results towards variations in the number of spatial dimensions. We map out the phase diagram of the model in space of spatial coupling K and dissipation strength α and find that it is qualitatively similar to that of the corresponding model in one spatial dimension. The dynamical critical exponent is found to be $z \approx 2$ along the transition line in accordance with Ref. [81].

Considering the action of the dissipative transverse field Ising model in Fourier space, the quadratic part of the action can be written as

$$S \sim (\mathbf{q}^2 + \omega^2 + |\omega|) \sigma_{\mathbf{q},\omega} \sigma_{-\mathbf{q},-\omega}, \tag{5.5}$$

if one neglects all prefactors. Taking the limit $\mathbf{q} \to 0$ and $\omega \to 0$, the dissipation term $|\omega|$ will always dominate the dynamic term ω^2. By using the scaling relation $\omega \sim q^z$ a balance is achieved between the spatial term and the dissipation term if $z = 2$. In this way the dynamical critical exponent is predictable by "counting powers" of the terms in the bare propagator. The estimate for z is

[1] The action is presented on discretized form.

a lowest order approximation, but in our experience this *naive scaling estimate* provides a reliable hint of the actual outcome of the simulations.
The action intended to describe orbital loop currents in cuprate superconductors, Eq. (1.2), prescribes a dissipation term in which the dissipative quantities are the bond variables rather than the variables themselves. Therefore, we also consider a dissipation term of this form in order to investigate if this alters the critical behavior. In particular, we are interested in how it affects spatio-temporal scaling compared to onsite dissipation. The dissipation term reads

$$S_{\text{diss}} = \frac{\alpha}{2} \sum_{\langle \mathbf{x},\mathbf{x}' \rangle} \sum_{\tau \neq \tau'} \left(\frac{\pi}{N_\tau} \right)^2 \frac{(\Delta\sigma_{\mathbf{x},\mathbf{x}',\tau} - \Delta\sigma_{\mathbf{x},\mathbf{x}',\tau'})^2}{\sin^2(\pi/N_\tau|\tau - \tau'|)}, \tag{5.6}$$

where the bond variables are given by $\Delta\sigma_{\mathbf{x},\mathbf{x}',\tau} = \sigma_{\mathbf{x},\tau} - \sigma_{\mathbf{x}',\tau}$ for nearest neighbor positions $\mathbf{x}$ and $\mathbf{x}'$. By use of naive scaling arguments we may predict the value $z = 1$ for the dynamical critical exponent. Physically this means that the bond dissipation term is less efficient in reducing temporal fluctuations compared to the onsite dissipation term. While (5.4) tends to align all spins along the imaginary time direction, (5.6) only contributes to order the Ising gradients. The numerical results of Paper I strongly suggests that the naive scaling estimate $z = 1$ is indeed realized in the $(1 + 1)$-dimensional bond dissipative model.

5.2 The dissipative Z_4 clock model

Partially motivated by the four-fold symmetry of the orbital currents introduced in Sec. 1.3 and partially motivated by the issue of variable *compactness* pertaining to the physics of resistively shunted Josephson junctions (see Sec. 5.3), we study two variants of a dissipative Z_4 model. The starting point is a set of angular variables $\{\theta_{x,\tau}\}$ residing on the vertices of a $(1+1)$-dimensional quadratic lattice. In order to impose the same four-fold symmetry as found in the orbital current theory the variables are parameterized as $\theta = 2\pi n/4$ with integer valued n. To investigate if the domain of these variables has any implications on the behavior of the model we consider both a compact and a noncompact version of the model. In the compact (C) case the parameterization variable n is restricted to only four values. θ is therefore always found within the primary interval. In the noncompact (NC) case there is no such restriction on n, θ is therefore free to wander outside the primary interval. The action describing the system is given by

$$S^{\text{C,NC}} = S_\tau^{\text{C,NC}} + S_x + S_{\text{diss}}, \tag{5.7}$$

where the quantum kinetic term for the compact and noncompact case, respectively, is given by

$$S_\tau^{\text{C}} = -K_\tau \sum_x^N \sum_\tau^{N_\tau} \cos(\theta_{x,\tau+1} - \theta_{x,\tau}) \tag{5.8}$$

and

$$S_\tau^{\mathrm{NC}} = \frac{K_\tau}{2} \sum_x^N \sum_\tau^{N_\tau} (\theta_{x,\tau+1} - \theta_{x,\tau})^2. \tag{5.9}$$

The spatial interaction is given by

$$S_x = -K \sum_x^N \sum_\tau^{N_\tau} \cos(\theta_{x+1,\tau} - \theta_{x,\tau}) \tag{5.10}$$

and the dissipation term is defined according to

$$S_{\mathrm{diss}} = \frac{\alpha}{2} \sum_x^N \sum_{\tau \neq \tau'} \left(\frac{\pi}{N_\tau} \right)^2 \frac{(\Delta\theta_{x,\tau} - \Delta\theta_{x,\tau'})^2}{\sin^2(\frac{\pi}{N_\tau}|\tau - \tau'|)}. \tag{5.11}$$

The manifest nonperiodic form of the dissipation term implies that this term must be reformulated in order to simulate the compact model. In addition, the kinetic term is treated differently in the two variants of the model. A thorough discussion of the formulation of the model may be found in Paper II and the Appendix therein.

In Sec. 3.4 we briefly mentioned the appearance of an intermediate critical phase in classical two-dimensional clock models with Z_p symmetry. The appearance of the intermediate phase found in this class of models depends on p, the number of discrete angles available to the spin on the unit circle. There are some controversies as to what value of p^* that separates the three-phase scenario from the two-phase scenario[83], however, $p = 4$ is undoubtedly in the Ising universality class.[2] It is therefore interesting that we find an intermediate critical phase in the quantum dissipative Z_4 model.

The critical phase and the phase transitions surrounding it are very similar to the quasiliquid phase and its adjoining transitions studied in variants of the two-dimensional classical clock model[84, 85, 64]. However, in order to generate the intermediate phase in the Z_4 model it is crucial to decompactify the variable θ as we do not observe this phase when the variables are not confined to the primary interval. By considering the distribution of the complex order parameter

$$m = \frac{1}{NN_\tau} \sum_{\mathbf{x},\tau} \mathrm{e}^{\mathrm{i}\theta_{\mathbf{x},\tau}} = |m| \mathrm{e}^{\mathrm{i}\phi} \tag{5.12}$$

in the complex plane the character of the various phases becomes evident. Consider first the noncompact case, where the variables are defined as $\theta = 2\pi n/4$, where $n \in \{0, \pm 1, \pm 2, \dots\}$. At weak dissipation strength the order parameter is peaked around the origin, corresponding to a disordered phase. This is shown in Fig. 5.1(b). Increasing the dissipation eventually drives the system into the intermediate phase where the order parameter develops a finite value as a finite size effect, Fig. 5.1(c). The order parameter is, however, free to rotate in the ϕ direction. This is the same effective wash-out of the excitation gap reported

[2] This can readily be shown by a simple transformation of the angular variables[24].

in discrete Z_p models[64]. Since the continuous symmetry of the order parameter in this phase is not exhibited by the Hamiltonian, this is an example of an emergent symmetry. Increasing the dissipation strength even further breaks the rotational symmetry of the order parameter when long range order is established. This can be seen from the order parameter plots as m relaxes into one of the four directions in the complex plane associated with the underlying Z_4 symmetry. The order parameter distribution corresponding to this phase is depicted in Fig. 5.1(d).
Contrasting the results of the noncompact dissipative clock model with a compact version of the same model makes it clear that it is imperative to decompactify the variables in order to observe the intermediate critical phase. The compact model features a single transition line in the phase diagram separating a disordered (symmetric) phase from a long-ranged ordered (broken Z_4 symmetry) phase. In terms of the distribution of the order parameter in the complex plane, this phase transition may be described as a redistribution of the order parameter weight from a Gaussian centered at the origin directly to a four-fold symmetric distribution. In Fig. 5.2 we show the order parameter distribution in the complex plane in the two phases.
As a last comment in this section we emphasize that on all phase transitions in this study, we measured spatio-temporal isotropy, i.e. $z = 1$.

5.3 Resistively shunted Josephson junction arrays

The quantum phase transition induced by dissipation in a single resistively shunted Josephson junction was first studied by Bulgadaev[86] and Schmid[87]. Since then this system has been investigated by several authors and by a broad array of methods including analytical, experimental and numerical work. See for instance Refs. [88] and [89] and references therein. The junction itself is made up, for example, of a thin oxide layer separating two superconductors or a constriction in a single superconductor. The main point is that there is a well-defined order parameter $\psi = |\psi|e^{i\theta}$ on each side of the junction. Due to "leakage" of the wavefunction from one side of the junction into the other, the superconducting grains become coupled by a Josephson potential[90]. This leakage means that Cooper pairs from one of the superconductors may tunnel through the barrier and enter the second superconductor, thereby probing the state of the order parameter in the adjacent superconductor. The phase difference between the two superconductors can be related to a voltage difference across the junction as well as a supercurrent flowing through the junction[90]. While the Cooper pairs tunnel through the junction, normal electrons may flow through the shunting resistor and dissipate energy. Modeling the shunt resistors as a coupling between phase differences across junctions and baths of oscillators, the oscillators may be integrated out in the same way as discussed in Sec. 3.1. The result is a self-interaction of the phase gradients along imaginary time.
It is now well-known[91] that the nonperiodic form of the dissipation term implies that the variables should be treated as noncompact. This means that rather than being defined on the interval $\theta \in [-\pi, \pi\rangle$, the variables must be al-

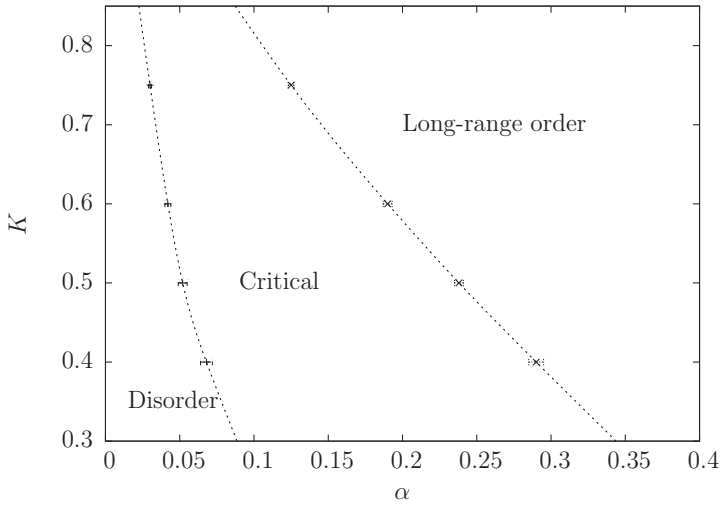

(a) The phase diagram of the quantum four state clock model with bond dissipation. K measures the spatial coupling between spins and α quantifies the dissipation strength. The diagram features three distinct phases: A disordered phase where the order parameter is distributed in the complex plane as shown in the leftmost panel below. An intermediate critical phase where the order parameter distribution is rotational symmetric as shown in the midmost panel. Lastly, there is a long-ranged ordered phase where the order parameter is confined in the four directions corresponding to the underlying Z_4 symmetry.

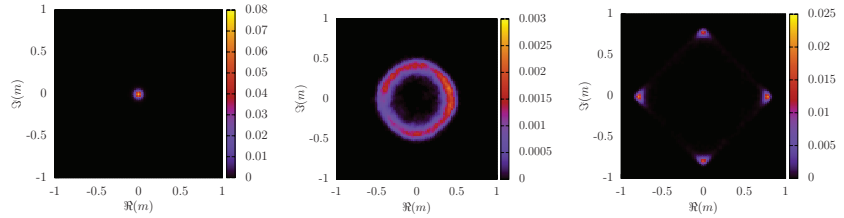

(b) Distribution of the order parameter m in the disordered phase.

(c) The rotationally symmetric order parameter distribution in the intermediate critical phase.

(d) Distribution of the order parameter in the long ranged ordered phase.

Figure 5.1: Inspecting the order parameter distribution in the complex plane reveals a clear distinction between the three phases of the noncompact Z_4 model. The color scale indicates relative density of the distribution.

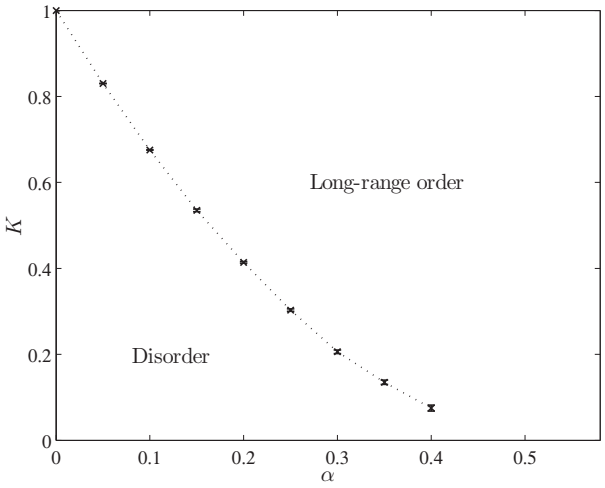

(a) The phase diagram of the compact Z_4 clock model with bond dissipation. In the space of spatial coupling K and dissipation strength α the model features a single transition line separating a disordered phase from a long ranged ordered phase.

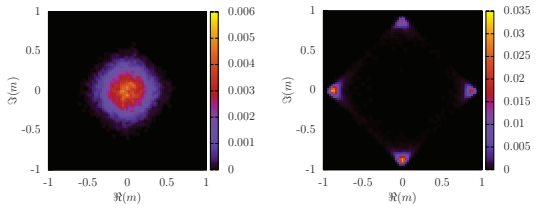

(b) Order parameter distribution in the disordered phase.

(c) Distribution of the order parameter in the ordered phase.

Figure 5.2: The order parameter distribution of the compact version of the clock model does not feature the rotational symmetric intermediate distribution.

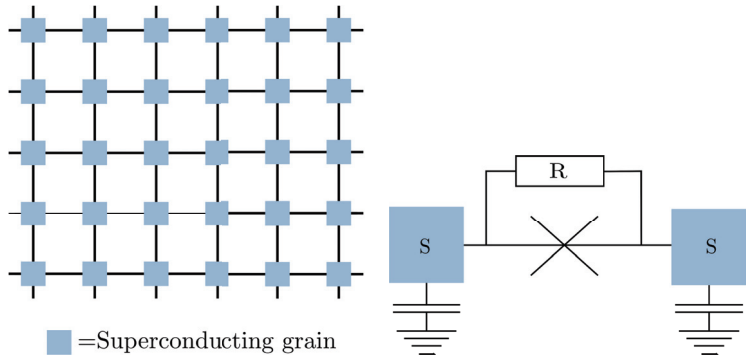

(a) A sketch of the two-dimensional lattice with a superconducting grain residing on each vertex.

(b) The action describes three interactions in the system: The capacitive coupling to ground, the Josephson tunnel junction and the shunting resistors.

Figure 5.3: A two-dimensional system of superconducting grains connected by Josephson tunnel junctions and shunting resistors.

lowed to take all real values $\theta \in \langle -\infty, \infty \rangle$[91]. The physical meaning behind this is that a sudden increment of a bond variable $\Delta\theta \rightarrow \Delta\theta + 2\pi$ describes a Cooper pair tunneling event between two neighboring grains. This tunneling will lead to a voltage imbalance over the barrier, leading to a dissipative, measurable current through the shunting resistors[91, 92]. Hence, the variables cannot be defined modulo 2π, since $\Delta\theta$ and $\Delta\theta + 2\pi$ represent physically distinguishable states.

Numerical work on dissipative Josephson junctions has mostly focused on a single junction where the only relevant variable is the phase difference between the two grains. The first Monte Carlo study of this system was presented in Ref. [93]. Considerable refined results on the same model were presented at a later stage in Ref. [88]. The numerical results confirmed the analytical result that the junction undergoes a superconductor-metal transition at a universal dissipation strength. This result originates with renormalization group arguments which may be found in Ref. [94].

In Paper IV we investigate a two-dimensional array of dissipative Josephson junctions. The physical system is made up of a two-dimensional cubic lattice with a superconducting grain residing at each grid point. Each superconducting grain is capacitively coupled to ground in addition to being coupled to its nearest neighbors by a Josephson potential and a shunting resistor. A sketch of such a system is given in Fig. 5.3.

In comparison with the single junction case we expect the added degrees of freedom associated with spatial fluctuations to be highly influential on the system behavior. This is in line with several papers that conjecture that the spatially extended junction system hosts (several) new phases[92, 95, 42, 96] in addition to the metallic and the superconducting phases.

The discretized action describing the array of quantum dissipative Josephson

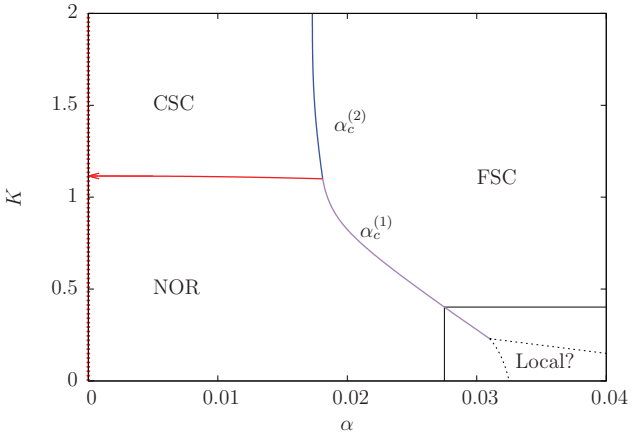

Figure 5.4: A schematic phase diagram in $K-\alpha$ space of the system defined by Eq. (5.13). NOR refers to the metallic normal phase with spatial and temporal disorder. In the CSC phase there is spatial quasi-long range order coinciding with temporal disorder. FSC refers to the fully bond-ordered superconducting phase with localized bond variables along imaginary time in addition to spatial stiffness. Refer to the text for further details. The red dotted line indicates that the limit $\alpha = 0$ is in principle ill-defined in this model. The presence of a finite dissipation term is essential for the decompatification of the variables. A hypothetical fourth, local phase was not observed in the simulations. The presence of such a phase could potentially facilitate a local quantum phase transition.

junctions reads[41]

$$S = \frac{K_\tau}{2}\sum_{\mathbf{x}}\sum_{\tau}^{N_\tau}(\theta_{\mathbf{x},\tau+1}-\theta_{\mathbf{x},\tau})^2 - K\sum_{\langle \mathbf{x},\mathbf{x}'\rangle}\sum_{\tau}^{N_\tau}\cos(\Delta\theta_{\mathbf{x},\mathbf{x}',\tau}) \qquad (5.13)$$
$$+\frac{\alpha}{2}\sum_{\langle \mathbf{x},\mathbf{x}'\rangle}\sum_{\tau\neq\tau'}\left(\frac{\pi}{N_\tau}\right)^2\frac{(\Delta\theta_{\mathbf{x},\mathbf{x}',\tau}-\Delta\theta_{\mathbf{x},\mathbf{x}',\tau'})^2}{\sin^2(\pi/N_\tau|\tau-\tau'|)}.$$

The three terms describe the capacitive coupling, the Josephson potential and the dissipation, respectively. As usual N_τ is the number of Trotter slices used to discretize the imaginary time and $\Delta\theta$ is the spatial lattice gradient.
By paying special attention to the anisotropy that exists between space and imaginary time we are able to conclude that the model features (at least) three distinct phases. In Fig. 5.4 we show a schematic phase diagram of the system in $K-\alpha$ space. Critical to the understanding of the nature of these phases is the reformulation of the noncompact variable θ according to $\theta \to \tilde{\theta} + 2\pi k$. The new field $\tilde{\theta}$ is compact (defined only on the primary interval $[-\pi,\pi\rangle$) and k is an integer-valued field keeping track of which 2π interval the original θ belonged to. Through this reformulation we may separate between the degrees of freedom relevant to spatial and temporal fluctuations.
The compact nature of the $\tilde{\theta}$-field enables the identification of spatial vortex excitations within the Trotter slices of the system. These excitations are iden-

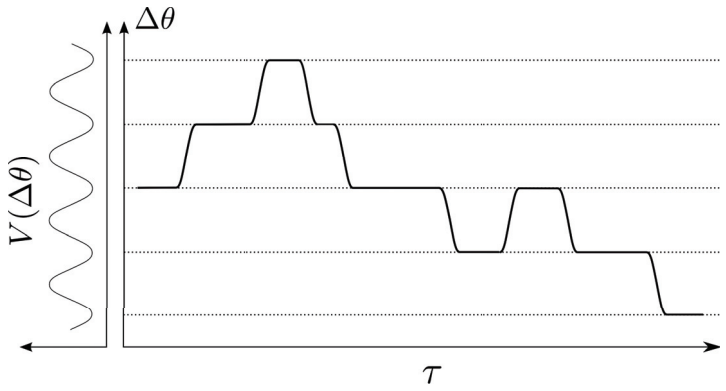

Figure 5.5: A sketch of $\Delta\theta(\tau)$ with several instantons and anti-instantons along the imaginary time direction. The plot along the left edge illustrates the extended Josephson potential and shows that the tunneling events take place between minima of the potential.

tified in the same way as the vortices discussed in Sec. 3.3. Onset of spatial order as measured by the helicity modulus may therefore be attributed to binding of vortices in the $\tilde{\theta}$-field. Additionally, we find that the degrees of freedom associated with the k-field describe instanton-like excitations in the temporal direction. Instantons are tunneling events of the bond variables, $\Delta\theta$, between minima of the extended Josephson potential. In terms of the k-field, this is a manifestation of the unbroken translational symmetry $\Delta k \to \Delta k + \Lambda$, where Λ is an integer.

In Fig. 5.5 we present a cartoon of $\Delta\theta(\tau)$ undergoing several tunneling events corresponding to instantons and anti-instantons. On the left side we indicate the Josephson potential in order to illustrate that $\Delta\theta(\tau)$ is located predominately in the vicinity of the minima except at the tunneling events.[3] Increasing dissipation will, at some critical value of α, suppress the tunneling events and trap $\Delta\theta(\tau)$ in one of the minima of the Josephson potential. To quantify this *localization transition* we use the mean squared displacement (MSD)

$$W^2_{\Delta\theta}(N_\tau) = \frac{1}{N_\tau}\left\langle \sum_\tau (\Delta\theta_\tau - \overline{\Delta\theta})^2 \right\rangle, \tag{5.14}$$

where $\overline{\Delta\theta} = (1/N_\tau)\sum_\tau \Delta\theta_\tau$. Fig. 5.6 shows a typical configuration of $\Delta\theta$ as a function of imaginary time in the critical superconducting (CSC) phase. As indicated in the figure $W_{\Delta\theta}$ is a measure of the characteristic deviation of $\Delta\theta$ from its mean value along the τ-direction. The localization of $\Delta\theta$ may be identified as the point where $W^2_{\Delta\theta}$ abruptly changes its scaling dependence on N_τ. Such a measure has been considered before[93, 88] in order to observe metal-superconductor transitions in a single junction. In these papers the superconducting state was associated with $W^2_{\Delta\theta}$ = constant while $W^2_{\Delta\theta}$ scales with N_τ in the metallic state. In the following, we will let $W^2_{\Delta\theta}$ = constant

[3] This is true as long as the Josephson coupling is relatively large.

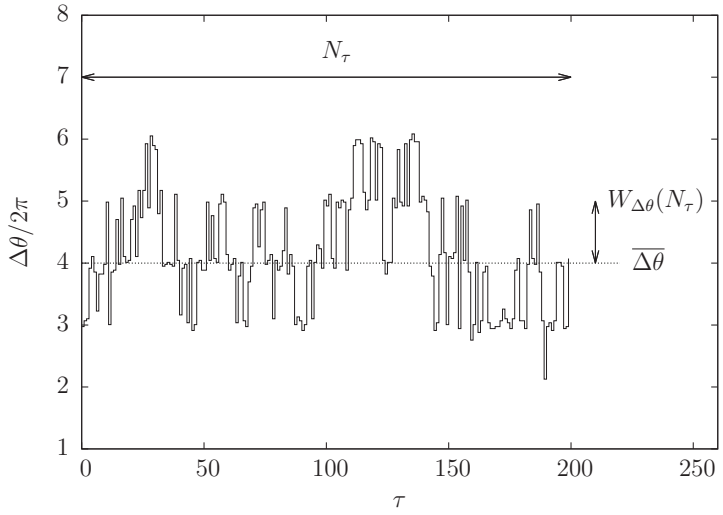

Figure 5.6: A plot of $\Delta\theta$ as a function of τ taken from the simulations in Paper IV. The mean squared displacement $W^2_{\Delta\theta}$ gives the characteristic squared deviation of $\Delta\theta$ from its mean value along imaginary time.

define temporal order, and conversely associate temporal disorder with $W^2_{\Delta\theta}$ diverging with N_τ. Spatial order and disorder are identified by $\Upsilon \neq 0$ and $\Upsilon = 0$, respectively.

In the phase diagram shown in Fig. 5.4 we find a normal phase (NOR) which is disordered in both space and time and a fully superconducting phase (FSC) which is ordered in space and time. Additionally, there is a critical superconducting phase (CSC) exhibiting finite helicity modulus and algebraically decaying spatial correlation functions. The transition between the NOR phase and the CSC phase is a purely spatial transition in the Berezinskii-Kosterlitz-Thouless universality class. The helicity modulus jumps discontinuously at the transition when the vortices in the $\tilde{\theta}$-field pair up. Inspecting the scaling behavior of $W^2_{\Delta\theta}$ in the NOR and CSC phases, we find no difference: The CSC phase is temporally disordered in exactly the same way as the normal phase. In both phases we find that $W^2_{\Delta\theta} \propto \ln N_\tau$. In this way, the ordering in space and the ordering in time are not necessarily coinciding.

Because the vortices are already tightly bound in the CSC phase, the transition from this phase into the fully superconducting phase (FSC) is mainly a temporal affair. The transition involves a suppression of instanton excitations and thereby a localization of $\Delta\theta$ into one of the potential minima. The character of the spatial order changes from quasi-long ranged to long-ranged as the localization transition couples the Trotter slices together along imaginary time. In this way the localization in imaginary time also affects the spatial fluctuations in a subtle way.

The phase transition from NOR to FSC is much more complicated than the two already considered. It appears to be a variant not previously considered in the context of superconductor-metal transitions. At the transition there is

concomitant binding of spatial vortices and a localization of $\Delta\theta$ along imaginary time upon entering the FSC phase from the NOR phase. The interplay between spatial point vortices and fluctuations in $\Delta\theta$ determines the character of the transition, but as thoroughly discussed in Paper IV, it is difficult to construct an order parameter that takes both spatial and temporal fluctuations into account. The compact magnetization measure $m = (1/V)\sum_{\mathbf{x},\tau} \exp[\mathrm{i}\theta_{\mathbf{x},\tau}]$ is only sensitive to fluctuations in the $\tilde{\theta}$-field and is completely oblivious to the state of the integer field k. Hence, the magnetization measure is not capable of describing the localization of $\Delta\theta$. Without a single order parameter that faithfully includes all relevant fluctuations the Binder analysis introduced in Sec. 4.6 is not useful. Consequently, we are unable to define a meaningful dynamical critical exponent z for this model.

5.3.1 Significance of the noncompactness on the orbital current model

The main motivation for this thesis is to study a model proposed to describe fluctuating loop currents in the copper-oxide sheets of cuprate superconductors. The specific form of the effective action intended to describe the loop-currents, Eq. (1.2), coincides with the action describing a two-dimensional array of spatially coupled, resistively shunted Josephson junctions (5.13). In this case θ no longer describes the angular direction of the loop current as indicated in Fig. 1.3, but gives the state of the order parameter phase at a given grain.
The resemblance between the models leads to a speculation whether the variables in Eq. (1.2) should be considered noncompact in a similar way as described in the previous section. The identical nonperiodic dissipation terms in Eq. (1.2) and Eq. (5.13), suggests to do so. On the other hand, considering θ as a variable parameterizing the angular state of the current loops suggests that a full rotation of the current pattern, $\theta \to \theta + 2\pi$, amounts to an identity operation. Following this line of thought, it is natural to argue that the variables should be treated as compact entities.
The results from Paper II, briefly introduced in Sec. 5.2, clearly show that the question of compactness is important. Defining the variables of the discrete clock model also outside the primary interval introduces a critical phase in addition to the fully ordered and the disordered phase. Although all phase transitions in this paper were spatio-temporally symmetric ($z = 1$) the results indicate that a decompactification of the variables has the potential of inducing novel physics. Consequently, it is important to compare the behavior of Eq. (1.2) with both compact and noncompact variables to look for the conjectured local quantum criticality in this model.
In Paper III we consider a compact version of Eq. (1.2) and show, both through Binder analysis and a direct inspection of correlation functions, that $z = 1$ at the only present phase transition line. In other words, the dissipation term is irrelevant in the renormalization group sense and the system undergoes a spatio-temporally isotropic transition in the 3D XY universality class. This result conforms well with naive scaling estimates. More importantly, the result indicates that the local quantum criticality ($z \to \infty$) predicted for this model[24]

does *not* occur with compact variables.
The compact model features two phases, a disordered phase with proliferated vortex-loops[97] and a phase with spontaneously broken $U(1)$ symmetry. Defining θ also outside the primary interval like in Sec. 5.3 and in Paper IV we observe much richer physics. The decompactification introduces instanton-like defects into the system, these defects may exist unpaired even in the presence of bound vortices. Increasing the dissipation strength from the CSC phase where this scenario is realized, the system undergoes a transition involving a localization of $\Delta\theta$ along imaginary time. Superficially, this might appear as a variant of local quantum criticality as it corresponds to a condensation of instantons from a state where the spatial defects are already tightly bound. This is, however, not the case. The boundedness of the vortices in the effectively decoupled Trotter slices corresponds to the strong coupling phase of the 2D XY model. The condensation of instantons thus occurs in a background of two-dimensional spatial spin waves, or in other words, fluctuations with infinite correlation length.
Considering all permutations of the two ordering variants, one could also imagine an additional fourth phase in the noncompact scenario. This phase would be characterized by having localized $\Delta\theta$ and proliferated vortices. The transition from the NOR phase into this putative local phase may be regarded as a purely temporal ordering coinciding with short-ranged spatial correlations. Due to this locality, such a transition could possibly be interpreted as a local quantum critical point ("$z = \infty$"). The most likely position of such a phase is at large dissipation strength and weak spatial coupling, corresponding to the lower right corner of Fig. 5.4. The simulations did not show any signs of such a fourth phase, and it therefore appears that the noncompact model does not feature local quantum criticality. However, since we are not able to perform a finite size scaling analysis in this case, this conclusion is not as well founded as the similar conclusion for the compact model.

5.4 Spin chains with non-ohmic dissipation

The spin-boson model in its most simple form describes a two-state system coupled to an infinite number of harmonic oscillators. Generalizations of this model are abundant in various branches of physics. The reader is referred to Refs. [98] and [80] for more comprehensive introductions to the model. In Paper V we consider a spatially extended variant of this model where each spin interacts with its spatial neighbors. Specifically, we consider a one-dimensional spin chain of length L in which each single spin couples to a private bath of oscillators with spectral density of the form $J(\omega) \propto \omega^s$. The model is also generalized in the sense that the Z_2 symmetry of the Ising spins in the original formulation of the model is replaced by higher symmetries. More particularly, we perform a comparative study of an Ising like Z_4 symmetry and a $U(1)$

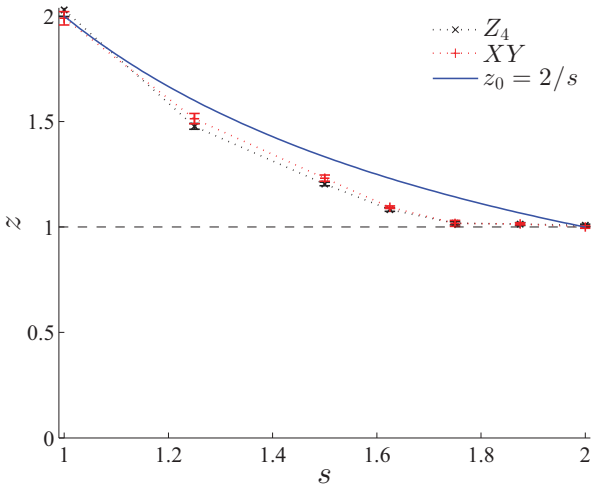

Figure 5.7: Dynamical critical exponent z as a function of s for both the Z_4 and the XY symmetry. The naive scaling estimate z_0, shown in blue, does not coincide with the calculated z for non-integer values of s.

symmetry. The discretized action describing the system reads

$$S = -K \sum_{\langle \mathbf{x},\mathbf{x}' \rangle} \sum_{\tau}^{L_\tau} \cos(\theta_{\mathbf{x},\tau} - \theta_{\mathbf{x}',\tau}) - K_\tau \sum_{\mathbf{x}}^{L} \sum_{\tau}^{L_\tau} \cos(\theta_{\mathbf{x},\tau+1} - \theta_{\mathbf{x},\tau}) \qquad (5.15)$$
$$-\frac{\alpha}{2} \sum_{\mathbf{x}}^{L} \sum_{\tau \neq \tau'} \left(\frac{\pi}{L_\tau} \right)^{1+s} \frac{\cos(\theta_{\mathbf{x},\tau} - \theta_{\mathbf{x},\tau'})}{\sin^{1+s}(\frac{\pi}{L_\tau}|\tau - \tau'|)},$$

where the angular brackets indicate a sum over nearest neighbors. We consider super-ohmic dissipation $1 \leq s \leq 2$ which has not received much attention in the literature. By varying the decay exponent s we are able to tune the effective dimensionality ($d_{\text{eff}} = d + z$) of the system and investigate the evolution of the critical exponents.

With a non-ohmic, onsite dissipation term the naive scaling estimate for the dynamical critical exponent is given by $z_0 = 2/s$. This results is exact for systems above the upper critical dimension ($d_{\text{eff}} > 4 = d_c^u$), but deviations may appear when the effective dimensionality is reduced below d_c^u. In Fig. 5.7 we show the evolution of z as a function of s. The calculated values decay notably faster than the blue curve which indicates the naive scaling estimate. As indicated by Fig. 2 in Paper V this discrepancy can not be accounted for by considering the scaling relation $z = z_0 - \eta$ which is known to be valid in the $s = 1$ limit[99]. Instead we find that the evolution of z may be described by the scaling relation

$$z = \max\left\{ \frac{2-\eta}{s}, 1 \right\}. \qquad (5.16)$$

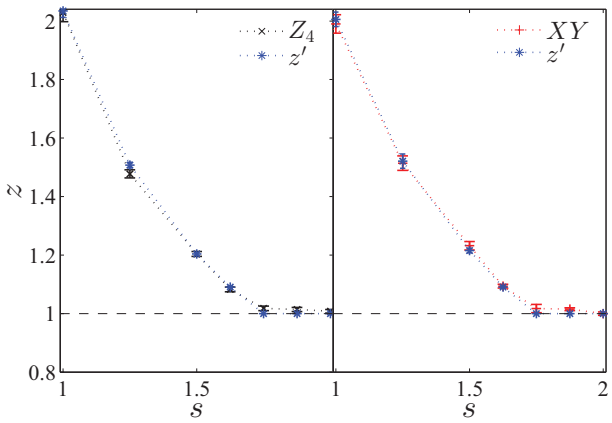

Figure 5.8: Dynamical critical exponent z as in Fig. 5.7, but compared with the scaling estimate $z' = (2-\eta)/s$. The values of η used in the scaling estimates are the same as reported in Fig. 2 in Paper V. The left panel correponds to the Z_4 model and the right panel to the XY model.

In Fig. 5.8 we show the same data for z as shown in Fig. 5.7, but compared with the Ansatz (5.16) instead of the naive scaling estimate z_0. Although there might still be some corrections to the finite size scaling, Eq. (5.16) seems to fit the data quite well.

Two additional features should be noted from Fig. 5.7. Firstly, the values of z calculated for the two different order parameter symmetries appear identical within statistical uncertainty.[4] Secondly, Fig. 5.7 suggests that z approaches unity for values $s < 2$, while naive scaling estimates would predict the dissipation to be irrelevant at $s = 2$. Although the dissipation term is highly anisotropic, the result conforms well with a previous analysis of classical models with isotropic long-ranged interactions on the form $1/r^{1+s}$[100]. In this work it was found that the system presents critical exponents similar to the corresponding short-range model already when s exceeds a value $s^* = 2 - \eta_{\mathrm{SR}}$. Here, η_{SR} denotes the anomalous dimension in the short-range model. In this way, s^* separates the basin of attraction corresponding to the fixed point with dissipation dominated criticality ($z \neq 1$) from the basin of attraction of the fixed point with Lorentz invariant ($z = 1$) criticality.

Since $\eta_{\mathrm{SR}} = 0.25$ in the limit $d_{\mathrm{eff}} \to 2$ for both the order parameter symmetries considered in Paper V, one might expect that $s^* = 1.75$. Because of the exceedingly slow crossover to asymptotic exponent values in the finite size scaling in this regime, we have not been able to firmly establish the exact value of s^*.

[4] The similarity between the Z_4 symmetry and the $U(1)$ symmetry is also seen in the evolution of η and the exponent combinations β/ν and γ/ν. In Sec. III E in Paper V we argue that the similarities between Z_4 and $U(1)$ are most likely a coincidence.

Chapter 6

Final remarks

The basic motivation and starting point of this thesis was to numerically investigate a model of putative fluctuating loop currents within the copper-oxide sheets of high-T_c cuprate superconductors. It is claimed that the model features a local quantum critical point: A phase transition at $T = 0$ with algebraically decaying correlation function in imaginary time, coinciding with vanishing spatial correlations. Such correlations are necessary for the loop current scenario to provide a microscopic foundation for the Marginal Fermi liquid behavior in the strange metal phase. We have also considered some less involved models to answer questions related to extended dissipative quantum systems in general.
In all papers in this thesis we introduce dissipation of the Caldeira-Leggett form to various systems and investigate how this effects the phase structure and critical properties. The dissipation comes about by coupling single degrees of freedom in the system to their own private baths of oscillators. One might argue that in order for the model to describe physical systems, these baths should also be coupled to each other, either directly, or indirectly via coupling through other spins. Some have reasoned that such local coupling to a bosonic bath introduces an intrinsic locality in the system, ultimately implying local quantum criticality[55]. From the results in this thesis and in Ref. [55], it is clear that this is not the case. Considering systems with a well defined order parameter and oscillator baths with ohmic spectral densities, we find that bond dissipation have a spatio-temporal isotropic ($z = 1$) transition. Corresponding systems with site dissipation have a slightly more anisotropic $z = 2$ transition. In both cases, however, the spatial correlation length diverges at criticality.
One may also debate whether the Caldeira-Leggett term (1.5) is an adequate way of describing dissipative effects in the context of loop currents. Starting from a more fundamental fermionic theory, a dissipation term differing from the Caldeira-Leggett form has been calculated. In this case dissipation arises from scattering of a loop-current order parameter off gapless particle-hole excitations at the Fermi level. The result is a non-local Landau damping kernel of the form $|\omega|/|\mathbf{q}|$[35, 101]. Needless to say, one might expect such a term and (1.5) to generate physics with essential differences.
The decompactification of the variables considered in Papers II and IV is a far more violent perturbation of the system than the mere presence of anisotropic

long ranged interactions. This is reflected by the appearance of a novel critical phase in both these papers.[1] The difference between compact and noncompact variables is particularly pronounced in the $(2+1)$-dimensional version of Eq. (1.2) with continuous symmetry. In this case completely different ordering effects are present when the phases are noncompact (instantons and spatial point vortices) compared with the more "standard" vortex loop proliferation in the compact case. As we discuss thoroughly in Paper IV it is not clear how an order parameter that faithfully describes all fluctuations of the system should be constructed in this case.[2]

At the very heart of the Marginal Fermi Liquid theory is the requirement that the correlations of the fluctuating loop currents at the quantum critical point should be local in space while algebraically decaying in imaginary time. We have not been able to directly observe such locality in any simulations on varieties of Eq. (1.2). Although it must be emphasized that due to the lack of an order parameter we have not performed any quantitative analysis of the transitions in Paper IV. In this paper we argue that in order for the system to present a local phase transition in the sense of a condensation of instantons without a divergent spatial correlation length, an additional local phase should have be present. However, there are arguments that the transition line separating the normal phase from the fully superconducting phase (NOR–FSC line in Fig. 5.4) presents a novel form of criticality where proliferation of instantons single-handedly drives the transition and space disorders as a "parasitic" effect[102]. In this way the system may disorder without producing a divergent spatial correlation length at criticality. The results presented in Paper IV contradicts this scenario in two ways. First of all, the phase transition separating the fully superconducting phase and the critical superconducting phase involves only proliferation of instantons. Hence, the unbinding of instantons does not necessarily affect the binding of spatial vortex defects. Secondly, a direct calculation of the spatial two-point correlation function in close proximity to the NOR–FSC line indicates that the transition is not local.

[1] These phases are fundamentally different and arise from from completely different mechanisms.

[2] It is also a possibility that no such order parameter exists.

Bibliography

[1] H. Kammerlingh-Onnes, Comm. Phys. Lab. Univ. Leiden (1911).

[2] J. Bardeen, L. N. Cooper, and J. R. Schrieffer, Phys. Rev. **108**, 1175 (1957).

[3] J. D. Patterson and B. C. Bailey, *Solid-State Physics (Introduction to the Theory)* (Springer, 2007).

[4] Bednorz and Müller, Zeitschrift für Physik **64**, 189 (1986).

[5] A. Sudbø and K. Fossheim, *Superconductivity, Physics and Applications* (Wiley, 2004).

[6] J. R. Waldram, *Superconductivity of Metals and Cuprates* (Institute of Physics Publishing, 1996).

[7] A. J. Leggett, Nature **2**, 134 (2006).

[8] S. Maekawa *et al*, *Physics of Transition Metal Oxides* (Springer, 2004).

[9] E. Abramhams, Journal of the Korean Physical Society **29** (1996).

[10] C. M. Varma, P. B. Littlewood, S. Schmitt-Rink, E. Abrahams, and A. E. Ruckenstein, Phys. Rev. Lett. **63**, 1996 (1989).

[11] T. Timusk and B. Statt, Rep. Prog. Phys. **62**, 61 (1998).

[12] O. Fischer, M. Kugler, I. Maggio-Aprile, C. Berthod, and C. Renner, Rev. Mod. Phys. **79**, 353 (2007).

[13] I. M. Vishik *et al.*, New Journal of Physics **12**, 105008 (2010).

[14] T. Yoshida, M. Hashimoto, I. M. Vishik, Z.-X. Shen, and A. Fujimori, Journal of the Physical Society of Japan **81**, 011006 (2012).

[15] C. M. Varma and B. Batlogg, Physics world , 33 (2000).

[16] W. S. Lee *et al.*, Nature **450**, 81 (2007).

[17] B. Fauque *et al.*, Phys. Rev. Lett. **96**, 197001 (2006).

[18] C. M. Varma, Phys. Rev. B **73**, 155113 (2006).

[19] P. A. Lee, N. Nagaosa, and X.-G. Wen, Rev. Mod. Phys. **78**, 17 (2006).

[20] S. Chakravarty, R. B. Laughlin, D. K. Morr, and C. Nayak, Phys. Rev. B **63**, 094503 (2001).

[21] C. M. Varma, Phys. Rev. Lett. **83**, 3538 (1999).

[22] C. M. Varma, Phys. Rev. B **55**, 14554 (1997).

[23] S. Sachdev, *Quantum Phase Transitions* (Cambridge University Press, 1999).

[24] V. Aji and C. M. Varma, Phys. Rev. Lett. **99** (2007).

[25] V. Aji and C. M. Varma, Phys. Rev. B **79**, 184501 (2009).

[26] H. A. Mook *et al.*, Phys. Rev. B **69**, 134509 (2004).

[27] V. Balédent *et al.*, Phys. Rev. Lett. **105**, 027004 (2010).

[28] Y. Li *et al.*, Nature **468**, 283 (2010).

[29] R.-H. He *et al.*, Science **331**, 1579 (2011).

[30] A. Kaminski *et al.*, Nature **416** (2002).

[31] J. E. Sonier *et al.*, Phys. Rev. Lett. **103**, 167002 (2009).

[32] S. Strässle, B. Graneli, M. Mali, J. Roos, and H. Keller, Phys. Rev. Lett. **106**, 097003 (2011).

[33] S. V. Borisenko *et al.*, Phys. Rev. Lett. **92**, 207001 (2004).

[34] G. J. MacDougall *et al.*, Phys. Rev. Lett. **101**, 017001 (2008).

[35] K. Børkje and A. Sudbø, Phys. Rev. B **77** (2008).

[36] J. Ashkin and E. Teller, Phys. Rev. **64**, 178 (1943).

[37] M. S. Grønsleth *et al.*, Phys. Rev. B **79**, 094506 (2009).

[38] V. Aji and C. M. Varma, Phys. Rev. B **82**, 174501 (2010).

[39] A. O. Caldeira and A. J. Leggett, Ann. Phys. (NY) **149**, 374 (1983).

[40] S. Tewari, J. Toner, and S. Chakravarty, Phys. Rev. B **73**, 064503 (2006).

[41] S. Chakravarty, G.-L. Ingold, S. Kivelson, and G. Zimanyi, Phys. Rev. B **37**, 3283 (1988).

[42] P. A. Bobbert, R. Fazio, G. Schön, and A. D. Zaikin, Phys. Rev. B **45**, 2294 (1992).

[43] R. Fazio and H. van der Zant, Phys. Rep. **355**, 235 (2001).

[44] L. Capriotti, A. Cuccoli, A. Fubini, V. Tognetti, and R. Vaia, Phys. Rev. Lett. **94**, 157001 (2005).

[45] T. Vojta, Reviews in Computational Chemistry **26**, 167 (2008).

[46] N. Goldenfeld, *Lectures on Phase Transitions and the Renormalization Group* (Addison Wesley, 1992).

[47] B. Widom, J. Chem. Phys. **43**, 3892 (1963).

[48] B. Widom, J. Chem. Phys. **43**, 3898 (1963).

[49] J. W. Negele and H. Orland, *Quantum Many Particle Systems* (Westview Press, 1995).

[50] A. Altland and B. Simons, *Condensed Matter Field Theory* (Cambridge, 2006).

[51] J. A. Hertz, Phys. Rev. B **14**, 1165 (1976).

[52] Q. Si, S. Rabello, K. Ingersent, and J. L. Smith, Nature **413**, 804 (2001).

[53] Q. Si and F. Steglich, Science **329**, 1161 (2010).

[54] R. Sknepnek, T. Vojta, and M. Vojta, Phys. Rev. Lett. **93**, 097201 (2004).

[55] P. Werner, *Dissipative Quantum Phase Transitions*, PhD thesis, ETH Zürich, 2005.

[56] G.-L. Ingold, Path integrals and their application to dissipative quantum systems, in *Coherent Evolution in Noisy Environments*, edited by A. Buchleitner and K. Hornberger, , Lecture Notes in Physics Vol. 611, pp. 1–53, Springer Berlin / Heidelberg, 2002.

[57] E. Ising, Z. Physik **31**, 253 (1925).

[58] L. Onsager, Phys. Rev. **65**, 117 (1944).

[59] N. D. Mermin and H. Wagner, Phys. Rev. Lett. **17**, 1133 (1966).

[60] J. M. Kosterlitz and D. J. Thouless, J. Phys. C: Solid State Phys. **6**, 1181 (1973).

[61] H. Weber and P. Minnhagen, Phys. Rev. B **37**, 5986 (1988).

[62] R. B. Potts, Mathematical Proceedings of the Cambridge Philosophical Society **48**, 106 (1952).

[63] S. Elitzur, R. B. Pearson, and J. Shigemitsu, Phys. Rev. D **19**, 3698 (1979).

[64] C. M. Lapilli, P. Pfeifer, and C. Wexler, Phys. Rev. Lett. **96**, 140603 (2006).

[65] J. J. Binney, N. J. Dowrick, A. J. Fisher, and M. E. J. Newman, *The Theory of Critical Phenomena (An Introduction to the Renormalization Group)* (Oxford, 1992).

[66] U. Wolff, Phys. Rev. Lett. **62**, 361 (1989).

[67] G. T. Barkema and M. E. J. Newman, Monte Carlo methods in chemical physics, in *New Monte Carlo Algorithms for Classical Spin Systems*, edited by D. Ferguson, J. I. Siepmann, and T. D. G., Wiley, New York, 1997.

[68] P. Werner and M. Troyer, Progress of Theoretical Physics Supplement **160**, 395 (2005).

[69] E. Luijten and H. W. J. Blöte, Int. J. Mod. Phys. C **6**, 359 (1995).

[70] E. Luijten, Monte Carlo simulation of spin models with long-range interactions, in *Computer Simulation Studies in Condensed Matter Physics XII*, edited by D. P. Landau, S. P. Lewis, and H. B. Schuettler, Springer, Heidelberg, 1999.

[71] K. Hukushima and K. Nemoto, J. Phys. Soc. Jpn. **65**, 1604 (1996).

[72] K. Hukushima, Phys. Rev. E **60**, 3606 (1999).

[73] B. Efron, Ann. Statist. **7**, 1 (1979).

[74] B. Efron, SIAM review **21**, 460 (1979).

[75] B. Efron, *The Jackknife, the Bootstrap and Other Resampling Plans* (Society for Industrial and Applied Mathematics, 1982).

[76] A. M. Ferrenberg and R. H. Swendsen, Phys. Rev. Lett. **63** (1989).

[77] S. Sachdev, Physics Today **64**, 29 (2011).

[78] K. Völker, Phys. Rev. B **58**, 1862 (1998).

[79] S. Chakravarty, Phys. Rev. Lett. **49**, 681 (1982).

[80] U. Weiss, *Quantum Dissipative Systems* (World Scientific, 2008).

[81] P. Werner, K. Völker, M. Troyer, and S. Chakravarty, Phys. Rev. Lett. **94**, 047201 (2005).

[82] M. Suzuki, Progress of Theoretical Physics **56**, 1454 (1976).

[83] A. F. Brito, J. A. Redinz, and J. A. Plascak, Phys. Rev. B **81**, 031130 (2010).

[84] S. K. Baek and P. Minnhagen, Phys. Rev. E **82**, 031102 (2010).

[85] S. K. Baek, P. Minnhagen, and B. J. Kim, Phys. Rev. E **80**, 060101(R) (2009).

[86] S. A. Bulgadaev, JETP Lett. **39**, 315 (1984).

[87] A. Schmid, Phys. Rev. Lett. **51**, 1506 (1983).

[88] P. Werner and M. Troyer, Phys. Rev. Lett. **95**, 060201 (2005).

[89] P. Werner and M. Troyer, Cluster Monte Carlo algorithms for dissipative quantum phase transitions, in *Understanding Quantum Phase Transitions*, edited by L. D. Carr, Taylor & Francis, Boca Raton, 2010.

[90] B. Josephson, Physics Letters **1**, 251 (1962).

[91] G. Schön and A. Zaikin, Phys. Rep. **198**, 237 (1990).

[92] S. V. Panyukov and A. D. Zaikin, J. Low Temp. Phys. **75**, 361 (1989).

[93] C. P. Herrero and A. D. Zaikin, Phys. Rev. B **65**, 104516 (2002).

[94] N. Nagaosa, *Quantum Field Theory in Condensed Matter Physics* (Springer, 1995).

[95] G. Refael, E. Demler, Y. Oreg, and D. S. Fisher, Phys. Rev. B **75**, 014522 (2007).

[96] P. Goswami and S. Chakravarty, Phys. Rev. B **73**, 094516 (2006).

[97] A. K. Nguyen and A. Sudbø, Phys. Rev. B **60**, 15307 (1999).

[98] K. Le Hur, Quantum phase transitions in spin-boson systems: Dissipation and light phenomena, in *Understanding Quantum Phase Transitions*, edited by L. D. Carr, Taylor & Francis, Boca Raton, 2010.

[99] S. Pankov, S. Florens, A. Georges, G. Kotliar, and S. Sachdev, Phys. Rev. B **69**, 054426 (2004).

[100] E. Luijten and H. W. J. Blöte, Phys. Rev. Lett. **89**, 025703 (2002).

[101] K. Børkje, *Theoretical Studies of Unconventional Order in Quantum Many-Particle Systems*, PhD thesis, NTNU, 2008.

[102] C. Varma and V. Aji, Private communication.

Paper I

Monte Carlo simulations of dissipative quantum Ising models.

Phys. Rev. B **81**, 104302 (2010).

PHYSICAL REVIEW B **81**, 104302 (2010)

Monte Carlo simulations of dissipative quantum Ising models

Iver Bakken Sperstad, Einar B. Stiansen, and Asle Sudbø
Department of Physics, Norwegian University of Science and Technology, N-7491 Trondheim, Norway
(Received 8 February 2010; published 16 March 2010)

The dynamical critical exponent z is a fundamental quantity in characterizing quantum criticality, and it is well-known that the presence of dissipation in a quantum model has significant impact on the value of z. Studying quantum Ising spin models using Monte Carlo methods, we estimate the dynamical critical exponent z and the correlation length exponent ν for different forms of dissipation. For a two-dimensional quantum Ising model with Ohmic site dissipation, we find $z \approx 2$ as for the corresponding one-dimensional case, whereas for a one-dimensional quantum Ising model with Ohmic bond dissipation, we obtain the estimate $z \approx 1$.

DOI: 10.1103/PhysRevB.81.104302 PACS number(s): 75.10.Hk, 64.60.De, 05.50.+q

I. INTRODUCTION

Conventionally, quantum criticality can be described by a quantum-to-classical mapping,[1] whereby a d-dimensional quantum model is represented by a $(d+1)$-dimensional classical model in which the extra dimension corresponds to imaginary time, τ. It is well-known since the work of Hertz[2] that this temporal dimension and the spatial dimensions do not necessarily appear on an equal footing. In the presence of dissipative terms in the action, for instance, long-range interactions are introduced in the imaginary time direction,[3,4] making the model behave as if it were $(d+z)$-dimensional rather than $(d+1)$-dimensional. The dynamical critical exponent z can be regarded as a measure of the anisotropy between the temporal dimension and the spatial dimensions, as defined by the scaling of the temporal correlation length, $\xi_\tau \sim \xi^z$. Here, $\xi \sim |K-K_c|^{-\nu}$ is the spatial correlation length upon approaching a quantum critical point $K=K_c$, with K being some arbitrary (nonthermal) coupling constant. Knowing the value of z is therefore of fundamental importance in the study of quantum phase transitions, especially since this critical exponent determines the appearance of the quantum critical regime at finite temperatures above the quantum critical point.[5,6] Such quantum critical points with an accompanying quantum critical region have been suggested to be responsible, for instance, for the anomalous behavior of the normal phase of high-T_c cuprate superconductors.[7,8]

To illustrate the effect of dissipation on the dynamical critical exponent, consider first a generic ϕ^4-type nondissipative quantum field theory. The bare inverse propagator can be obtained from the quadratic part of the action as $\mathbf{q}^2+\omega^2$, meaning that one has isotropic scaling between the spatial dimensions and the temporal dimension, i.e., $z=1$. Adding local Ohmic dissipation by coupling each spin to a bath of harmonic oscillators,[3] the inverse propagator is modified to $\mathbf{q}^2+\omega^2+|\omega|$. Assuming a phase transition to an ordered state and taking the limit $\mathbf{q}\to\mathbf{0}$, $\omega\to 0$, the dissipative term $|\omega|$ will always dominate over the dynamic term ω^2, and so, by using $\omega \sim q^z$, we may naively make the prediction $z=2$. Note that according to this argument, the dynamical critical exponent for a given action is independent of the spatial dimensionality of the system. We will refer to these scaling arguments as naive scaling, and postpone any discussion of caveats and other possible scaling choices to Sec. IV.

If one replaces this Ohmic site dissipation with dissipation that also couples in space and not just in time, this situation may change significantly. A common form of dissipation in the context of arrays of resistively shunted Josephson junctions and related models, is the Ohmic dissipation of gradients, i.e., of the bond variable that is the difference of the quantum phase between the superconducting elements.[9] In Fourier space, this bond dissipation corresponds to an inverse propagator $\mathbf{q}^2+\omega^2+\mathbf{q}^2|\omega|$. (See, however, Sec. IV.) Once again letting $\mathbf{q}\to\mathbf{0}$, $\omega\to 0$, we can from naive scaling expect the dissipation to be weaker than in the onsite case since in this limit $\mathbf{q}^2|\omega| \ll \mathbf{q}^2$ for any positive z. A possible value is therefore $z=1$, for which the spatial term balances the dynamic term and dissipation can be considered perturbatively irrelevant in renormalization group sense.

Simple arguments of the kind given above have been the approach most commonly used whenever a dynamical critical exponent is to be determined. In recent years there has however been progress toward calculating the corrections to these lowest-order estimates for z both by field-theoretical renormalization group methods[10–12] and by Monte Carlo methods.[12–15] In addition, there has also been considerable recent interest in dissipative systems exhibiting more exotic forms of quantum criticality where the critical exponents are varying continuously.[16–18]

The most notable advance from our point of view is, however, the work by Werner *et al.*[13] justifying numerically the naive scaling estimate for the Ising spin chain with site dissipation by extensive Monte Carlo simulations. More precisely, it was found that the dynamical critical exponent was universal and satisfied $z=2-\eta$, with an anomalous scaling dimension $\eta \approx 0.015$. Apart from Ref. 13, almost no Monte Carlo simulations have been performed on extended quantum dissipative models. (See, however, Refs. 15 and 19 for reviews of Monte Carlo simulation for dissipative systems and quantum phase transitions.) The present work can therefore be regarded as a natural extension of the work done by Werner *et al.*, but more importantly as a first step toward more complex dissipative quantum models with bond dissipation. For instance, the dissipative XY model with bond dissipation is very interesting both as a model of granular superconductors or other systems which may be modeled as Josephson junction arrays.[9] In particular, such a dissipative XY model[20] and related Ashkin-Teller models[21,22] have been proposed to describe quantum critical fluctuations of loop-current order in cuprate superconductors.

Finding a value of z is also of considerable interest for purely classical models that include strongly anisotropic interactions. The reason is simply that performing a finite-size analysis to find the critical coupling or critical exponents requires a choice of system sizes that reflects an anisotropy in the scaling of the correlation lengths. In other words, one ideally needs to know the relative correlation length exponent $\nu_\tau/\nu = z$ *a priori* for the finite-size analysis to be correct.

In this work, we seek to employ Monte Carlo simulations of Ising models to answer the following questions: (1) can we confirm numerically that the dynamical critical exponent is indeed independent of dimensionality? (Neglecting the assumed small η) (2) how will the dynamical critical exponent for Ising variables change if one replaces the site dissipation with dissipation that also acts in space? The first question will be addressed in Sec. II, where we study the two-dimensional (2D) quantum Ising model with site dissipation. In Sec. III, we turn to the second question by studying a one-dimensional (1D) quantum Ising chain with bond dissipation in a similar manner. The results will be related to the naive scaling arguments for z, after which we conclude in Sec. V.

II. 2D QUANTUM ISING MODEL WITH SITE DISSIPATION

We first consider a quantum Ising spin model in two spatial dimensions coupled to a bath of harmonic oscillators,[3] i.e., a higher-dimensional version of the model considered in Ref. 13. In Fourier space, the quadratic part of the action for this model can be written as

$$S = \sum_{\mathbf{q}} \sum_{\omega} \left(\tilde{K}\mathbf{q}^2 + \tilde{K}_\tau \omega^2 + \frac{\alpha}{2}|\omega| \right) \sigma_{\mathbf{q},\omega}\sigma_{-\mathbf{q},-\omega}, \tag{1}$$

where σ is the Ising field. The discretized real space representation on a $L \times L \times L_\tau$-lattice then reads

$$\begin{aligned} S = &- K \sum_{x=1}^{L} \sum_{y=1}^{L} \sum_{\tau=1}^{L_\tau} [\sigma_{x,y,\tau}\sigma_{x+1,y,\tau} + \sigma_{x,y,\tau}\sigma_{x,y+1,\tau}] \\ &- K_\tau \sum_{x=1}^{L} \sum_{y=1}^{L} \sum_{\tau=1}^{L_\tau} \sigma_{x,y,\tau}\sigma_{x,y,\tau+1} \\ &+ \frac{\alpha}{4} \sum_{x=1}^{L} \sum_{y=1}^{L} \sum_{\tau \neq \tau'}^{L_\tau} \left(\frac{\pi}{L_\tau} \right)^2 \frac{(\sigma_{x,y,\tau} - \sigma_{x,y,\tau'})^2}{\sin^2(\pi/L_\tau|\tau - \tau'|)}. \end{aligned} \tag{2}$$

We have assumed a spatially isotropic system, so that $K_x = K_y = K$. Periodic boundary conditions are implicit in the imaginary time direction and are also applied for the spatial directions. Note that our representation is equivalent to that of Ref. 13, although superficially appearing slightly different.

We could, as Werner *et al.*, take a quantum Ising model in a transverse magnetic field as a starting point, and the field would then give rise to the quantum dynamics of the spins as represented by the second line in the action in Eq. (2). However, in this work we are not interested in the effect of a transverse field per se, and will therefore treat the dynamic term as a phenomenological term of unspecified origin. (See, however, Sec. IV). In the following, we will fix the value of the dynamic coupling of the Ising field to $K_\tau = -1/2 \ln(\tanh 1) \approx 0.1362$ and vary the spatial coupling K. For the $(1+1)$-dimensional model,[13] this choice ensures that $K_c = 1$ for $\alpha = 0$, whereas in the $d = 2$ case it is chosen primarily for computational convenience, and to allow for direct comparison with the $d = 1$ case. For the Monte Carlo simulations, we have used an extension of the Wolff cluster algorithm[23] by Luijten and Blöte,[24] which very effectively treats the long-range interaction in the imaginary time direction. We have mainly used an implementation of the Mersenne Twister[25] random number generator (RNG), but also confirmed that other RNGs yielded consistent result. We also make use of Ferrenberg-Swendsen[26] reweighting techniques which enable us to vary K continuously after the simulations have been performed.

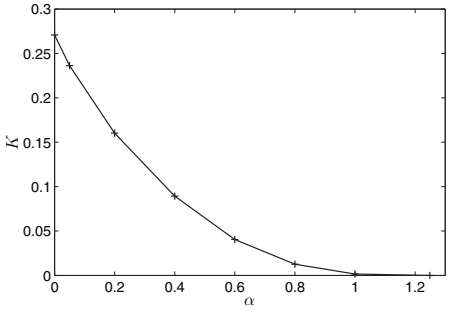

FIG. 1. Phase diagram for the 2D quantum Ising model with site dissipation for $K_\tau = -1/2 \ln(\tanh 1)$. The ordered phase is found for large values of spatial coupling K and dissipation strength α.

We will first present the phase diagram for this model in the α-K plane, as shown in Fig. 1. The phase diagram for the $(2+1)$-dimensional model is very similar to that for its $(1+1)$-dimensional counterpart, with a disorder-order phase transition for increasing dissipation and/or spatial coupling. Along the α-axis, a temporally ordered state is reached at $\alpha = \alpha_c$ through a purely dissipative phase transition when $K = 0$, in which case the model is simply a collection of decoupled $(0+1)$-dimensional dissipative two-level systems. The long-range interaction in the temporal chains decays as $1/|\tau_i - \tau_j|^2$, accordingly, the phase transition is of a kind closely related to the Kosterlitz-Thouless transition,[27] in which the ordered phase consists of tightly bound kinks and antikinks.

With the same temporal coupling values as for the $d = 1$ case, we can with relative ease determine the critical dissipation strength α_c for the independent subsystems, see the result stated in Ref. 13.

We have chosen a somewhat more quantitative approach to determine the dynamical critical exponent z than the one given in the presentation of Werner *et al.*, so we will use the exposition of our results to detail the method. This method is essentially the same as the one applied by the authors of Refs. 28 and 29 for spin glasses in a transverse field, but as it is rather scantily described in the literature, we include it here for completeness.

The basis of our approach is as follows. For systems with isotropic scaling, a well-known method to determine the

value of the critical coupling is to calculate the Binder ratio

$$Q = \frac{\langle m^4 \rangle}{\langle m^2 \rangle^2}, \tag{3}$$

and use this to plot the Binder cumulant $g \equiv 1 - Q/3$ as a function of coupling for several (e.g., cubic, in the $(2+1)$-dimensional case) system sizes. The Binder cumulant at the critical coupling is independent of system size (to leading order in L), and the crossing point of $g(K)$ for two different system sizes thus defines the (pseudo)critical point.

However, this finite-size scaling approach breaks down when the system size scales anisotropically. In this case, the scaling at criticality is given as a function with two independent scaling variables instead of just one,

$$Q(L, L_\tau) = \mathcal{G}\left(\frac{L}{\xi}, \frac{L_\tau}{\xi_\tau}\right), \tag{4}$$

and anisotropic systems according to $L_\tau \propto L^z$ are the appropriate choice instead of cubic systems. Hence, given the value of z, one should also observe data collapse as a function of L_τ / L^z for the Binder cumulant curves at the critical point.

In order to find z self-consistently, we consider first the Binder cumulant as a function of L_τ for given α, K and L. For very small L_τ, the system appears effectively two-dimensional, and consequently the increased influence of fluctuations makes this system more disordered than the corresponding three-dimensional system. In the opposite limit of $L_\tau \to \infty$ the system appears effectively one-dimensional, and with $L_\tau \gg \xi_\tau$ the system is again disordered. As g is a measure of the degree of order in the system, $g \to 0$ in both the above limits, and accordingly g must have a maximum for some finite value $L_\tau = L_\tau^*$. One way of interpreting L_τ^* is as the temporal size for which the system appears as isotropic as it possibly can be (or optimally three-dimensional), the anisotropic interactions taken into account.

The details of our procedure are as follows. First, we sample the Binder ratio as a function of coupling K for a large number of system sizes. For each value of L, we choose at least 14 values of L_τ close to the presumed peak position L_τ^* for the extent of the imaginary time dimension. The procedure for estimating z then follows in three steps. For each K, curves of the Binder cumulant g for all L are plotted as a function of L_τ, corresponding to the plot shown in panel (a) of Fig. 2. Second, a fourth order polynomial fit is made to these curves, localizing the points (L_τ^*, g^*) defining the peaks of the functions $g(L_\tau)$ with good precision. The obtained values for the peak Binder cumulants for each L are then plotted as a function of K, as shown in panel (b) of Fig. 2. A value for the critical coupling K_c can be found by estimating the value K to which the crossing point for two subsequent values of L converges for $1/L \to 0$. The third step for finding the dynamical critical exponent is a simple finite-size scaling analysis of the peak positions L_τ^* of the curves $g(L_\tau)$ as shown in panel (c) of Fig. 2, assuming the relation $L_\tau^* = aL^z$, with a being a nonuniversal prefactor. Finally, one may

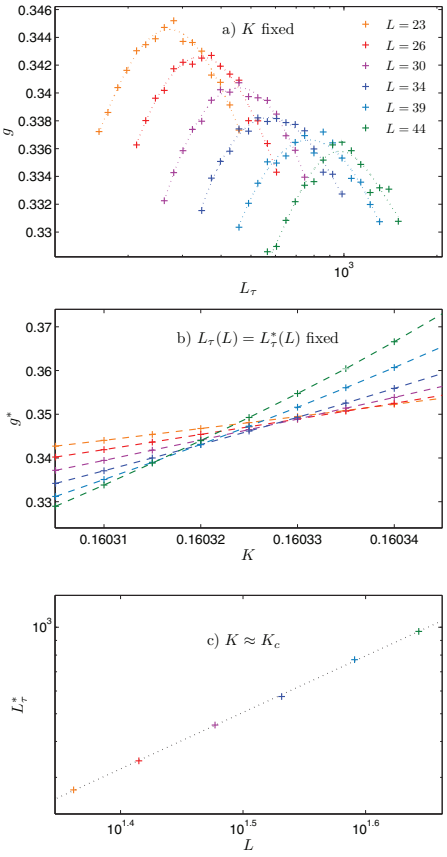

FIG. 2. (Color online) Illustration of the procedure for estimating the dynamical critical exponent z, as described in the text, here for the 2D quantum Ising model with site dissipation and $\alpha = 0.2$. (a) The Binder cumulant g as a function of temporal system size L_τ for a number of spatial system sizes L at $K = 0.160312$. (b) The peak value Binder cumulant g^* as a function of coupling K. (c) Finite-size analysis of the peak position of L_τ^* as a function of spatial system size L at criticality, $K_c = 0.160312(2)$, which yields the estimate $z = 1.97(3)$. The straight line represents a least-squares fit to the data points.

check the self-consistency of the obtained values for K_c and z by plotting the putative data collapse of the Binder cumulant as a function of L_τ / L^z, cf. Eq. (4).

Before moving on, we comment on the two interrelated (subleading) finite-size effects in the crossing point of Fig. 2: the crossing point between two subsequent Binder curves moves toward lower coupling for increasing system size, and accordingly the Binder cumulant at the crossing point decreases for increasing L. Consequently, the value of $g^*(K = K_c)$ will never be independent of system size L for finite systems. However, in our experience, this vertical deviation from collapse of the Binder curves—which is particularly evident when focusing on the peak of the Binder curves as in our analysis—does not itself affect the finite-size

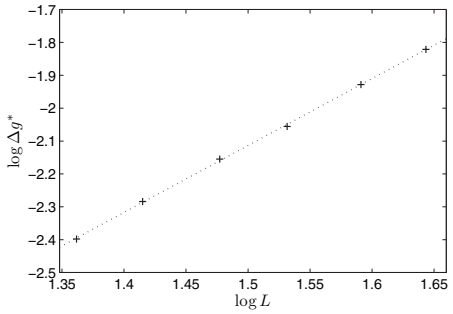

FIG. 3. Finite-size analysis for obtaining $1/\nu$ for the 2D quantum Ising model. Here we have evaluated the slope of the Binder cumulant g^* around $K=0.160312$ for $\alpha=0.2$, which yields $\nu=0.49(1)$. The straight line represents a least-squares fit to the data points.

estimate for z. More important is a possible horizontal deviation. Likewise, a slow convergence of the crossing points to K_c complicates the determination of the critical coupling for finite systems. The resulting uncertainty in z is dominated by this uncertainty in K_c, at least for the $d=2$ case.

It might be possible to obtain better precision for the critical coupling by using the finite-size analysis technique presented in Ref. 30 for the crossing points, but in the present case with an additional (and unknown) finite-size effect in z, this more rigorous approach seems by no means straightforward. To ensure that finite-size effects are negligible, we have checked the dependence of z on the lowest value of L included in the fitting procedure. In the analysis illustrated in Fig. 2, we have only retained system sizes such that the value of z seems to have converged. For the case $\alpha=0.2$ considered above, the resulting estimate is $z=1.97(3)$. No significant variation in the dynamical critical exponent is observed for stronger dissipation, and we conclude that we have $z\approx 2$ along the critical line. However, we have not been able to determine conclusively whether or not one has exactly anomalous scaling dimension $\eta=0$ in the relation $z=2-\eta$, which might be expected[10] since the value $d+z$ lies at the upper critical dimension for this phase transition for $d=2$.

We also give an estimate of the correlation length exponent ν using the peak values $g^*(K)$ of the Binder cumulant. The leading order scaling properties of the Binder ratio can be stated as[31] $Q(K,L)=\tilde{\mathcal{G}}([K-K_c]L^{1/\nu})$, and assuming negligible finite-size effects in the obtained dimensions $L_\tau^*(L)$, one finds the finite-size relation

$$\log\frac{\mathrm{d}g^*}{\mathrm{d}K} = C + \frac{1}{\nu}\log L, \tag{5}$$

The slope $\mathrm{d}g^*/\mathrm{d}K$ is estimated by the finite difference Δg^* over a small coupling interval around K_c, and C is an unimportant constant. The resulting finite-size analysis for $\alpha=0.2$ is illustrated in Fig. 3, and we find $\nu=0.49(1)$. This is very close to the expected (mean-field) value $\nu=1/2$ (Ref. 10), which is reasonable given that $z\approx 2$.

We finally note that, whereas increasing α does not lead to a significant change of z, it certainly does increase the prefactor a of the scaling relation $L_\tau \sim L^z$ and thereby the peak position L_τ^*. This reflects the increased anisotropy of the interactions, and can be seen also for $\alpha=0$ when K and K_τ are allowed to vary freely. At criticality one has $a=1$ for $K_\tau=K$, with increasing a for increasing anisotropy K_τ/K. In fact, for the analytically solvable 2D Ising model there even exists an exact mapping between system size anisotropy (i.e., a) and interaction anisotropy (i.e., K_τ/K).[32]

III. QUANTUM ISING CHAIN WITH BOND DISSIPATION

In this section, we will consider a $(1+1)$-dimensional quantum Ising model where the dissipative quantities of interest are bond variables involving Ising spins, rather than individual Ising spins themselves. The specific form of this dissipation kernel has been proposed as a candidate for describing the origin of the anomalous normal state properties of the cuprate high-T_c superconductors,[20] but in that case involving two sets of Ising spin on each lattice point. Such a model, unlike the one we will consider, may be mapped onto a four-state clock model, and may be approximated by an XY model with a fourfold symmetry breaking field, which in the classical case in two spatial dimensions is perturbatively irrelevant near criticality on the disordered side. Due to the degrees of freedom in our model being Ising spins with a spin gap, the present model should therefore not be regarded as directly comparable to a dissipative XY model that the authors of Ref. 20 consider. It should rather be regarded as a simple, but spatially extended model system, illustrating how bond dissipation can affect a quantum phase transition, which is certainly an important question on its own right.

In Fourier space, the action is given by

$$S = \sum_{\mathbf{q}}\sum_{\omega}\left(\tilde{K}\mathbf{q}^2 + \tilde{K}_\tau\omega^2 + \frac{\alpha}{2}|\omega|\mathbf{q}^2\right)\sigma_{\mathbf{q},\omega}\sigma_{-\mathbf{q},-\omega}. \tag{6}$$

The real space representation of this system is given by the action

$$S = -K\sum_{x=1}^{L}\sum_{\tau=1}^{L_\tau}\sigma_{x,\tau}\sigma_{x+1,\tau} + K_\tau\sum_{x=1}^{L}\sum_{\tau}^{L_\tau}\sigma_{x,\tau}\sigma_{x,\tau+1} + \frac{\alpha}{2}\sum_{x=1}^{L}\sum_{\tau\neq\tau'}^{L_\tau}\left(\frac{\pi}{L_\tau}\right)\frac{(\Delta\sigma_{x,\tau}-\Delta\sigma_{x,\tau'})^2}{\sin^2(\pi/L_\tau|\tau-\tau'|)}, \tag{7}$$

cf. the site dissipation case in Eq. (2). Here, $\Delta\sigma_{x,\tau}\equiv\sigma_{x+1,\tau}-\sigma_{x,\tau}$.

The interpretation of this representation remains mostly the same as in the previous section. The only difference is that the coupling to the heat bath is given in terms of the Ising field gradients rather than the Ising fields themselves. In the limit $\mathbf{q}\to\mathbf{0}$, $\omega\to 0$, we may anticipate from the Fourier representation of the action that the last term becomes irrelevant, which implies the value $z=1$ for the dynamical critical exponent. It is also evident from Eq. (7) that the bond dissipation is less effective than site dissipation in reducing quantum fluctuations. While site dissipation tends to align all

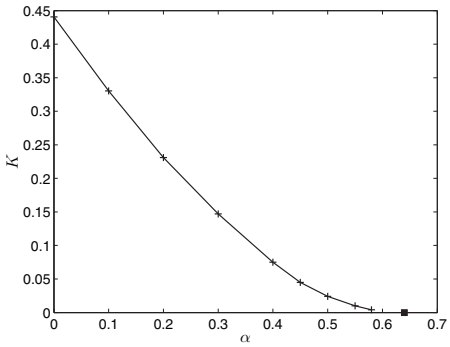

FIG. 4. Phase diagram of the quantum Ising chain with bond dissipation for $K_\tau=\ln(1+\sqrt{2})/2$. The ordered phase is found for large values of spatial coupling K and dissipation strength α. The filled square on the α axis represents an upper bracket for critical coupling α_c when the spatial coupling is tuned to zero, see the text.

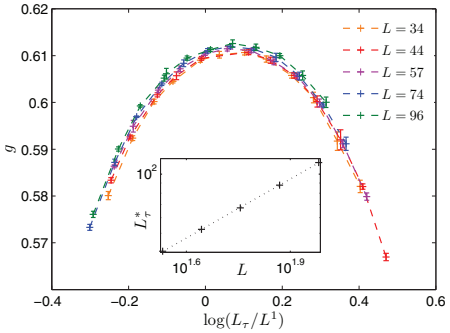

FIG. 5. (Color online) Data collapse of the Binder cumulant for $z=1$ at $K_c=0.3306$ for the 1D quantum Ising chain with bond dissipation and $\alpha=0.1$. The error bars are obtained from a jackknife analysis in the reweighting procedure. *Inset:* finite-size analysis resulting in dynamical critical exponent $z=1.007(15)$. The straight line represents a least-squares fit to the data points.

spins in the temporal direction, the bond dissipation tends to align the *difference* of nearest-neighbor spins along the Trotter slices. At least in the presence of a finite coupling $K\neq 0$, this is a less effective way of reducing temporal fluctuations of individual spins than onsite dissipation.

When expanding the dissipative term, it becomes clear that it contributes to both ferromagnetic and antiferromagnetic long-range interaction. This renders the system intractable to the Luijten-Blöte variant cluster algorithm used in the previous section. This algorithm builds up clusters with sizes comparable to the entire system and flips these as a whole, resulting in extreme correlations.[33] No cluster algorithm that effectively handles competing interactions has come to the authors' attention.

In the Monte Carlo simulations, we have therefore used a parallel tempering[34,35] algorithm which adequately handles the critical slowing down in the critical regime. A number of independent systems perform random walks in the space of coupling values, and this enables the systems to effectively explore a rugged energy landscape like the one generated by the dissipation term in Eq. (7).

The coupling values are distributed according to the iteration procedure introduced by Hukushima,[36] which renders the accept ratio of the attempted exchange of two adjacent coupling values independent of the coupling value. Consequently, the systems are allowed to wander relatively freely through the space of coupling values, although even more sophisticated distribution algorithms are available in that respect.[35]

The parameter K_τ is fixed at $\ln(1+\sqrt{2})/2\approx 0.4407$, the critical coupling K_c is thus the same as for the isotropic 2D Ising model when the dissipation strength is tuned to zero. Anticipating $z=1$, this choice also ensures that the simulations will be performed for convenient values of L and L_τ. The further steps necessary to find information about the critical properties are the same as discussed in Sec. II. The phase diagram of the system in the α-K plane is shown in Fig. 4.

For this model, the critical exponents are extracted for the two dissipation strengths $\alpha=0.1$ and 0.2. In Fig. 5, we show the results for the dynamical critical exponent for $\alpha=0.1$ as illustrated by the collapse of the Binder cumulant curves discussed in Sec. II for the value $z=1$. The results confirm the proposed value of z based in naive scaling arguments, and it appears that the bond dissipation term is indeed irrelevant.

The value of the dynamical critical exponent is very sensitive to finite-size effects and therefore challenging to obtain with the algorithm we have used given the limitations this entails. Increasing the dissipation strength makes these challenges more apparent, so to illustrate the dependence of z on system size we plot in Fig. 6 z as a function of system size for a fixed $K=K_c$ for $\alpha=0.2$. Note that three adjacent L values have been used to calculate every value for z, $\langle L\rangle$ denoting the average of these. The evolution of z is clearly seen to approach $z\approx 1$ in the thermodynamic limit. Even larger dissipation strengths tend to require much larger system sizes not practically feasible with the current algorithm. Results for such dissipation strengths are therefore not included here.

We have also attempted to extract the correlation length exponent ν for both dissipation strengths. When discarding

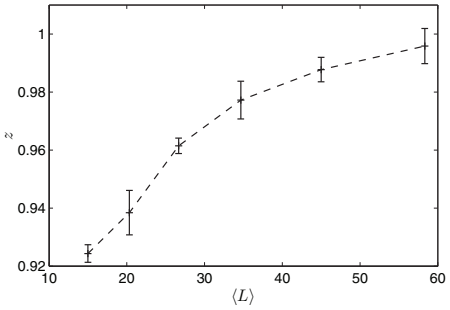

FIG. 6. The evolution of z as a function of system size for the 1D quantum Ising chain with bond dissipation with $\alpha=0.2$. Every point is calculated for the same coupling value $K_c=0.231$ from three adjacent system sizes, and the error bars are obtained from the least-squares fit in the finite-size analysis.

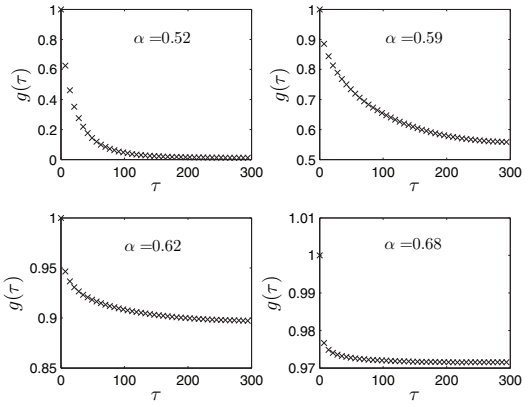

FIG. 7. The temporal spin-spin correlation function $g(\tau)=\langle\sigma_{x,\tau}\sigma_{x,0}\rangle$ for the 1D quantum Ising chain with bond dissipation at $K=0$ with $L=20$ and $L_\tau=600$. The decay of the correlation function is illustrated for four different dissipation strengths as the system goes from the disordered phase ($\alpha=0.52$) to the ordered phase ($\alpha=0.68$).

the smallest system sizes where finite-size effects are expected to be important, the values are found to be $\nu=1.00(2)$ for $\alpha=0.1$ and $\nu=1.005(8)$ for $\alpha=0.2$. This corresponds well with the exact value $\nu=1$ expected for the universality class of a 2D Ising model.

Sufficiently strong dissipation brings the critical coupling K_c toward zero, and, as indicated on the α-axis of the phase diagram in Fig. 4, the model undergoes a purely dissipative phase transition at some critical dissipation strength α_c. The ground state at $K=0$ consists of columns in the direction of imaginary time of ordered Ising spins. However, the direction of ordering is in general not uniform, as can be seen from Eq. (7), since a column can be flipped as a whole with no cost of energy. This nonuniform order prohibits the use of Binder cumulant curves to determine the critical coupling, so the exact value of α_c is difficult to deduct from the simulations. These obstacles make an estimate of the dynamical critical exponent unfeasible by our methods. Furthermore, since this phase transition is not of Kosterlitz-Thouless nature, any variety of the method of Ref. 27 also seem to be inapplicable to this model.

To corroborate that, there is in fact a phase transition to an ordered state for increasing α also at $K=0$, we present in Fig. 7 results for the temporal spin-spin-correlation $g(\tau)=\langle\sigma_{x,\tau}\sigma_{x,0}\rangle$. It is clear that this correlation function decays exponentially to zero for low dissipation strengths, while in the opposite limit of strong dissipation the correlation function quickly decays to some finite value. The character of the correlation function as α is tuned through the intermediate region is better illustrated in Fig. 8, where we have extracted the temporal correlation length ξ_τ. The diverging correlation length signifies a critical region with algebraic decay of the correlation function. The spatial correlation length ξ, on the other hand, we have found to be vanishing also in the critical region, and the behavior of the system depends only very weakly on its spatial extent L. From a crude finite-size analysis based on Fig. 8, we obtain the value $\alpha_c \leq 0.64$ as a best estimate for a upper bracket of the critical coupling, as we indicated in the phase diagram in Fig. 4.

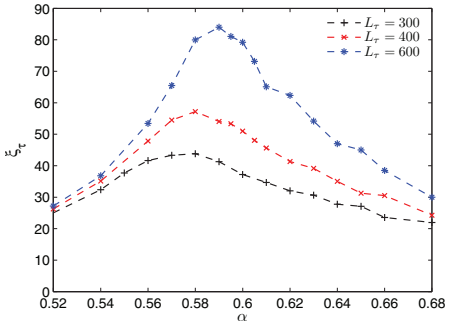

FIG. 8. (Color online) The temporal correlation length ξ_τ as a function of dissipation strength α for the 1D quantum Ising chain with bond dissipation at $K=0$. Because of the extremely anisotropic scaling in this limit, and to be sure to avoid any spatial finite-size effects, we have chosen to fix $L=20$.

IV. DISCUSSION

We will begin the discussion of our results by taking a closer look at the scaling arguments presented in Sec. I for finding the dynamical critical exponent. As indicated here, one important caveat of such arguments is that they only tell what exponent is naively expected to the lowest order approximation, and in general field-theoretical methods (see, e.g., Ref. 10) are needed to ascertain how higher order corrections modify this estimate. Furthermore, with several terms in the quadratic part of the action, it is not always obvious which terms should be required to balance at the critical point, or for which phase transitions this is valid.

For site dissipation, one obtains $z=2$ by balancing the spatial term and the dissipative term, since the dynamic term will be subdominant to the dissipative term for all positive z. For the bond dissipation case, a similar argument excludes the possibility $z=2$ for which the dissipative term would balance the dynamic term, since they both would be subdominant to the spatial term for all $z>1$. It is therefore interesting to ask if the possibility $z=0$, or alternatively $z\ll 1$, can be considered. In the limit that z is strictly zero, a dissipative term on the form $|\omega|$ would balance the dynamic term whereas a dissipative term on the form $\mathbf{q}^2|\omega|$ would balance the spatial term, but in the latter case both would be subdominant to the dynamic term. One interpretation is that $z=0$ in both cases would imply unrestrained quantum fluctuations resulting in spatial correlations being infinitely stronger than temporal correlations, so that each Trotter slice is essentially independent. In this interpretation, a strictly vanishing dynamical critical exponent may however be considered unphysical since we are assuming a transition to uniform order for the entire $(d+1)$-dimensional system by taking the limit $\mathbf{q}\to\mathbf{0}$, $\omega\to 0$.

Likewise, tuning $K_\tau\to 0$ may be considered unphysical since one removes the origin of the quantum nature of the

system. For this reason one cannot say that there will exist a quantum phase transition with $z=0$ for the bond dissipation model even if the ω^2 term had been removed from the action. The origin of the ω^2 term in a physical quantum model can be a transverse magnetic field in the Ising case or a Josephson charging energy in the XY case, and the interpretation of the prefactor K_τ is in general the inertia of the degrees of freedom. Even though we have chosen to operate with a nonspecific parameter K_τ, we therefore do not regard taking $K_\tau=0$ admissible in our simulations.

The opposite limit of $z=\infty$ may similarly be interpreted as spatially local criticality with correlations in the imaginary time direction independent of (the vanishing) correlations in the spatial directions, see, e.g., Refs. 16, 17, and 20. This is trivially the case in the limit $K=0$ for site dissipation with $\alpha>\alpha_c$, although one may argue that z is undefined in that case as the system is strictly decoupled in the spatial directions. The same argument cannot be applied to bond dissipation. For that model, the system does not experience dimensional reduction as $K\to 0$, but is still dependent (although very weakly) on the spatial extent of the $(d+1)$-dimensional system. We should however note that the approach taken here for determining the dynamical critical exponent is not applicable when z is either strictly zero or infinite, and also for a constant value $z\gg 1$ it would be very difficult to determine the dynamical critical exponent for practically attainable lattice sizes. If, on the other hand, one has $z\to\infty$ in the sense of activated dynamical scaling, the method is in principle feasible.[19]

Before continuing the discussion of the bond dissipation, we comment further on the relation between the real space representation of $\mathbf{q}^2|\omega|$ and the form of the bond dissipation used in Eq. (7). When Fourier transforming $\mathbf{q}^2|\omega|\sigma_{\mathbf{q},\omega}\sigma_{-\mathbf{q},-\omega}$ from Eq. (6) and discretizing the resulting differential operators, we arrive at

$$S_{\mathbf{q}^2|\omega|} \propto -\left(\frac{\pi}{L_\tau}\right)^2 \frac{\Delta\sigma_{x,\tau}\cdot\Delta\sigma_{x,\tau'}}{\sin^2(\pi/L_\tau|\tau-\tau'|)}. \tag{8}$$

Now, writing out the last term of Eq. (7) and comparing with Eq. (8) shows that the Fourier space representation of the bond dissipation can be written as

$$S_{\text{bond}} = (\mathbf{q}^2|\omega| + C'\mathbf{q}^2)\sigma_{\mathbf{q},\omega}\sigma_{-\mathbf{q},-\omega}. \tag{9}$$

Here, C' depends weakly on dimensions for finite systems. In other words, the bond dissipation is of the same form as $\mathbf{q}^2|\omega|$ dissipation, but with renormalized spatial nearest-neighbor coupling, which however does not alter the critical exponents of the model. This extra term originates with the counterterm introduced to cancel out the renormalization of the bare potential that arises due to the coupling with a heat bath.[3] For the Ising model, this renormalization is responsible for stabilizing ferromagnetic order at $K>0$.

We will now turn to the analysis of simulations on finite lattices, in particular with respect to the scaling relation $L_\tau = aL^z$ and the system anisotropy expressed by it. To interpret our results, it is useful to consider the dependence of both z and a on the dissipation strength α, and the variation in these quantities can be understood as follows. If the dissipation term is relevant and thus determining the universality class, we may assume that the value of z will be given by the form of this term even for infinitesimal $\alpha>0$ in the thermodynamic limit. In this case, increasing the dissipation strength α further will therefore not change z, but the prefactor a will have to change to reflect the increased interaction anisotropy. Correspondingly, when the dissipation term is an irrelevant perturbation, the dynamical critical exponent will remain $z=1$ in the thermodynamic limit. Upon increasing α, the dissipation will never grow strong enough to alter the universality class, but the nonuniversal prefactor a will in general change also in this case, and whether it increases or decreases is determined by how the dissipation changes the overall interaction anisotropy.

Regarding the evolution of a upon increasing α for the bond dissipation case, there are now two effects that must be considered separately. One implicit effect is that increasing α decreases $K=K_c$ at criticality, thereby increasing the anisotropy ratio K_τ/K, which results in a much larger a for large values of α. The other effect is that arising explicitly from the dissipation term and its contribution to the effective coupling strength in the imaginary time direction. Whereas a site dissipation term obviously increases the anisotropy when increasing the dissipation strength while keeping the other coupling values fixed, such an enhancement of a does not appear for bond dissipation. This can be seen—as we have checked—by evaluating a for increasing α for isotropic short-range coupling, i.e., $K_\tau=K$. One possible interpretation of this result is that although bond dissipation does not change universality, it favors $z<1$ behavior, which can also be recognized from Fig. 6. In other words, the dissipation term contributes to making the temporal dimension less ordered than the spatial dimension, in strong contrast to the case of site dissipation. This would in part explain why one needs much longer simulations and larger systems to obtain reliable results for strong bond dissipation.

Given that the exceedingly strong finite-size effects thwart a precise determination of z for higher values of α, one should in general also consider the possibility of continuously varying critical exponents. However, we have shown that $z\approx 1$ for $\alpha=0.1$ and presented solid arguments favoring that this is the case also for $\alpha=0.2$, as it is obviously also in the limit $\alpha=0$. Therefore, if the exponents are in fact continuously varying, they begin to vary only for dissipation strengths above $\alpha>0.2$, and would furthermore have to be varying very slowly.

V. CONCLUSION

This work represents a further step toward simulations of physically interesting extended quantum systems with dissipation. Using Monte Carlo methods, we have studied a model similar to that by Werner *et al.*,[13] but with higher spatial dimensionality, as well as a model with one spatial dimension but with bond dissipation instead of site dissipation. We have found that the $(2+1)$-dimensional model with site dissipation has a dynamical critical exponent very close to the corresponding $d=1$ model, i.e., $z\approx 2$. Bond

dissipation, on the other hand, is fundamentally different, and our results strongly suggest that this form of dissipation is irrelevant to the universality class, i.e., $z \approx 1$ and nonvarying. We therefore believe that the same dynamical critical exponent also applies to $(2+1)$-dimensional models with bond dissipation for the same degrees of freedom, although we have not been able to reach sufficiently large systems to show this convincingly by numerical means. In both cases, the numerical estimates for the dynamical critical exponent is consistent with those found by naive scaling arguments on the quadratic part of the action.

ACKNOWLEDGMENTS

We thank Steinar Kragset for his contribution during the early phases of this project. We also acknowledge discussions with Egil V. Herland, Mats Wallin, and Chandra M. Varma.

[1] M. Suzuki, Prog. Theor. Phys. **56**, 1454 (1976).
[2] J. A. Hertz, Phys. Rev. B **14**, 1165 (1976).
[3] A. O. Caldeira and A. J. Leggett, Ann. Phys. **149**, 374 (1983).
[4] S. Chakravarty, Phys. Rev. Lett. **49**, 681 (1982).
[5] S. L. Sondhi, S. M. Girvin, J. P. Carini, and D. Shahar, Rev. Mod. Phys. **69**, 315 (1997).
[6] M. Vojta, Rep. Prog. Phys. **66**, 2069 (2003).
[7] D. M. Broun, Nat. Phys. **4**, 170 (2008).
[8] C. M. Varma, P. B. Littlewood, S. Schmitt-Rink, E. Abrahams, and A. E. Ruckenstein, Phys. Rev. Lett. **63**, 1996 (1989).
[9] S. Chakravarty, G.-L. Ingold, S. Kivelson, and A. Luther, Phys. Rev. Lett. **56**, 2303 (1986).
[10] S. Pankov, S. Florens, A. Georges, G. Kotliar, and S. Sachdev, Phys. Rev. B **69**, 054426 (2004).
[11] S. Sachdev, P. Werner, and M. Troyer, Phys. Rev. Lett. **92**, 237003 (2004).
[12] P. Werner, M. Troyer, and S. Sachdev, J. Phys. Soc. Jpn. Suppl. **74**, 67 (2005).
[13] P. Werner, K. Völker, M. Troyer, and S. Chakravarty, Phys. Rev. Lett. **94**, 047201 (2005).
[14] L. F. Cugliandolo, G. S. Lozano, and H. Lozza, Phys. Rev. B **71**, 224421 (2005).
[15] P. Werner and M. Troyer, Prog. Theor. Phys. Suppl. **160**, 395 (2005).
[16] S. Tewari, J. Toner, and S. Chakravarty, Phys. Rev. B **72**, 060505(R) (2005).
[17] S. Tewari and J. Toner, EPL **74**, 341 (2006).
[18] P. Goswami and S. Chakravarty, Phys. Rev. B **73**, 094516 (2006).
[19] T. Vojta, Rev. Comput. Chem. **26**, 167 (2008).
[20] V. Aji and C. M. Varma, Phys. Rev. B **79**, 184501 (2009).
[21] V. Aji and C. M. Varma, Phys. Rev. Lett. **99**, 067003 (2007).
[22] K. Børkje and A. Sudbø, Phys. Rev. B **77**, 092404 (2008).
[23] U. Wolff, Phys. Rev. Lett. **62**, 361 (1989).
[24] E. Luijten and H. Blöte, Int. J. Mod. Phys. C **6**, 359 (1995).
[25] M. Matsumoto and T. Nishimura, ACM Trans. Model. Comput. Simul. **8**, 3 (1998).
[26] A. M. Ferrenberg and R. H. Swendsen, Phys. Rev. Lett. **63**, 1195 (1989).
[27] E. Luijten and H. Meßingfeld, Phys. Rev. Lett. **86**, 5305 (2001).
[28] M. Guo, R. N. Bhatt, and D. A. Huse, Phys. Rev. Lett. **72**, 4137 (1994).
[29] H. Rieger and A. P. Young, Phys. Rev. Lett. **72**, 4141 (1994).
[30] L. Wang, K. S. D. Beach, and A. W. Sandvik, Phys. Rev. B **73**, 014431 (2006).
[31] A. M. Ferrenberg and D. P. Landau, Phys. Rev. B **44**, 5081 (1991).
[32] G. Kamieniarz and H. W. J. Blöte, J. Phys. A **26**, 201 (1993).
[33] D. Kandel, R. Ben-Av, and E. Domany, Phys. Rev. Lett. **65**, 941 (1990).
[34] K. Hukushima and K. Nemoto, J. Phys. Soc. Jpn. **65**, 1604 (1996).
[35] H. Katzgraber, Modern Computation Science, Oldenburg, Germany, 16-28 August 2009 (unpublished).
[36] K. Hukushima, Phys. Rev. E **60**, 3606 (1999).

Paper II

Criticality of compact and noncompact quantum dissipative Z_4 models in $(1+1)$ dimensions.

Phys. Rev. B **83**, 115134 (2011).

PHYSICAL REVIEW B **83**, 115134 (2011)

Criticality of compact and noncompact quantum dissipative Z_4 models in (1 + 1) dimensions

Einar B. Stiansen, Iver Bakken Sperstad, and Asle Sudbø
Department of Physics, Norwegian University of Science and Technology, N-7491 Trondheim, Norway
(Received 15 December 2010; revised manuscript received 4 February 2011; published 28 March 2011)

Using large-scale Monte Carlo computations, we study two versions of a (1 + 1)D Z_4-symmetric model with ohmic bond dissipation. In one of these versions, the variables are restricted to the interval $[0,2\pi\rangle$, while the domain is unrestricted in the other version. The compact model features a completely ordered phase with a broken Z_4 symmetry and a disordered phase, separated by a critical line. The noncompact model features three phases. In addition to the two phases exhibited by the compact model, there is also an intermediate phase with isotropic quasi-long-range order. We calculate the dynamical critical exponent z along the critical lines of both models to see if the compactness of the variable is relevant to the critical scaling between space and imaginary time. There appears to be no difference between the two models in that respect, and we find $z \approx 1$ for the single phase transition in the compact model as well as for both transitions in the noncompact model.

DOI: 10.1103/PhysRevB.83.115134 PACS number(s): 75.40.Mg, 64.60.De, 05.30.Rt

I. INTRODUCTION

The standard way of introducing dissipation in a quantum mechanical system is to couple some variable describing the system to the degrees of freedom of an external environment.[1] The environment is modeled as a bath of harmonic oscillators which couple linearly to the system variables. The oscillator degrees of freedom, appearing in the action to second order, may be integrated out to produce an effective theory for the composite system given in terms of the system variables.

The presence of a dissipative term introduces strongly retarded (nonlocal in time) self-interactions of the system variables. This long-range interaction in imaginary time may have serious consequences for the quantum critical behavior of the system. This effect can usually be described by a dynamical critical exponent z defined by the anisotropy of the divergence of the correlation lengths at criticality, $\xi_\tau \sim \xi^z$, where ξ and ξ_τ are the correlation lengths in space and imaginary time, respectively. An Ising spin chain with site dissipation was shown by extensive Monte Carlo simulations in Ref. 2 to have $z \approx 2$. The same model, augmented to two spatial dimensions, was investigated by the present authors in Ref. 3. The result $z = 1.97(3)$ suggests that the dynamical critical exponent is independent of the number of spatial dimensions, in agreement with naive scaling arguments which make no reference to dimensionality.[4] On the other hand, when coupling the reservoir to bond variables involving Ising spins the dissipation term was found to be irrelevant to the universality class, i.e., $z \approx 1$.[3] In general, dissipation suppresses certain types of quantum fluctuations, though the larger value of z for site dissipation signifies that bond dissipation is far less effective than site dissipation in reducing fluctuations.

Ohmic dissipation in terms of gradients or bonds is common in models describing shunted Josephson junctions or granular superconductor systems.[5,6] Here, the bonds represent the difference of the quantum phases between the superconducting grains. In this context it is well known that the coupling of the environment to the system may affect the natural domain of the system variables.[7] For Josephson junctions, this means that the domain of the phase variables reflects quantization of the charges on each superconducting grain. If the charges are quantized in units of Cooper pairs, $2e$, the domain of the quantum phase is 2π periodic. Ohmic shunting leads to an unbounded $-\infty < \theta < \infty$ domain,[7] reflecting a continuous transfer of charges across the junction. We will henceforth refer to the variable defined on a restricted 2π interval as *compact* and the extended variable as *noncompact*.

Moreover, dissipation in terms of bonds has also been proposed in an effective model describing the low-energy physics of fluctuating loop currents to describe anomalous normal state properties of high-T_c cuprates.[8,9] A quantum statistical mechanical model for such degrees of freedom has been derived from a microscopic three-band model of the cuprates.[10] The classical part of the derived action consists in its original form of two species of Ising variables within each unit cell, coupled by a four-spin Ashkin-Teller term. This model has been proven, through large-scale Monte Carlo simulations, to support a phase transition with a nondivergent nonanalyticity in the specific heat on top of an innocuous background.[11] The breaking of the Ising-like symmetry describes a suggested ordering of loop currents upon entering the pseudogap phase of the cuprates. Neglecting the Ashkin-Teller interaction term present in this theory, the classical model may be mapped onto a four-state clock model, with the basic variable being an angle parametrizing the four possible current loop orientations.[8,10,11]

The quantum version of this model includes a kinetic energy term describing the quantum dynamics of the angle variables. Adding dissipation of angle differences as in the Caldeira-Leggett approach for Josephson junctions, the model has been reported to exhibit local quantum criticality. Local quantum criticality in this context means that the model exhibits a fluctuation spectrum which only depends on frequency, but is independent of the wave vector.[8] This essentially implies a dynamical critical exponent $z \to \infty$. A point which quite possibly is of importance in this context, is that while the starting point in Ref. 8 is a model with two Ising-like variables, the actual dissipative quantum model discussed is one with global $U(1)$ symmetry.

While the physical picture of fluctuating configurations of current loops suggests an identification of the angles θ and

$\theta + 2\pi$, the presence of the clearly noncompact dissipation term makes this not entirely obvious. It is therefore the intent of this work to investigate if the restriction of the variable domain influences the dynamical critical exponent z, and thereby if it may have consequences for possible manifestations of local quantum criticality in similar models. Since it is still an open question exactly what the consequences are of how the variable domains are defined in dissipative quantum models, a numerical comparison of the compact and noncompact case is of general interest. We will therefore not restrict the interpretation of the model to Ising variables associated with loop currents, although the Z_4 symmetry reflecting this starting point will be maintained. Moreover, due to the long-ranged interactions in the imaginary-time direction, the Monte Carlo computations are extremely demanding. Since we are interested in a proof of principle of the importance of compactness versus noncompactness, we will in this paper limit ourselves to a $(1 + 1)$D model.

We will perform Monte Carlo simulations on two versions of a dissipative Z_4 model described in more detail in Sec. II, one with compact variables (i.e., a clock model) and one with noncompact variables. The simulation details are described in Sec. III, after which we present the results, first for the noncompact case in Sec. IV, then for the compact case in Sec. V.

Our main finding is that, although the critical scaling of space and imaginary time is equal for both cases, i.e., $z = 1$, there is a major difference in phase structure. Whereas the compact model displays a conventional order-disorder phase transition, the noncompact model develops an intermediate phase characterized by power-law decay in spin correlations (quasi-long-range order) and a $U(1)$ symmetric distribution of the complex order parameter. The appearance of this intermediate phase is related to the fact that the kinetic energy term must be treated differently for the compact and noncompact cases, as we discuss in detail in the Appendix.

It is well established that this kind of critical phase occurs in classical 2D Z_q clock models and XY models with Z_q anisotropy,[12–14] but only for larger values of q than we are considering. It is remarkable that the noncompact model presented in this paper exhibits a critical phase with emergent $U(1)$ symmetry, when the dissipationless starting point is a pure $Z_4 = Z_2 \times Z_2$ model (i.e., a double Ising model) with the angle variables restricted to four discrete values by a *hard* constraint. We will discuss this in more detail in Sec. VI, after which we summarize our results in Sec. VII.

II. THE MODEL

The starting point for our model is a chain of N_x quantum rotors, or equivalently planar spins, the alignment of which is described by a set of angle variables $\{\theta_x\}$. Although these variables could also be denoted as the phases of the quantum rotors, we will refer to them simply as angles. Requiring that the spins satisfy Z_4 symmetry, the angles can be parametrized as $\theta = 2\pi n/4$ with integer n, making our model similar to a four-state (or Z_4) clock model. Being quantum spins, their dynamics is described by their evolution in imaginary time τ, with N_τ denoting the number of Trotter slices used to discretize the imaginary time dimension. The variables $\{\theta_{x,\tau}\}$ are thus defined on the vertices of a $(1 + 1)$D quadratic lattice of size $N_x \times N_\tau$.

In order to investigate if the restriction on the angle variable is relevant to the dynamical critical exponent z or not, we will consider two variants of this model, with the complete action for both stated below for later reference. In the compact (C) case, we restrict the parametrization variable n to just four values, so that the angle θ is restricted to one primary interval, corresponding to the four primary states of the four-state clock model. In the noncompact (NC) case we have no such restriction, and n can take any integer values. The general form of the action is

$$S^{\mathrm{C,NC}} = S_\tau^{\mathrm{C,NC}} + S_x + S_{\mathrm{diss}}, \tag{1}$$

where the kinetic energy for the compact and the noncompact case, respectively, is given by

$$S_\tau^{\mathrm{C}} = -K_\tau \sum_{x=1}^{N_x} \sum_{\tau=1}^{N_\tau} \cos(\theta_{x,\tau+1} - \theta_{x,\tau}), \tag{2}$$

$$S_\tau^{\mathrm{NC}} = \frac{K_\tau}{2} \sum_{x=1}^{N_x} \sum_{\tau=1}^{N_\tau} (\theta_{x,\tau+1} - \theta_{x,\tau})^2. \tag{3}$$

The spatial interaction defines a periodic potential

$$S_x = -K \sum_{x=1}^{N_x} \sum_{\tau=1}^{N_\tau} \cos(\theta_{x+1,\tau} - \theta_{x,\tau}), \tag{4}$$

and the dissipation term is defined according to

$$S_{\mathrm{diss}} = \frac{\alpha}{2} \sum_{x=1}^{N_x} \sum_{\tau \neq \tau'}^{N_\tau} \left(\frac{\pi}{N_\tau}\right)^2 \frac{(\Delta\theta_{x,\tau} - \Delta\theta_{x,\tau'})^2}{\sin^2\left(\frac{\pi}{N_\tau}|\tau - \tau'|\right)}. \tag{5}$$

The bond variable or angle difference is written as $\Delta\theta_{x,\tau} = \theta_{x+1,\tau} - \theta_{x,\tau}$.

Note that the only apparent difference between the compact and the noncompact model is the form of the kinetic energy term. When the angles are compact the short-range temporal interaction is given by a cosine term, in contrast to noncompact angles for which a quadratic form of the kinetic term must be used. The reason for this difference can be traced to the fact that, whereas canonical conjugate variables of compact angles are discrete due to the 2π periodicity of the quantum wave functions, no such restriction applies when the angles are noncompact. From a qualitative point of view the two separate forms of the temporal interaction term is expected. Considering the imaginary time history of a single variable, it is clear that a cosine interaction in imaginary time will render the ground state of the noncompact model massively degenerate. A Trotter slice may be shifted by 2π relative to the neighboring Trotter slices without any penalty in the action. However, a quadratic interaction term in the imaginary time direction lifts this degeneracy and tends to localize the angle variables.

There is nothing new about the derivation of these different kinetic terms, but as the difference is crucial to the phase structure of our models and is also rarely discussed in the literature, we include the derivation in the Appendix. In addition, in order to simulate the compact model we also need

an appropriate reinterpretation of the dissipation term. We find it natural to postpone this to Sec. V.

The action is on a form identical to the model in Sec. III in Ref. 3 apart from the nature of the variables and the resultant treatment of the dissipation term. However, we still expect the scaling arguments presented in Ref. 3 to be valid since no reference to the actual type of variable is used. The action in Fourier space may be written

$$S \sim (\mathbf{q}^2 + \omega^2 + |\omega|\mathbf{q}^2)\theta_q\theta_{-q}, \tag{6}$$

neglecting any prefactors. Taking the limit $\mathbf{q} \to 0, \omega \to 0$ we anticipate that the term $\sim|\omega|\mathbf{q}^2$ describing the dissipation is subdominant for all positive z. Accordingly, we expect at least naively that $z = 1$ for both compact and noncompact variables. This will be investigated in detail in our simulations, and we make no assumption of the veracity of naive scaling applied to this problem.

III. DETAILS OF THE MONTE CARLO COMPUTATIONS

When expanding the dissipative term, it becomes clear that it contributes both to ferromagnetic and antiferromagnetic long range interactions. This renders the system intractable to the Luijten-Blöte[15] extension of the Wolff cluster algorithm[16] which has been used with great success in systems with noncompeting interactions. Also, for the case of noncompact variables there does not exist a straightforward way of defining (pseudo)spin projections, a necessary point for the Wolff embedding technique.[16] Considerable progress has been made in constructing new effective algorithms for long range interacting systems with extended variables.[17–19] However, these algorithms are presently restricted to (0 + 1)D systems, and do not seem to generalize easily to $N_x > 1$.[18] Furthermore, the basic degrees of freedom in these algorithms are the phase *differences* between two superconducting grains in an array of Josephson junctions. Our aim is to investigate the ordering of the phases themselves. Hence, the existing nonlocal algorithms may not be utilized. In the Monte Carlo simulations, we have therefore used a parallel tempering algorithm[20,21] in which several systems (typically 16 or 32) are simulated simultaneously at different coupling strengths.

A Monte Carlo sweep corresponds to proposing a local update by the Metropolis-Hastings algorithm for every grid point in the system in a sequential way. For the case of noncompact variables the proposed new angles are generated by randomly choosing to increase or decrease the value, then propagating the value by randomly choosing the increment on the interval $\{\frac{\pi}{2}, \pi, \frac{3\pi}{2}, 2\pi\}$. In the case of compact variables, a new angle value in the primary interval is randomly chosen. After a fixed number of Monte Carlo sweeps (typically $3 - 10$) a parallel tempering move is made. In this move, a swap of configurations between two neighboring coupling values is proposed, and the swap is accepted with probability Ξ_{PT} given by

$$\Xi_{PT} = \begin{cases} 1 & \text{if } \Delta < 0, \\ \mathrm{e}^{-\Delta} & \text{if } \Delta \geqslant 0. \end{cases} \tag{7}$$

Here, $\Delta = \kappa'(\bar{S}[X;\kappa'] - \bar{S}[X';\kappa']) - \kappa(\bar{S}[X;\kappa] - \bar{S}[X';\kappa])$, where κ is the coupling value varied, representing in our case K or α, and X represents the angle configuration. $\bar{S}$ indicates the term of the action proportional with the coupling parameter κ.

All Monte Carlo simulations were initiated with a random configuration. Depending on system sizes various numbers of sweeps were performed for each coupling value. For the phase transition separating the disordered state from the critical phase in the noncompact model $5 - 10 \times 10^6$ sweeps were made. Also, $1 - 5 \times 10^5$ sweeps at each coupling value were discarded for equilibration. For the compact model and the second transition of the noncompact model as much as 30×10^6 sweeps where performed and typically 5×10^5 sweeps discarded.

The Mersenne-Twister[22] random number generator was used in all simulations and the random number generator on each CPU was independently seeded. It was confirmed that other random number generators yielded consistent results. We also make use of the Ferrenberg-Swendsen reweighting technique,[23] which enables us to continuously vary the coupling parameter after the simulations have been performed.

IV. RESULTS: NONCOMPACT MODEL

In this section we consider the noncompact version of the dissipative Z_4 model. Using Eqs. (3), (4), and (5) we have the following action:

$$S^{\mathrm{NC}} = S_\tau^{\mathrm{NC}} + S_x + S_{\mathrm{diss}}. \tag{8}$$

In contrast to the compact model, the angle variables are in this case not restricted to the primary interval. The variables are straightforwardly generalized to take the values $\theta = 2\pi n/4$, where $n = 0, \pm 1, \pm 2, \ldots$. We seek to fix K and K_τ and investigate how the system behaves under the influence of increasing dissipation strength controlled by the dimensionless parameter α.

The kinetic coupling strength has been fixed to $K_\tau = 0.4$ for computational reasons, as this ensures that the simulations will be performed at convenient values of N_x and N_τ. We have performed simulations at four different spatial coupling constants $K = 0.4$, 0.5, 0.6, and 0.75. These choices are also made for computational convenience, as the limit of vanishing dissipation as well as the limit $K \to 0$ are both very computationally demanding. For all coupling values there is a disordered phase at low values of the dissipation strength. In this phase the noncompact angles exhibit wild fluctuations and consequently $\langle \mathrm{e}^{\mathrm{i}\theta_{x,\tau}} \rangle = 0$. However, we also have $\langle \mathrm{e}^{\mathrm{i}\Delta\theta_{x,\tau}} \rangle \neq 0$ in this phase, a trivial consequence of the cosine potential acting as an external field on the bond variables. The bond variables occasionally drift from one minimum of the extended cosine potential to another. As the dissipation strength is increased, fluctuations in these variables are suppressed, and the system features two consecutive phase transitions separated by a critical phase. This intermediate phase is characterized by power-law decay of spatiotemporal

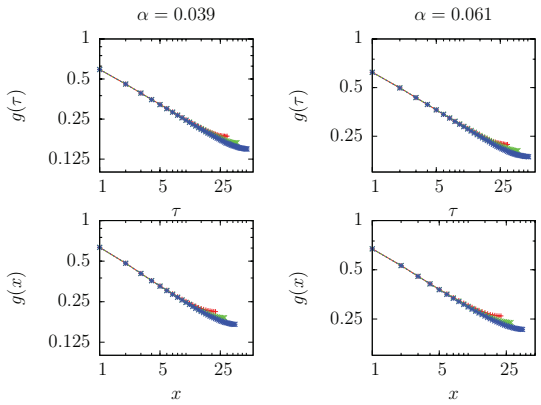

FIG. 1. (Color online) Correlation functions, Eq. (9), at two values of the dissipation strength α within the critical phase for spatial coupling $K = 0.75$. System sizes are $N_x = 44,57,74$, with optimal choices of N_τ at $\alpha_c^{(1)}$, see text. Top row: Correlation functions for the temporal direction. Bottom row: Correlation functions for the spatial direction.

spin correlations on the form

$$g(\mu) = \langle e^{i(\theta_\mu - \theta_0)} \rangle, \quad \mu \in (x, \tau). \tag{9}$$

The correlation functions for both spatial and imaginary time direction are shown in Fig. 1 for two different dissipation strengths both within the the critical phase.

A very similar critical phase, as well as phase transitions associated with it, has recently enjoyed increased interest in various versions of classical clock models.[24–26] We will proceed under the assumption that a similar picture is valid in our case. Indeed, simulations performed on a classical 2D six-state clock give qualitatively very similar results for all observables considered below, which supports the supposition that these two phenomena are related.

Considering the complex order parameter of the system,

$$m = \frac{1}{N_x N_\tau} \sum_{x,\tau} e^{i\theta_{x,\tau}} = |m| e^{i\phi}, \tag{10}$$

the intermediate critical phase can be identified by observing the distribution of m in the complex plane.[26] In the disordered phase, the order parameter is a Gaussian peak centered at the origin. In the intermediate phase, quasi-long-range order develops in the complex order parameter, and so $|m|$ acquires a nonzero value as a finite-size effect. The order parameter is, however, free to rotate in the ϕ direction. This can be described as the vanishing of the excitation gap naively expected for discrete Z_q models, or equivalently as an emergent $U(1)$ symmetry.[27] This symmetry is broken at a larger value of the dissipation strength, when true long range order is established when the magnetization selects one of the four well-defined directions in the complex plane originating with the underlying Z_4 symmetry. Typical distributions of the complex order parameter in the three phases is shown in Fig. 2.

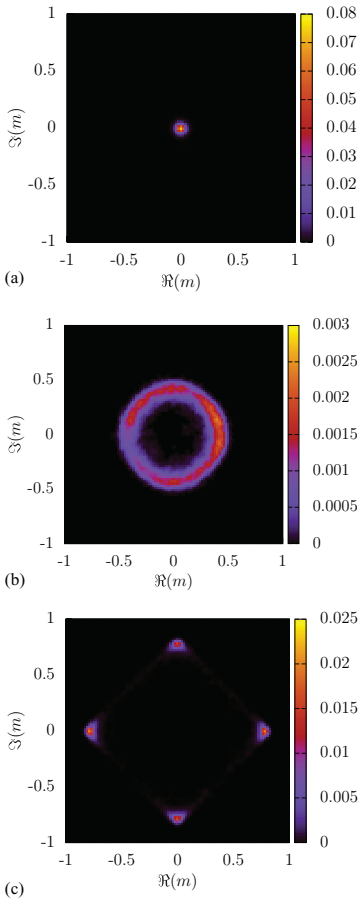

FIG. 2. (Color online) Evolution of the complex order parameter when dissipation strength α is increased for $K = 0.75$ and system size $N_x = 74$, $N_\tau = 103$ which corresponds to a near optimal aspect ratio at the phase transition at $\alpha \approx \alpha_c^{(1)}$. The color scale indicates relative density of the distribution. (a) Two dimensional Gaussian distribution of the order parameter in the complex plane corresponding to the disordered phase with $\alpha = 0.0 < \alpha_c^{(1)}$. (b) Intermediate critical phase exhibiting a finite-size-induced nonvanishing $|m|$ that rotates in the ϕ direction. The critical phase exists in a finite interval of dissipation strengths $\alpha_c^{(1)} < \alpha = 0.04 < \alpha_c^{(2)}$. The remaining anisotropy is attributed to insufficient sampling.[28] (c) The rotational symmetry of the intermediate critical phase is broken and long-range order is established as the order parameter relaxes into one of the four directions in the complex plane. The long-range ordered phase corresponds to the strong dissipation limit, $\alpha = 0.18 > \alpha_c^{(2)}$.

Although not presented here, we have also confirmed that the susceptibility of the order parameter diverges over a finite interval of dissipation strengths, also a clear evidence of a critical phase.

The phase transition between the disordered state and the intermediate critical phase at dissipation strength $\alpha = \alpha_c^{(1)}$ is

detected by the Binder cumulant $g = 1 - Q/3$, where

$$Q = \frac{\langle |m|^4 \rangle}{\langle |m|^2 \rangle^2}. \tag{11}$$

The brackets indicate ensemble averaging. The scaling at criticality of the Binder cumulant for anisotropic systems is given in terms of two independent scaling variables,[2]

$$g(N_x, N_\tau) = \mathcal{G}\left(\frac{N_x}{\xi}, \frac{N_\tau}{\xi^z}\right). \tag{12}$$

At a critical point the correlation length ξ diverges, and one should be able to observe data collapse of the Binder cumulant as a function of N_τ/N_x^z for the correct value of z. The value of $g(N_x, N_\tau)$ is independent of N_x at the critical coupling, this may be used to align the plots of g as a function of N_τ horizontally. The exponent z can then be found by optimal collapse of data onto a universal curve. The cumulant curves have a maximum at $N_\tau = N_\tau^*$. At this temporal size, the system appears as isotropic as it can be, the anisotropic interactions taken into account. See Ref. 3 for a thorough discussion of this finite-size analysis.

In the intermediate phase, the system is critical over a finite interval of dissipation strengths. According to the scaling Eq. (12), curves of the Binder cumulant for increasing system sizes will therefore merge in this interval for $N_x \to \infty$.[29] For systems of finite sizes as considered here, the curves will however intersect close to the transition instead, and we find $\alpha_c^{(1)}$ by inspecting the convergence of the crossing points. As discussed in Ref. 3, the functional form of this convergence is unknown in our case (cf. also Sec. VI and Ref. 29), and all we can do is to report our best estimate for the $N_x \to \infty$ transition point. The uncertainty estimated accordingly is not insignificant, but the effective critical exponent z is found to not be very sensitive to this error in α_c.

By further increasing the dissipation strength, the rotational symmetry of the global order parameter is broken at $\alpha = \alpha_c^{(2)}$. The Binder cumulant given by Eq. (11) will not pick up this transition because $|m|$ does not contain any information on the angular direction of the global magnetization. Therefore, we consider an alternative magnetization measure[26,27]

$$m_\phi = \langle \cos(4\phi) \rangle, \tag{13}$$

where ϕ is the global phase as indicated by Eq. (10). This anisotropy measure vanishes when ϕ is evenly distributed and tends toward unity when the excitation gap opens and ϕ gets localized. We show in Fig. 3 both order parameters for the system $N_x = 74$, $N_\tau = 103$ as a function of α. This N_τ corresponds to the nearest integer N_τ^* at $\alpha \approx \alpha_c^{(1)}$. Actually, the optimal N_τ decreases with increasing α, so the given system size does not represent an optimally chosen aspect ratio for other dissipation strengths. The rotational symmetry of the complex order parameter is clearly seen to be broken at a higher dissipation strength than the onset of the intermediate critical phase.

Because ϕ measures a global rotation of the order parameter, extremely long simulations is needed to explore the ϕ space with a local update algorithm. This limits the efficiency of constructing a Binder cumulant from m_ϕ and extracting $\alpha_c^{(2)}$ from a universal point because this would involve calculating

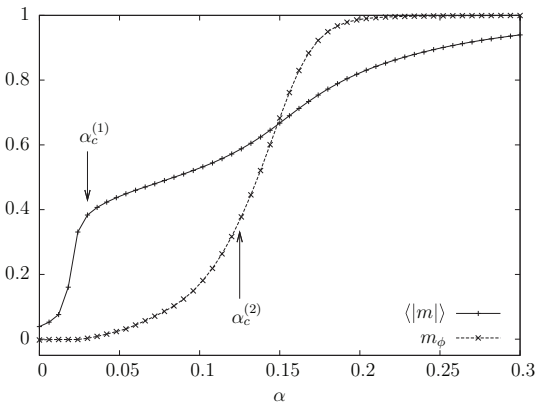

FIG. 3. The order parameter $\langle |m| \rangle$ and the anisotropy measure m_ϕ of the noncompact Z_4 model with $K = 0.75$ and system size $N_x = 74$, $N_\tau = 103 \approx N_\tau^*$. This size represents a near optimal aspect ratio at $\alpha \approx \alpha_c^{(1)}$. The two phase transitions are indicated by arrows, note that the intermediate critical phase $\alpha_c^{(1)} < \alpha < \alpha_c^{(2)}$ features a rotationally symmetric order parameter distribution.

moments of a already statistically compromised ensemble. To alleviate these difficulties, we instead make a scaling ansatz for the anisotropy measure itself,

$$m_\phi = \mathcal{M}_\phi\left(\frac{N_x}{\xi}, \frac{N_\tau}{\xi^z}\right), \tag{14}$$

based on the fact that the naive scaling dimension of this magnetization measure is zero. Near criticality, we expect m_ϕ to scale with system size in the same way as the Binder cumulant Eq. (12). Hence, we may calculate a dynamical critical exponent for this transition by exactly the same procedure as in Sec. V and Ref. 3. Again we expect a merging of m_ϕ curves as $\alpha \to \alpha_c^{(2)}$ from above in the limit of large N_x, but for the present system sizes we use the crossing points of m_ϕ curves to estimate $\alpha_c^{(2)}$. In Fig. 4, we plot the resulting phase diagram in the $\alpha - K$ plane. The intermediate phase is evidently very wide also when compared to the uncertainty assigned to the transition line, and we feel confident that it is a genuine phase and not merely an effect of the admittedly moderate finite system sizes we are restricted to.

We extract the dynamical critical exponent z along both of the critical lines $\alpha_c^{(1)}$ and $\alpha_c^{(2)}$ for all spatial coupling strengths. The data collapse of the Binder cumulant g at $K = 0.75$ and $\alpha = 0.030 \approx \alpha_c^{(1)}$ is shown in Fig. 5. Increasing the dissipation strength further brings the system to the second phase transition at $\alpha = 0.125 \approx \alpha_c^{(2)}$, the collapse of m_ϕ at this point is shown in Fig. 6.

In Table I, we present the numerical estimates of the dynamical critical exponent. The values of z are obtained using the scaling relation $N_\tau^* = a N_x^z$, with uncertainties based on a bootstrap analysis. These uncertainties also include the uncertainty in α_c. Within the accuracy of the simulations, the value of the critical exponent is $z = 1$ for all the coupling values at both phase transitions (although precise results are harder to obtain for the second). This is in accordance with the scaling argument presented in Sec. II.

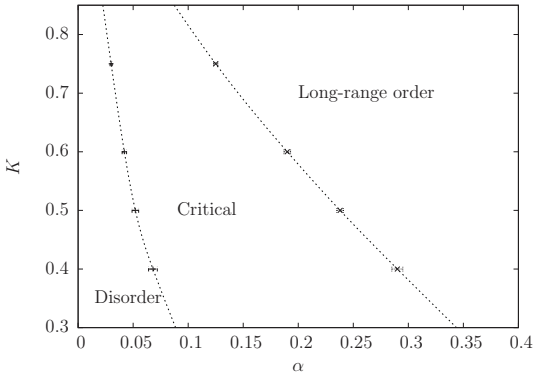

FIG. 4. Phase diagram for the noncompact model, Eq. (8) with $K_\tau = 0.4$. The dotted lines are guides to the eye. For fixed K the model features two consecutive phase transitions surrounding the intermediate critical phase (with quasi-long-range order). The simulation results (symbols along the dotted lines) are restricted to a region in coupling space amenable to simulations.

V. RESULTS: COMPACT MODEL

We now turn to the compact version of the dissipative Z_4 model,

$$S^{\mathrm{C}} = S_\tau^{\mathrm{C}} + S_x + S_{\mathrm{diss}}, \tag{15}$$

where the three terms are given by Eqs. (2), (4), and (5), respectively. Note that we now use a kinetic term S_τ^{C} having the same cosine-form as the spatial interaction term S_x. Regarding the use of the same dissipation term S_{diss} as in the noncompact case, one may argue that adding a Caldeira-Leggett term for the angle differences $\Delta\theta$ is a rather artificial way to model dissipation for a compact clock model in the first place, since its variance under 2π translations of θ implicitly

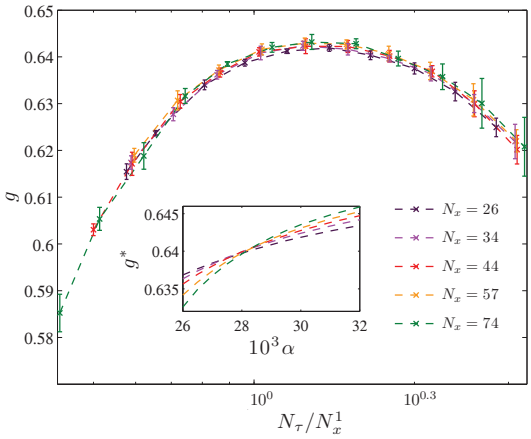

FIG. 5. (Color online) Data collapse of the Binder cumulant, $g = 1 - Q/3$, with Q given by Eq. (11), for the noncompact Z_4 model at $K = 0.75$ and $\alpha = 0.030 \approx \alpha_c^{(1)}$ with $z^{(1)} = 1$. Inset: Intersection of the Binder cumulant as a function of dissipation strength.

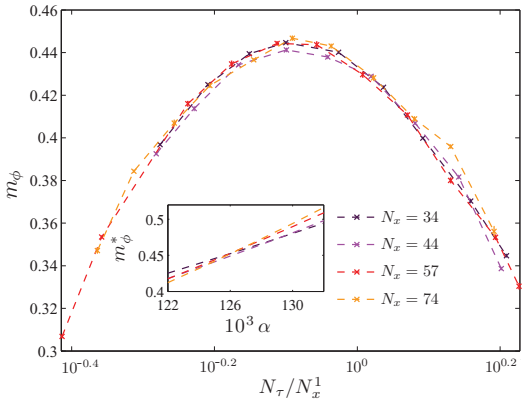

FIG. 6. (Color online) Data collapse of the anisotropy measure m_ϕ, Eq. (13), for the noncompact Z_4 model at $K = 0.75$ and $\alpha = 0.125 \approx \alpha_c^{(2)}$ with $z^{(2)} = 1$. The actual uncertainties are probably larger than indicated by the error bars for reasons discussed in the text. Inset: Intersection of the anisotropy measure as a function of dissipation strength.

assumes noncompact variables. However, adding exactly such a dissipation term is crucial for the demonstration of local quantum criticality in a similar Z_4 model[8] that is not obviously noncompact. Therefore, our motivation for the comparative study in the present section of a compactified version of the action (8) is to investigate whether an equivalent dissipation term for compact variables gives the model the same critical properties as reported for noncompact variables in the previous section, and thus whether the compactness of the variables as such is essential. Constructing an appropriate compactified version of the dissipative model does, however, require a reinterpretation of the variables in the Caldeira-Leggett term, so we will begin with a careful discussion of how we should treat this term in our simulations.

We first impose the following restriction on the interpretation of the compactified dissipation term: The term as a whole should be invariant under translations $\theta \to \theta + 2\pi$, since these two states are indistinguishable. As a corollary, any configurations that are physically indistinguishable when the angles are restricted to four values $\theta \in \{-\pi, -\pi/2, 0, \pi/2\}$ (or any equivalent parametrization) should give the same contribution to the dissipation term. Consequently, we cannot simply simulate the model with the dissipation term (5) as it stands, because the angle differences $\Delta\theta_{x,\tau}$ now only make physical sense modulo 2π. We therefore have to bring

TABLE I. Numerical estimates for critical coupling and critical exponents $z^{(1),(2)}$ for the two phase transitions $\alpha_c^{(1),(2)}$ of the noncompact model.

K	$\alpha_c^{(1)}$	$z^{(1)}$	$\alpha_c^{(2)}$	$z^{(2)}$
0.75	0.030(2)	0.99(1)	0.125(2)	1.01(2)
0.6	0.042(2)	0.99(2)	0.190(3)	0.96(3)
0.5	0.053(2)	1.02(2)	0.238(3)	0.97(3)
0.4	0.068(4)	0.97(3)	0.287(5)	0.99(4)

$\Delta\theta_{x,\tau}$ back to the primary interval $[-\pi,\pi\rangle$, as is well known for phase differences in superconducting systems without dissipation and other realizations of the (compact) XY model. Furthermore, we also choose to do the same for the difference between the two (compactified) $\Delta\theta_{x,\tau}$ terms in Eq. (5), as the alternative would result in different Boltzmann factors being associated with physically equivalent situations. Our procedure then is equivalent to requiring that the entire difference $\Delta\theta_{x,\tau} - \Delta\theta_{x,\tau'}$ should be restricted to the primary interval $[-\pi,\pi\rangle$, i.e., treating the dissipation term as a 2π-periodic function.

The details of the Monte Carlo simulations are described in Sec. III also for the compact model. The only difference that may be of any consequence is that we found it more convenient to vary the spatial coupling while fixing the dissipation strength in this case, but we have checked that the direction in coupling space taken by the simulations has no impact on the result.

The dissipationless ($\alpha = 0$) four-state clock model is completely isomorphic to the Ising model with interaction $K/2$. Thus, we may employ the criterion $\sinh(K_c)\sinh(K_\tau) = 1$ in order to calculate K_c for a fixed value of K_τ. The temporal coupling parameter is fixed at $K_\tau = -\ln(\tanh\frac{1}{2}) \approx 0.7719$ such that $K_c = 1$ when the dissipation is tuned to zero.

The most striking difference we found when compactifying the angles is that the intermediate phase with quasi-long-range order vanishes. This means that one has only a single disorder-order phase transition, as is the result one would usually expect for any model with Z_4 symmetry. We have verified that the Z_4 symmetry and the apparent $U(1)$ symmetry of the complex order parameter (in the disordered phase) are spontaneously broken simultaneously at a single critical point. This is found by observing that the inflection points of magnetization curves for m and m_ϕ coincide asymptotically, in contrast to the curves shown in Fig. 3 for the noncompact case.

The phase diagram for the compact Z_4 model with bond dissipation is shown in Fig. 7. It differs considerably from that

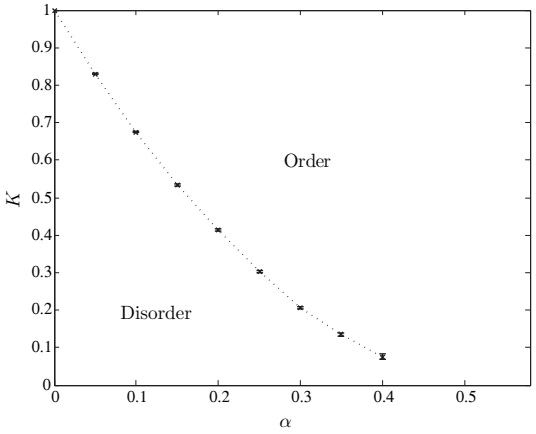

FIG. 7. Phase diagram for the compact model of Eq. (15) with $K_\tau = -\ln(\tanh\frac{1}{2})$, the dotted line indicating a critical line separating the disordered phase from a phase with long-range order. The line is not drawn beyond $\alpha = 0.4$ because of increasing uncertainties.

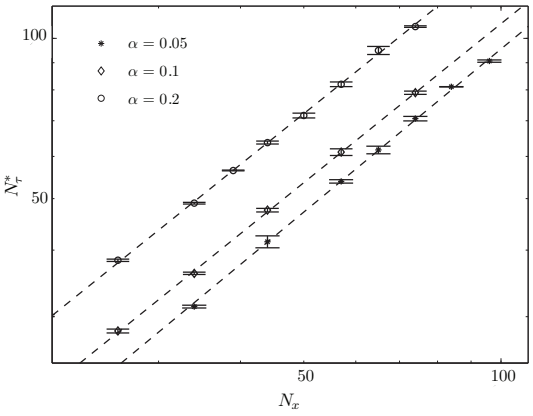

FIG. 8. Finite-size analysis of the maximum N_τ^* of the cumulant curves as a function of spatial system size N_x used to obtain the dynamical critical exponent z for the compact model. The dashed lines show the power-law fits, cf. Table II for the results.

of its noncompact counterpart, not only in the evident absence of any intermediate critical phase, but also in that the limit $\alpha \to 0$ is well behaved. Here, the model is reduced to two uncoupled 2D Ising models, for which exact results are known and simulations are straightforward. In the limit of $K \to 0$ the simulations are on the other hand very difficult for the same reasons as those investigated by us in a similar model in Ref. 3. Therefore, we have not strived to extend the phase diagram all the way down to the α axis in this work. Due to the qualitative difference in the kinetic terms for the compact and noncompact model, it is not possible to make quantitative comparison between the position of the phase transition line in Fig. 7 and the two phase transition lines in Fig. 4.

Turning next to the nature of the critical line in the phase diagram, we show in Fig. 8 and Table II results for the three points along the line for which we made the most effort to extract the dynamical critical exponent. These points are chosen so that the relative influence of the dissipation term should be qualitatively comparable with that for the points $(\alpha_c^{(1)}, K)$ chosen for the first transition of the noncompact model. As for the noncompact model here and the Ising model with bond dissipation studied in Ref. 3, there is no significant variation in the dynamical critical exponent from the expected value $z = 1$, although the tendency to greater finite-size effects for increasing α remains for both the compact and the noncompact model.

TABLE II. Critical coupling K_c and dynamical critical exponent z for different values of the dissipation strength α for the compact model.

α	K_c	z
0.05	0.8303(4)	1.02(2)
0.1	0.6753(7)	0.99(2)
0.2	0.414(2)	0.99(2)

VI. DISCUSSION

The models discussed in this paper are in some sense generalizations of the Ising spin system with bond dissipation discussed in Ref. 3. For the compact Z_4 model the modifications come from the increase of the number of states from $q = 2$ to $q = 4$, while one for the noncompact model adds an additional extension of the configuration space. The phase diagram for the compact model is very much like that observed for the dissipative Ising model,[3] both featuring a single order-disorder phase transition line. The noncompact model on the other hand exhibits much richer physics in the sense that it presents, for fixed K and K_τ, two phase transitions surrounding an intermediate critical phase with power-law decaying spin correlations and emergent $U(1)$ symmetry. The most pressing question then pertains to the occurrence of this phase: Why is the discrete structure of the angle variables rendered irrelevant in a region of parameter space for our Z_4 model, when such behavior is previously known to occur only in Z_q models with $q > 4$? Even our compactified model differs from a pure $Z_4 = Z_2 \times Z_2$ clock model, since the dissipation term couples the two underlying Z_2 models in a nontrivial way. Such models can no longer be expected *a priori* to behave as an Ising model, and there is in principle no reason why they may not even present intermediate phases. The absence of such a phase in our compact model does however indicate that we must turn to the other obvious difference between our model and a Z_4 clock model, namely that the variables in our noncompact model are free to drift outside the primary interval. Somehow, this added degree of freedom is enough to close the excitation gap.

As observed in Fig. 4, the underlying Z_4 symmetry stemming from the discreteness of the variables is irrelevant in the intermediate phase. Consequently, the system displays an effective continuous symmetry. Since $z = 1$, the effective long-wavelength low-energy propagator is on a Gaussian form $1/(\omega^2 + q^2)$. In addition, the system is effectively two dimensional due to $z = 1$. In two dimensions, Gaussian fluctuations are sufficient to induce a critical phase given a continuous symmetry. This is analogous to the mechanism producing a critical phase in the classical 2D XY model with an $Z_{q>4}$ anisotropy[12] [soft constraint with underlying $U(1)$ symmetry], and also for classical $Z_{q>4}$ clock models[14] (hard constraint). The difference in our case is that the underlying symmetry is $Z_{q=4}$.

To comment further on the origin of the critical phase, it appears that the quadratic form of the kinetic energy in the problem is essential for observing it. This quadratic short-range interaction term in imaginary time facilitates Gaussian fluctuations. Were we to use a cosine-like form of this term for noncompact variables (as one does for compact variables), this intermediate phase would not be found. The kinetic energy term is bounded from below, but not from above. Upon entering the intermediate phase from the ordered side, this term tends to suppress strong θ fluctuations, much more so than a kinetic term which is bounded from below *and* above, such as a cosine-like term. Only at even lower values of the dissipation are the excitation energies of larger θ fluctuations so low that wild θ fluctuations are possible due to the boundedness of the spatial coupling. At this point, the system disorders completely. If the quadratic kinetic energy term is replaced by a cosine-like term, wild θ fluctuations are facilitated precisely at the critical point where the Z_4 symmetry becomes irrelevant, and the system disorders directly from the Z_4-ordered state. Hence, for a compact model there will only be one phase transition separating the Z_4-ordered state from the completely disordered phase.

We now comment on the critical scaling between space and imaginary time in the models we have studied. For the compact case one has the conventional case of a critical line along which the correlation length diverges as $\xi \sim |K - K_c|^{-\nu}$ in space and $\xi_\tau \sim |K - K_c|^{-z\nu}$ in imaginary time, with z appearing to remain equal to unity along the line. This picture is no longer valid in the noncompact case, as ξ and ξ_τ are formally infinite in the entire intermediate critical phase, and z cannot be defined from the anisotropy of their divergence in this region. Furthermore, supposing that the intermediate phase shares qualities with the corresponding phase in classical $Z_{q>4}$ models, the correlation lengths can be expected to diverge exponentially as this critical phase is approached from either side as for the Kosterlitz-Thouless (KT) transition, and not as a power law as for conventional critical points. However, as long as the correlation length *does* diverge, and this divergence is exponential both in space and imaginary time, the dynamical critical exponent is still well defined through $\xi_\tau \sim \xi^z$. Therefore, our finite size analysis is valid as $\alpha \to \alpha_c^{(1)^-}$ and $\alpha \to \alpha_c^{(2)^+}$ irrespective of whether these points turns out to possess KT criticality or not. At both phase transitions we have $z = 1$, signaling equally strong divergence of correlation lengths in space and imaginary time.

To infer from simulations on finite systems that the correlation length in fact diverges exponentially is exceedingly difficult,[29–31] and we have not attempted to determine the exact nature of the phase transitions, but leave this an open question. The phase transitions (one or both) may be in the KT universality class, or it may belong to a class of related topological phase transitions.[25] This identification of the exact universality class is controversial even for classical clock models.[24,32,33]

If we generalize the noncompact action in Sec. IV by redefining the phase space such that the variable can take on all real values, Eq. (8) may represent the action for a one-dimensional array of Josephson junctions.[5,6] Recent theoretical work[34,35] report that such systems may display local quantum criticality, in the sense that the spatial coupling renormalizes to zero at the quantum phase transition so that the behavior is essentially $(0 + 1)$ dimensional. This suggests that local quantum criticality need not be restricted to $(2 + 1)$D models such as the one presented in Ref. 8, but that similar unconventional criticality may be found in $(1 + 1)$D as well. Although it should be remembered that our $(1 + 1)$D model has discrete angle variables, our simulations do not show any traces of local critical behavior, in the sense that the scaling of Binder cumulants do not give $z \gg 1$.

Strictly speaking, the dynamical critical exponent is not well defined inside the intermediate phase, and the isotropic behavior is instead maintained by the decay exponents for the power-law spin correlation functions in space and time being equal. Nevertheless, for finite N_x one may still assume the

scaling relation $N_\tau^* = aN_x^z$ and use the ordinary procedure to extract the (effective) exponent z as long as the system is critical, which yields $z \approx 1$ in the entire intermediate phase. We may then inspect how the nonuniversal prefactor a changes as a reflection of the anisotropy of the interaction in time and space. In the noncompact model it is possible to investigate the development of a at constant K_τ/K and varying α without leaving the critical region. We find that a decreases for increasing α, indicating that the dissipation term contributes to making the temporal dimension less ordered than the spatial one. This is also in contrast with a tendency toward $(0+1)$D behavior when increasing the dissipation strength, as suggested in the models mentioned above.

VII. CONCLUSIONS

We have performed Monte Carlo simulations on two distinct Z_4-symmetric dissipative lattice models. In one model the phase variables are only defined on the interval $[0,2\pi\rangle$, while the other model has no restrictions on the variables. The different domains of the variables have implications for the short-range interaction term in imaginary time, which again leads to essential differences in the behavior of the two models. The compact model features only one phase transition in which the Z_4 symmetry is spontaneously broken. On the other hand, the noncompact model displays three phases, namely a disordered phase with exponentially decaying spin correlations, an intermediate critical phase with quasi-long-range order, and finally a long-range ordered phase.

Along the phase-transition line of the compact model, we find the dynamic critical exponent $z = 1$, independent of the dissipation strength. In the noncompact model, we find the value $z = 1$ for both phase transitions and the power-law decay exponents for space and imaginary time are equal in the entire phase exhibiting quasi-long-range order.

We have shown that the issue of compactness versus noncompactness of the fundamental variables of the Z_4 models have important ramifications for their long-distance, low-energy physics.

ACKNOWLEDGMENTS

The authors acknowledge useful discussions with Egil V. Herland, Mats Wallin, and Henrik Enoksen. A.S. was supported by the Norwegian Research Council under Grant No. 167498/V30 (STORFORSK). E.B.S. and I.B.S thank NTNU for financial support. The work was also supported through the Norwegian consortium for high-performance computing (NOTUR).

APPENDIX: QUANTUM-TO-CLASSICAL MAPPING FOR COMPACT AND NONCOMPACT VARIABLES

In this appendix we will outline the quantum-to-classical mapping for a quantum rotor model and show how the kinetic term in the resulting classical model depends on whether the variables are interpreted as compact or noncompact. We will first reproduce the derivation as given in Refs. 36 and 37, for the case of compact variables, after which we will generalize and reinterpret it for the noncompact case. Although there is nothing novel about this derivation, the form of the kinetic term often seems to be taken for granted in the literature, and a correct interpretation of the classical action in the noncompact case is crucial for our results. As a starting point we take the (dissipationless) Hamiltonian $H_0 = T + U$ for a spatially extended system of particles, each moving on a ring. The kinetic energy of the rotors is given by

$$T = -\frac{1}{2I}\sum_x \frac{\partial^2}{\partial\theta_x^2}, \tag{A1}$$

where I is some inertia parameter. The (periodic) potential energy is given by Josephson-like coupling of the rotors,

$$U = -K\sum_x \cos(\hat{\theta}_{x+1} - \hat{\theta}_x), \tag{A2}$$

with K being the coupling strength. Here we have used the angle representation where we for simplicity let θ be a continuous variable, and $\hat{\theta}$ is the corresponding operator. Characteristic of a rotor model is the invariance of the system upon translations of the angle $\theta \to \theta + 2\pi$. The eigenfunctions describing the system should therefore be 2π periodic, a requirement which immediately yields discretized angular momenta and energy levels.

The partition function of the rotor system may be given by

$$\mathcal{Z} = \mathrm{Tr}(\mathrm{e}^{-\beta(T+U)}). \tag{A3}$$

We let $k_B = 1$ such that β equals inverse temperature. The trace may be evaluated by introducing a path integral over M time slices between $\tau = 0$ and $\tau = \beta$, with the width of the time slices given by $\Delta\tau = \beta/M$. For every time step indexed by τ, we insert a complete set of states,

$$\mathcal{Z} \approx \lim_{M\to\infty}\int \mathcal{D}\theta \prod_{\tau=0}^{M-1} \langle\theta(\tau+1)|\mathrm{e}^{-\Delta\tau T}\mathrm{e}^{-\Delta\tau U}|\theta(\tau)\rangle. \tag{A4}$$

Here, $|\theta(\tau)\rangle$ is an angular eigenstate of all rotors with Trotter index τ. Since $|\theta(\tau)\rangle$ is an eigenstate of $\hat{\theta}$ we get

$$\mathrm{e}^{-\Delta\tau U}|\theta(\tau)\rangle = |\theta(\tau)\rangle\mathrm{e}^{K\cos(\theta_{x+1,\tau}-\theta_{x,\tau})}. \tag{A5}$$

A general matrix element describing the kinetic energy is given by

$$T_{x,\tau} = \langle\theta_x(\tau+1)|\mathrm{e}^{-\Delta\tau T}|\theta_x(\tau)\rangle. \tag{A6}$$

Next, for each τ we insert a complete set of eigenstates of the kinetic energy $|n_x(\tau)\rangle$. Because θ and n are conjugate variables, we have the identity $\langle n_x(\tau)|\theta_x(\tau)\rangle = \exp[-in_{x,\tau}\theta_{x,\tau}]$. Inserting this, we get the general form of the matrix element for the kinetic energy

$$T_{x,\tau} = \sum_{n_{x,\tau}} \mathrm{e}^{in_{x,\tau}\theta_{x,\tau+1}}\mathrm{e}^{-in_{x,\tau}\theta_{x,\tau}}\mathrm{e}^{-\frac{1}{2I}\Delta\tau n_{x,\tau}^2}. \tag{A7}$$

Using the Poisson summation formula, we may write the summation over integer-valued angular momenta in Eq. (A7)

as an integral over the continuous field $\tilde{n}$ at the cost of introducing another summation variable m:

$$\begin{aligned} T_{x,\tau} &= \sum_{m=-\infty}^{\infty} \int \mathrm{d}\tilde{n} \mathrm{e}^{\mathrm{i}\tilde{n}(\theta_{x,\tau+1}-\theta_{x,\tau})-\frac{1}{2I}\Delta\tau\tilde{n}^2} \mathrm{e}^{2\pi\mathrm{i}m\tilde{n}} \\ &= \sum_{m=-\infty}^{\infty} \mathcal{C}\mathrm{e}^{-\frac{I}{2\Delta\tau}(\theta_{x,\tau+1}-\theta_{x,\tau}-2\pi m)^2} \\ &\approx \mathcal{C}\mathrm{e}^{K_\tau \cos(\theta_{x,\tau+1}-\theta_{x,\tau})}, \end{aligned} \tag{A8}$$

where $K_\tau = \frac{I}{\Delta\tau}$, and $\mathcal{C} = \sqrt{\frac{2\pi I}{\Delta\tau}}$ is a constant prefactor which is henceforth dropped from the expressions. The last approximation of Eq. (A8) is the Villain approximation of the cosine function, which is known not to alter the universality class of the phase transition.

Reintroducing the matrix elements to the partition function and renaming $\Delta\tau K \to K$, we get

$$Z = \int \mathcal{D}\theta \mathrm{e}^{K_\tau \sum_\tau \sum_x \cos(\theta_{x,\tau+1}-\theta_{x,\tau})} \mathrm{e}^{K \sum_\tau \sum_x \cos(\theta_{x+1,\tau}-\theta_{x,\tau})}, \tag{A9}$$

i.e., an anisotropic XY model in $(1+1)$ dimensions. Note however, that we were able to cast the kinetic energy matrix element into the form of a sequence of Gaussians because the angular momentum eigenvalues where restricted to integer values. This is only the case when the canonical conjugate variable θ is restricted to a $[0,2\pi\rangle$ interval. In other words, the partition function given in Eq. (A9) reflects the interpretation of Eqs. (A1) and (A2) in terms of rotors.

Equations (A1) and (A2) may also describe particles moving in an extended potential, in which case the state of the system after a 2π translation is distinguishable from the state prior to the translation. Introducing dissipation to this system by coupling $\Delta\theta$ to a bosonic bath explicitly breaks the peri odicity of the quantum Hamiltonian, and consequently the variable θ should be treated as an extended variable from the outset. This necessitates a modification of the above procedure as the summation over the eigenstates in Eq. (A7) has to be replaced by an integral over a continuum of momentum states. Then, the kinetic energy matrix element instead becomes

$$\begin{aligned} T_{x,\tau} &= \int \mathrm{d}n_{x,\tau} \mathrm{e}^{\mathrm{i}n_{x,\tau}(\theta_{x,\tau+1}-\theta_{x,\tau})-\frac{1}{2I}\Delta\tau n_{x,\tau}^2} \\ &= \mathrm{e}^{-\frac{I}{2\Delta\tau}(\theta_{x,\tau+1}-\theta_{x,\tau})^2}, \end{aligned} \tag{A10}$$

where a constant factor has been ignored. Inserting this expression into the kinetic part of the partition function yields

$$\begin{aligned} \mathcal{Z}_\tau &= \lim_{M\to\infty} \int \mathcal{D}\theta \mathrm{e}^{-\frac{I}{2}\sum_{\tau=0}^{M-1}\Delta\tau(\frac{\theta_{x,\tau+1}-\theta_{x,\tau}}{\Delta\tau})^2} \\ &\equiv \int \mathcal{D}\theta \mathrm{e}^{-\frac{I}{2}\int_0^\beta \mathrm{d}\tau(\frac{\partial\theta_x}{\partial\tau})^2}. \end{aligned} \tag{A11}$$

The continuum expression for the action is the one conventionally stated in the literature both for compact and noncompact variables. However, it is always implicit that the imaginary time dimension is discrete by construction,[38] and for most numerical computations it has to be treated as such in any case. One then has to choose one of two alternative discretizations of the short-range interaction in the imaginary time direction, depending on the interpretation of the system and the compactness of the variables. As shown above, the cosine-like term of Eq. (2) is the natural discretization for compact variables, whereas the quadratic term used in Eq. (3) is associated naturally to noncompact variables.

[1] A. O. Caldeira and A. J. Leggett, Ann. Phys. (NY) **149**, 374 (1983).
[2] P. Werner, K. Völker, M. Troyer, and S. Chakravarty, Phys. Rev. Lett. **94**, 047201 (2005).
[3] I. B. Sperstad, E. B. Stiansen, and A. Sudbø, Phys. Rev. B **81**, 104302 (2010).
[4] J. A. Hertz, Phys. Rev. B **14**, 1165 (1976).
[5] S. Chakravarty, G.-L. Ingold, S. Kivelson, and A. Luther, Phys. Rev. Lett. **56**, 2303 (1986).
[6] S. Chakravarty, G.-L. Ingold, S. Kivelson, and G. Zimanyi, Phys. Rev. B **37**, 3283 (1988).
[7] G. Schön and A. D. Zaikin, Phys. Rep. **198**, 237 (1990).
[8] V. Aji and C. M. Varma, Phys. Rev. Lett. **99**, 067003 (2007).
[9] V. Aji and C. M. Varma, Phys. Rev. B **79**, 184501 (2009).
[10] K. Børkje and A. Sudbø, Phys. Rev. B **77**, 092404 (2008).
[11] M. S. Grønsleth, T. B. Nilssen, E. K. Dahl, E. B. Stiansen, C. M. Varma, and A. Sudbø, Phys. Rev. B **79**, 094506 (2009).
[12] J. V. José, L. P. Kadanoff, S. Kirkpatrick, and D. R. Nelson, Phys. Rev. B **16**, 1217 (1977).
[13] H. H. Roomany and H. W. Wyld, Phys. Rev. B **23**, 1357 (1981).
[14] S. Elitzur, R. B. Pearson, and J. Shigemitsu, Phys. Rev. D **19**, 3698 (1979).
[15] E. Luijten and H. Blöte, Int. J. Mod. Phys. C **6**, 359 (1995).
[16] U. Wolff, Phys. Rev. Lett. **62**, 361 (1989).
[17] P. Werner and M. Troyer, Phys. Rev. Lett. **95**, 060201 (2005).
[18] P. Werner, G. Refael, and M. Troyer, J. Stat. Mech.: Theory Exp. (2005) P12003.
[19] P. Werner and M. Troyer, Prog. Theor. Phys. Suppl. **160**, 395 (2005).
[20] K. Hukushima and K. Nemoto, J. Phys. Soc. Jpn. **65**, 1604 (1996).
[21] H. G. Katzgraber, Modern Computation Science, Oldenburg, Germany, 16-28 August 2009, (unpublished).
[22] M. Matsumoto and T. Nishimura, ACM Trans. Model. Comput. Simul. **8**, 3 (1998).
[23] A. M. Ferrenberg and R. H. Swendsen, Phys. Rev. Lett. **63**, 1195 (1989).
[24] C. M. Lapilli, P. Pfeifer, and C. Wexler, Phys. Rev. Lett. **96**, 140603 (2006).
[25] S. K. Baek and P. Minnhagen, Phys. Rev. E **82**, 031102 (2010).
[26] S. K. Baek, P. Minnhagen, and B. J. Kim, Phys. Rev. E **80**, 060101(R) (2009).
[27] J. Lou, A. W. Sandvik, and L. Balents, Phys. Rev. Lett. **99**, 207203 (2007).
[28] J. Hove and A. Sudbø, Phys. Rev. E **68**, 046107 (2003).
[29] D. Loison, J. Phys.: Condens. Matter **11**, L401 (1999).

[30]E. Luijten and H. Meßingfeld, Phys. Rev. Lett. **86**, 5305 (2001).
[31]M. Itakura, J. Phys. Soc. Jpn. **70**, 600 (2001).
[32]C.-O. Hwang, Phys. Rev. E **80**, 042103 (2009).
[33]S. K. Baek, P. Minnhagen, and B. J. Kim, Phys. Rev. E **81**, 063101 (2010).
[34]S. Tewari, J. Toner, and S. Chakravarty, Phys. Rev. B **72**, 060505(R) (2005).
[35]S. Tewari, J. Toner, and S. Chakravarty, Phys. Rev. B **73**, 064503 (2006).
[36]M. Wallin, E. S. Sørensen, S. M. Girvin, and A. P. Young, Phys. Rev. B **49**, 12115 (1994).
[37]S. L. Sondhi, S. M. Girvin, J. P. Carini, and D. Shahar, Rev. Mod. Phys. **69**, 315 (1997).
[38]J. W. Negele and H. Orland, *Quantum Many-Particle Systems* (Perseus Books, Reading, MA 1998).

Paper III

Quantum criticality in a dissipative (2+1)-dimensional XY model of circulating currents in high-T_c cuprates.

Phys. Rev. B **84**, 180503 (2011).

RAPID COMMUNICATIONS

PHYSICAL REVIEW B **84**, 180503(R) (2011)

Quantum criticality in a dissipative (2+1)-dimensional XY model of circulating currents in high-T_c cuprates

Iver Bakken Sperstad, Einar B. Stiansen, and Asle Sudbø

Department of Physics, Norwegian University of Science and Technology, N-7491 Trondheim, Norway

(Received 20 September 2011; revised manuscript received 14 October 2011; published 8 November 2011)

We present large-scale Monte Carlo results for the dynamical critical exponent z and the spatio-temporal two-point correlation function of a (2+1)-dimensional quantum XY model with bond dissipation, proposed to describe a quantum critical point in high-T_c cuprates near optimal doping. The phase variables of the model, originating with a parametrization of circulating currents within the CuO_2 unit cells in cuprates, are compact, $\{\theta_{\mathbf{r},\tau}\} \in [-\pi,\pi\rangle$. The dynamical critical exponent is found to be $z \approx 1$, and the spatio-temporal correlation functions are explicitly demonstrated to be isotropic in space-imaginary time. The model thus has a fluctuation spectrum where momentum and frequency enter on equal footing, rather than having the essentially momentum-independent marginal Fermi-liquid-like fluctuation spectrum previously reported for the same model.

DOI: 10.1103/PhysRevB.84.180503 PACS number(s): 74.72.Kf, 74.20.Mn, 74.40.Kb, 71.10.Hf

Quantum critical points describe systems with diverging length scales at zero temperature, and have come into much focus in recent years as possible descriptions of anomalous phenomena in strongly correlated fermion systems and systems with competing orders.[1] One prime example of this is represented by the high-T_c superconducting cuprates, where various types of quantum critical phenomena have been proposed as essential for understanding the many unusual normal-state transport properties these systems exhibit. This has, over the past quarter of a century, represented one of the major challenges in condensed-matter physics.[2]

One successful phenomenological framework is to describe the the normal phase around optimal doping as a marginal Fermi liquid (MFL),[3] the weakest possible violation of having a nonzero quasiparticle residue at the Fermi surface. Among the merits of the MFL phenomenology is that it describes transport properties in this strange metallic phase in good accordance with experiments. This follows naturally from the essentially momentum-independent, linear-in-frequency, fluctuation spectrum of the MFL hypothesis.[3]

More recent works have pursued a more microscopic foundation of MFL. The underlying picture is that there exists a quantum critical point (QCP) residing at $T = 0$ beneath the superconducting dome.[4] The degrees of freedom associated with this QCP are circulating currents within the unit cells of the CuO_2 layers. The main idea is that the MFL phenomenology arises from the quantum critical fluctuations of these currents above the QCP at $T > T_c$. It has also been demonstrated how the same fluctuations may give rise to d-wave high-T_c superconductivity.[5] The ordering of such circulating currents upon lowering the temperature from the strange metal region into the pseudogap region is a candidate for a possible competing order in this part of the phase diagram.[6] Magnetic order conforming with such circulating currents has in fact been observed in several experiments.[7–11] It must be mentioned that others argue that such signatures may have a quite different origin,[12–15] and also numerical results disagree on the presence of such circulating currents,[16–18] but the model remains one of the central theories of the physics of high-T_c cuprates.[2,19]

A remarkable implication of a q-independent fluctuation spectrum, such as that posited in MFL theory, is that the associated QCP exhibits *local* quantum criticality (LQC). Defining the dynamical critical exponent z from the scaling of momentum and frequency at the quantum critical point, $\omega \sim q^z$, this means that, formally, $z = \infty$. It is a highly nontrivial question as to how such a remarkable property of a quantum critical point can arise in an extended system. Recently, it was argued[20,21] that precisely such local criticality is found in a (2+1)-dimensional quantum XY model with bond dissipation of the Caldeira-Leggett[22] form. The angle variables of this model were associated with circulating current degrees of freedom, as will be explained below.

The results of Ref. 20 would imply that the previously hypothesized MFL fluctuation spectrum has been derived from a microscopic theory applicable to cuprates. In a broader perspective, it is of considerable interest to investigate in detail if such unusual behavior can occur in model systems of condensed matter, as related variants of locality have also been considered in the context of gauge/gravity duality[23] and QCPs in disordered systems and heavy fermion compounds.[1]

From naive scaling arguments[24,25] applied to the dissipative model proposed in Ref. 20, one might expect that dissipation is irrelevant in the renormalization group sense. The result would then not be LQC, but instead conventional quantum criticality with isotropic scaling $z = 1$. Here, we report results from Monte Carlo simulations performed directly on the (2+1)-dimensional quantum XY model with bond dissipation and compact angle variables, considered in Ref. 20. Our results strongly indicate that in this model $z = 1$.

The dissipative (2+1)-dimensional [(2+1)D] XY action considered in Ref. 20 takes the form

$$\begin{aligned} S = &-K \sum_{\langle \mathbf{r},\mathbf{r}'\rangle} \sum_{\tau=1}^{L_\tau} \cos(\Delta\theta_{\mathbf{r},\mathbf{r}',\tau}) \\ &-K_\tau \sum_{\mathbf{r}} \sum_{\tau=1}^{L_\tau} \cos(\theta_{\mathbf{r},\tau+1} - \theta_{\mathbf{r},\tau}) \\ &+\frac{\alpha}{2} \sum_{\langle \mathbf{r},\mathbf{r}'\rangle} \sum_{\tau\neq\tau'}^{L_\tau} \left(\frac{\pi}{L_\tau}\right)^2 \frac{(\Delta\theta_{\mathbf{r},\mathbf{r}',\tau} - \Delta\theta_{\mathbf{r},\mathbf{r}',\tau'})^2}{\sin^2\left(\frac{\pi}{L_\tau}|\tau-\tau'|\right)} \end{aligned} \quad (1)$$

when put on a cubic $L \times L \times L_\tau$ lattice. The bond variables are given by $\Delta\theta_{\mathbf{r},\mathbf{r}',\tau} = \theta_{\mathbf{r},\tau} - \theta_{\mathbf{r}',\tau}$, where the sum over $\mathbf{r}$ and $\mathbf{r}'$

goes over nearest neighbors in the x-y plane. Periodic boundary conditions are implicit in the imaginary time direction, and are also applied in the spatial directions.

Such a model has previously been employed as an effective description of a resistively shunted Josephson junction array,[26] and it may also be viewed as a generic quantum rotor model with dissipative currents. A third possible interpretation in the context of high-T_c cuprates is as follows. Suppose the angles θ *a priori* can take only four possible values. These four values then represent the directions of a pseudospin associated with the four possible ordered circulating current patterns within each CuO_2 unit cell (see, e.g., Fig. 1 of Ref. 27). The first two terms represent the standard interaction energies in space-imaginary time of these circulating currents in neighboring unit cells, and have been derived from microscopics.[27] The last term is the term responsible for dissipating the ordered circulating currents.[20]

In Eq. (1), the angles are continuous variables. We will discuss a possible *a posteriori* justification for this later in this Rapid Communication by showing that an added fourfold anisotropy term is perturbatively irrelevant. Reference 20, moreover, appears to treat $\theta_{\mathbf{r},\tau}$ as compact variables, also in the presence of a dissipation term that apparently renders the action nonperiodic in the angle variables.[28] In order to investigate numerically the same model considered in Ref. 20, we therefore *compactify* the expression $\Delta\theta_{\mathbf{r},\mathbf{r}',\tau} - \Delta\theta_{\mathbf{r},\mathbf{r}',\tau'}$ so that it is defined modulo 2π. We will discuss alternative choices later.

The calculations of Ref. 20 were not restricted to any specific parameter regime, but predicted that every point on the $T = 0$ quantum critical surface in $\alpha - K - K_\tau$ (parameter) space (for $\alpha > 0$) should be a local QCP. Accordingly, we choose convenient coupling constants when searching for LQC in our simulations, and for the results presented here, the dissipation strength is fixed at $\alpha = 0.05$.

The phase diagram (not shown) is qualitatively very similar to those found for related compact (1+1)D models with bond dissipation.[25,29] It features a single critical surface that separates a disordered from a fully ordered phase, and which is continuously connected to the 3D XY critical line at $\alpha = 0$. For similar models in (1+1) dimensions, only the region of relatively moderate dissipation was accessible to simulations, as increasing α increases finite-size effects, resulting in apparent values $z < 1$ for the dynamical critical exponent. As expected, this problem is no less severe in (2+1) dimensions. Available system sizes are restricted by the absence of cluster algorithms to treat models with bond dissipation appropriately,[25] and we are therefore confined to local Metropolis updates.

To locate the phase transition, we vary the spatial coupling K and use the crossing point for different system sizes L of the Binder cumulant $g = 1 - \langle|m|^4\rangle/(2\langle|m|^2\rangle^2)$. Here, $m = \sum_{\mathbf{r},\tau} \exp[i\theta_{\mathbf{r},\tau}]$ is the order parameter of the $U(1)$-symmetric degrees of freedom. Due to the anisotropy of the interactions, we have to calculate g for multiple values of L_τ for each spatial system size L, as described in more detail, e.g., in Ref. 25. The value $L_\tau = L_\tau^*$ where the function $g(L_\tau)$ reaches its maximum corresponds to the *optimal* temporal extent for which the system appears as isotropic as it can be, the anisotropic interactions taken into account.

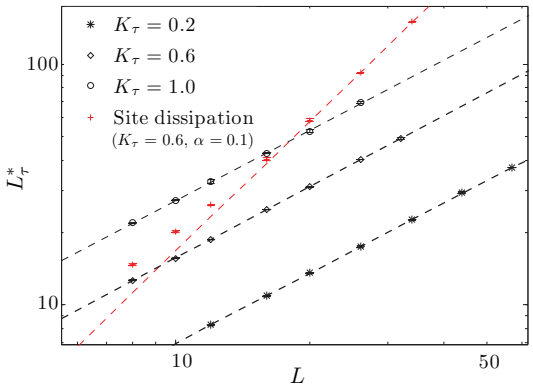

FIG. 1. (Color online) Finite-size analysis of the maximum L_τ^* of the Binder cumulant curves $g(L_\tau)$ as a function of spatial system size L. For the black data points, the dynamical critical exponents z as given in Table I are obtained from the slope of the fitting lines (dashed). The red (gray) points show similar results for site dissipation for comparison, where a fit of the three largest systems yields $z = 1.84(3)$.

For a conventional QCP, at which the correlation length ξ_τ in imaginary time scales with the correlation length ξ in space as $\xi_\tau \sim \xi^z$ with a finite z, we expect to observe the scaling relation $L_\tau^* \sim L^z$. This scaling procedure then allows one to extract the dynamical critical exponent z from Binder cumulant data. For a local QCP formally having $z = \infty$, we expect this scaling to break down. Our strategy to search for possible LQC in the model (1) is therefore to perform the above procedure *assuming* conventional criticality, and then look for indications that this hypothesis should be rejected.

The results of this finite-size analysis is shown in Fig. 1, with the values of the dynamical critical exponent z given in Table I. Here, we have chosen three different values of the quantum coupling K_τ in order to investigate both the limit of relatively weak quantum coupling and the opposite limit leading to relatively strong system anisotropy.

The results show that the effective dynamical critical exponent is $z \lesssim 1$ for all the parameter sets considered, and we expect that we could obtain $z \approx 1$ if we were able to reach higher values of L. (For a smaller value $\alpha = 0.02$, we obtained $z = 1$ within statistical uncertainty.) It is conceivable that signatures of LQC would be visible only for systems larger than the admittedly moderate system sizes accessible to present algorithms. However, were that the case, the true

TABLE I. Critical coupling K_c and dynamical critical exponent z for different values of the quantum coupling K_τ, but for the same dissipation strength $\alpha = 0.05$. Uncertainty estimates for z have been calculated by a bootstrap procedure, including the uncertainty in K_c.

K_τ	K_c	z
0.2	0.48068(5)	0.968(8)
0.6	0.28244(4)	0.985(8)
1.0	0.18008(5)	0.970(11)

$z \to \infty$ nature of the model would likely reveal itself as strongly increasing effective values of z as a finite-size effect for increasing L. For comparison, we have also carried out simulations with equivalent parameters of a (2+1)D XY model with *site* dissipation, for which $z = 2$ is expected.[25,30] The results are included in Fig. 1, and already for system sizes comparable to those for bond dissipation, we observe (finite-size) crossover behavior with $z \to 2$. For bond dissipation, we observe no tendency toward $z > 1$ for either of the parameter sets, and it is hard to imagine how crossover to $z \to \infty$ scaling should be much slower than crossover to $z = 2$ scaling.

For all results reported here, we have used parallel tempering[31] to reduce autocorrelation times, and to ensure that the simulations are well equilibrated. To emulate the continuous $U(1)$ symmetry, the simulations are made for Z_q clock models, with $q = 128$ for $K_\tau = 0.2, 1.0$, and $q = 32$ for $K_\tau = 0.6$. The nature of the criticality remains unchanged also when increasing to $q = 1024$. The results are obtained using an implementation of the Mersenne Twister[32] random number generator, but other random number generators produced consistent results.

Although we found no indication of LQC from the scaling of the Binder cumulant, we also considered the correlations of the order parameter field directly

$$C(\mathbf{r} - \mathbf{r}', \tau - \tau') = \langle e^{i\theta_{\mathbf{r},\tau}} e^{-i\theta_{\mathbf{r}',\tau'}} \rangle. \tag{2}$$

The correlation functions presented here are obtained for the parameter set $K_\tau = 0.6$, with $L_\tau = L_\tau^*$ and $K = K_c$ as obtained from the previous simulations, and therefore serve as a self-consistency check of the Binder scaling procedure. From Fig. 2, it is evident that the correlation function at the critical point decays isotropically in space-imaginary time. In other words, there are no signs of locality.

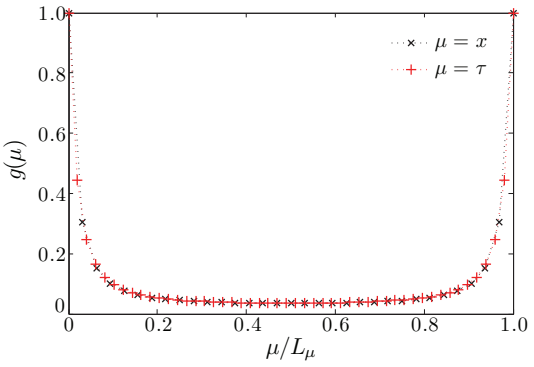

FIG. 2. (Color online) Correlation functions at the critical point $K_c = 0.282\,44$ for dissipation strength $\alpha = 0.05$ and quantum coupling $K_\tau = 0.6$. The system size $L = 32$, $L_\tau = 49 \approx L_\tau^*$ corresponds to the rightmost data point of the midmost data series in Fig. 1. The correlation function is defined in the spatial direction as $g(x) = g(|\mathbf{r} - \mathbf{r}'|) = C(\mathbf{r} - \mathbf{r}', 0)$ and in the temporal direction as $g(\tau) = C(\mathbf{0}, \tau)$, with C defined in Eq. (2). Also, $L_x \equiv L$. Error bars are smaller than the linewidth, and the dotted lines are guides to the eye.

Furthermore, we have verified that the same conclusion may be drawn for the other values of K_τ considered, and also for larger system sizes with aspect ratios found from extrapolation based on the power law shown in Fig. 1. As an additional test, we compared the correlation functions shown here with those obtained by setting $\alpha = 0$ in Eq. (1). Letting $K_\tau > K$, values of L_τ and K_c were determined by the same procedure as for the dissipative model. There is no indication that adding dissipation changes the scaling of the temporal correlation length ξ_τ with respect to the spatial correlation length ξ.

Depending on how $\Delta\theta_{\mathbf{r},\mathbf{r}',\tau}$ is interpreted in the dissipation term, it may be argued either that the correct treatment is to compactify only the gradients $\Delta\theta_{\mathbf{r},\mathbf{r}',\tau}$, restricting them to the interval $[-\pi, \pi\rangle$, or to do so to the difference $\Delta\theta_{\mathbf{r},\mathbf{r}',\tau} - \Delta\theta_{\mathbf{r},\mathbf{r}',\tau'}$ as well. Although we have chosen the latter, as in Ref. 29, we also performed simulations with the former compactification scheme. The results are qualitatively similar, with the difference merely amounting to a renormalization of the dissipative coupling α. In other words, the absence of LQC in this model is not contingent on the choice of compactification scheme.

As explained in connection with Eq. (1), the underlying circulating current degrees of freedom are most naturally described by discrete, Z_4-symmetric variables. In Ref. 21, it was argued that a model with continuous $U(1)$ symmetry nonetheless would be a correct description. The result of LQC would then also apply to the four-state model of the original degrees of freedom since a fourfold anisotropy field, given by

$$S_4 = h_4 \sum_{\mathbf{r},\tau} \cos(4\theta_{\mathbf{r},\tau}), \tag{3}$$

would be irrelevant at the critical point of the action (1). We have investigated the effect of a fourfold anisotropy in our simulations by including the term (3) in the action. Using the approach of Ref. 33, we find the same result for the dissipative (2+1)D XY model as reported there for the classical 3D XY model, namely, that the h_4 term is perturbatively irrelevant.

The soft constraint represented by a (finite) anisotropy term is not obviously the same as the hard constraint constituted by the discrete Z_4 variables of the original model (the limit $h_4 = \infty$). We may only speculate whether a putative LQC fixed point for a $U(1)$ theory might survive in the limit $h_4 \to \infty$, but note that our simulations showed no signs of locality neither when enforcing a soft nor a strong Z_4 constraint on the variables.[34]

Finally, we briefly consider variants of LQC other than that of Ref. 21, which predicts a strictly infinite z for $\xi_\tau \sim \xi^z$ so that ξ is strictly vanishing at criticality. Another conceivable sense in which $z \to \infty$ is by activated dynamical scaling,[35] i.e., scaling on the form $\ln \xi_\tau \sim \xi^\psi$. In this case, as we expect also in the first case, locality would manifest itself in our simulations as a strongly increasing value of $z > 1$ as the thermodynamical limit was approached. This is not observed in our results. We have also verified explicitly, by an appropriate modification of the scaling,[35] that our results are not consistent with activated dynamical scaling.

In conclusion, we find no signs of local quantum criticality in the compact (2+1)D XY model with bond dissipation, but instead conventional quantum criticality with indications of

isotropic scaling of imaginary time and space. This implies that the fluctuation spectrum of the model is a function of the combination $\sqrt{q^2+\omega^2}$, rather than being dependent only on the frequency ω, but not on the momentum q (which would be a hallmark of local quantum criticality). Our results therefore differ in a fundamental way from those obtained from the same model in Ref. 20.

The authors acknowledge useful discussions with Egil V. Herland, Chandra M. Varma, and Vivek Aji. A.S. was supported by the Norwegian Research Council under Grant No. 205591/V30 (FRINAT). E.B.S. and I.B.S thank NTNU for financial support. The work was also supported through the Norwegian consortium for high-performance computing (NOTUR).

[1] H. v. Löhneysen, A. Rosch, M. Vojta, and P. Wölfle, Rev. Mod. Phys. **79**, 1015 (2007).
[2] J. Zaanen, in *100 Years of Superconductivity*, edited by H. Rogalla and P. H. Kes (Taylor & Francis, London, 2011) (in press) (e-print arXiv:1012.5461).
[3] C. M. Varma, P. B. Littlewood, S. Schmitt-Rink, E. Abrahams, and A. E. Ruckenstein, Phys. Rev. Lett. **63**, 1996 (1989).
[4] C. M. Varma, Phys. Rev. B **55**, 14554 (1997).
[5] V. Aji, A. Shekhter, and C. M. Varma, Phys. Rev. B **81**, 064515 (2010).
[6] C. M. Varma, Phys. Rev. B **73**, 155113 (2006).
[7] B. Fauqué, Y. Sidis, V. Hinkov, S. Pailhès, C. T. Lin, X. Chaud, and P. Bourges, Phys. Rev. Lett. **96**, 197001 (2006).
[8] A. Kaminski, S. Rosenkranz, H. M. Fretwell, J. C. Campuzano, H. R. Z. Li, W. G. Cullen, H. You, C. G. Olson, C. M. Varma, and H. Höchst, Nature (London) **416**, 610 (2002).
[9] Y. Li, V. Balédent, G. Yu, N. Barišić, K. Hradil, R. A. Mole, Y. Sidis, P. Steffens, X. Zhao, P. Bourges, and M. Greven, Nature (London) **468**, 283 (2010).
[10] Y. Li, V. Balédent, N. Barišić, Y. Cho, B. Fauqué, Y. Sidis, G. Yu, X. Zhao, P. Bourges, and M. Greven, Nature (London) **455**, 372 (2008).
[11] V. Balédent, B. Fauqué, Y. Sidis, N. B. Christensen, S. Pailhès, K. Conder, E. Pomjakushina, J. Mesot, and P. Bourges, Phys. Rev. Lett. **105**, 027004 (2010).
[12] J. E. Sonier, V. Pacradouni, S. A. Sabok-Sayr, W. N. Hardy, D. A. Bonn, R. Liang, and H. A. Mook, Phys. Rev. Lett. **103**, 167002 (2009).
[13] S. Strässle, B. Graneli, M. Mali, J. Roos, and H. Keller, Phys. Rev. Lett. **106**, 097003 (2011).
[14] S. V. Borisenko, A. A. Kordyuk, A. Koitzsch, T. K. Kim, K. A. Nenkov, M. Knupfer, J. Fink, C. Grazioli, S. Turchini, and H. Berger, Phys. Rev. Lett. **92**, 207001 (2004).
[15] G. J. MacDougall, A. A. Aczel, J. P. Carlo, T. Ito, J. Rodriguez, P. L. Russo, Y. J. Uemura, S. Wakimoto, and G. M. Luke, Phys. Rev. Lett. **101**, 017001 (2008).
[16] M. Greiter and R. Thomale, Phys. Rev. Lett. **99**, 027005 (2007).
[17] S. Nishimoto, E. Jeckelmann, and D. J. Scalapino, Phys. Rev. B **79**, 205115 (2009).
[18] C. Weber, A. Läuchli, F. Mila, and T. Giamarchi, Phys. Rev. Lett. **102**, 017005 (2009).
[19] M. Vojta, Adv. Phys. **58**, 699 (2009).
[20] V. Aji and C. M. Varma, Phys. Rev. Lett. **99**, 067003 (2007).
[21] V. Aji and C. M. Varma, Phys. Rev. B **79**, 184501 (2009).
[22] A. O. Caldeira and A. J. Leggett, Ann. Phys. (NY) **149**, 374 (1983).
[23] T. Faulkner, N. Iqbal, H. Liu, J. McGreevy, and D. Vegh, Science **329**, 1043 (2010).
[24] J. A. Hertz, Phys. Rev. B **14**, 1165 (1976).
[25] I. B. Sperstad, E. B. Stiansen, and A. Sudbø, Phys. Rev. B **81**, 104302 (2010).
[26] S. Chakravarty, G.-L. Ingold, S. Kivelson, and A. Luther, Phys. Rev. Lett. **56**, 2303 (1986).
[27] K. Børkje and A. Sudbø, Phys. Rev. B **77**, 092404 (2008).
[28] G. Schön and A. D. Zaikin, Phys. Rep. **198**, 237 (1990).
[29] E. B. Stiansen, I. B. Sperstad, and A. Sudbø, Phys. Rev. B **83**, 115134 (2011).
[30] P. Werner, M. Troyer, and S. Sachdev, J. Phys. Soc. Jpn. Suppl. **74**, 67 (2005).
[31] K. Hukushima and K. Nemoto, J. Phys. Soc. Jpn. **65**, 1604 (1996).
[32] M. Matsumoto and T. Nishimura, ACM Trans. Model. Comput. Simul. **8**, 3 (1998).
[33] M. Caselle and M. Hasenbusch, J. Phys. A **31**, 4603 (1998).
[34] Here, we focused on the *perturbative* relevance of h_4. A substantial $h_4 > 1$ does seem to change the nature of the phase transition. The observation of diverging Binder cumulants $g \to -\infty$ points to a first-order phase transition both for the strongly anisotropic XY case and for the Z_4 case.
[35] T. Vojta, Rev. Comput. Chem. **26**, 167 (2008).

Paper IV

Three distinct types of quantum phase transitions in a (2+1)-dimensional array of dissipative Josephson junctions.

Phys. Rev. B **85**, 224531 (2012).

PHYSICAL REVIEW B **85**, 224531 (2012)

Three distinct types of quantum phase transitions in a $(2+1)$-dimensional array of dissipative Josephson junctions

Einar B. Stiansen, Iver Bakken Sperstad, and Asle Sudbø
Department of Physics, Norwegian University of Science and Technology, N-7491 Trondheim, Norway
(Received 22 December 2011; revised manuscript received 11 April 2012; published 25 June 2012)

We have performed large-scale Monte Carlo simulations on a model describing a $(2+1)$-dimensional array of dissipative Josephson junctions. We find three distinct stable quantum phases of the system. The most ordered state features long-range spatial ordering in the phase θ of the superconducting order parameter, but temporal ordering only in spatial gradients $\Delta\theta$, not in θ. Significantly, the most ordered state therefore does not have three-dimensional (3D) XY ordering. Rather, it features two-dimensional (2D) spin waves coexisting with temporally disordered phases θ. There is also an intermediate phase featuring quasi-long-range spatial order in θ coexisting with a gas of instantons in $\Delta\theta$. We briefly discuss possible experimental signatures of such a state, which may be viewed as a local metal and a global superconductor. The most disordered state has phase disorder in all spatio-temporal directions, and may be characterized as a gas of proliferated vortices coexisting with a gas of $\Delta\theta$ instantons. The phase transitions between these phases are discussed. The transition from the most ordered state to the intermediate state is driven by proliferation of instantons in $\Delta\theta$. The transition from the intermediate state to the most disordered state is driven by the proliferation of spatial point vortices in the background of a proliferated $\Delta\theta$-instanton gas, and constitutes a Berezinskii-Kosterlitz-Thouless phase transition. The model also features a direct phase transition from the most ordered state to the most disordered state, and this transition is neither in the 2D XY nor in the 3D XY universality class. It comes about via a simultaneous proliferation of point vortices in two spatial dimensions and $\Delta\theta$ instantons, with a complicated interplay between them. The results are compared to, and differ in a fundamental way from, the results that are found in dissipative quantum rotor systems. The difference originates with the difference in the values that the fundamental degrees of freedom can take in the latter systems compared to dissipative Josephson junction arrays.

DOI: 10.1103/PhysRevB.85.224531 PACS number(s): 74.81.Fa, 05.30.Rt, 74.40.Kb, 74.50.+r

I. INTRODUCTION

In general, dissipation suppresses quantum fluctuations and may support states of spontaneously broken symmetry. A remarkable consequence of this is the dissipation-driven quantum phase transition in a single resistively shunted Josephson junction in which the phase difference is localized in a minimum of the periodic Josephson potential.[1] In the parameter space of Josephson coupling and dissipation strength, this corresponds physically to a phase diagram with one metallic phase and one superconducting phase. While the behavior of a single dissipative Josephson junction is theoretically well understood, the picture is less complete for spatially extended systems. Other than the fully disordered phase and the fully ordered phase expected from the single-junction system, the phase diagram of arrays of dissipative Josephson junctions is conjectured to host additional phases in both one[2–7] and two[2,8,9] dimensions. These new, exotic phases can broadly be characterized by having various combinations of global and/or local phase fluctuations or order.

Most of the analytical works on similar models have been based on mean-field analyses or perturbative renormalization group arguments. Since these approaches are valid in a limited region of the parameter space, in particular regions far away from phase transitions, a nonperturbative approach is of importance. Previous numerical work on models of dissipative Josephson junctions has mostly focused on lower-dimensional systems. The first Monte Carlo simulation of a single dissipative Josephson junction was presented in Ref. 10, where a fluctuation measure of the imaginary-time path of the phase difference was introduced to characterize the localization transition. Improved and extended results for the same model were later reported in Ref. 11. For one spatial dimension, Ref. 12 reported four physically distinct phases for a dissipative Josephson junction chain. This simulation was performed on a dual model and not directly on the phase degrees of freedom. A model for a $(2+1)$-dimensional [$(2+1)$D] dissipative Josephson junction array (JJA) has been treated numerically by Ref. 13. In essence, their results support the simplest scenario for a zero-temperature phase diagram,[14,15] with one phase with and another without spatio-temporal order. This is also what was found in a large-scale Monte Carlo simulation on the dissipative $(2+1)$D XY quantum rotor model.[16]

Finally, our investigations are also motivated by a rather different physical system which can be described by a closely related model. In Ref. 17, a quantum XY model with bond dissipation in two spatial dimensions was used to describe quantum critical fluctuations in cuprate high-T_c superconductors. The principal result of analytical work on this model is that the dissipation-driven quantum critical point is local, in the sense that the fluctuation spectrum is frequency dependent but momentum independent.[17] Although the physical system we have in mind primarily is that of a Josephson junction array, we return to a discussion of the possibilities of local quantum criticality later in the paper.[18]

The purpose of this paper is to numerically investigate the phase diagram of a specific model of a $(2+1)$-dimensional dissipative Josephson junction array. We pay special attention to the manifest anisotropy that exists between the spatial and temporal dimensions. To be specific, the fluctuations of the quantum paths of the phase gradients will be explicitly

characterized in terms of roughening transitions, allowing us to consider the (temporal) localization transition separately from the onset of (spatial) phase coherence. In particular, we will identify a partially superconducting phase with spatial, but no temporal phase coherence. This corresponds to a dissipative JJA which may sustain a nonzero Josephson current, but where one nonetheless has voltage fluctuations over each junction. We investigate two phase transitions where the spatio-temporal aspects are well separated and can be characterized in terms of either a spatial vortex-antivortex unbinding, or proliferation of instantonlike defects. We also discuss a direct quantum phase transition from an ordered state to a disordered state involving simultaneous disordering in space and imaginary time. This corresponds to a quantum phase transition on a dissipative JJA where one transitions from a state sustaining a Josephson current and allowing no voltage fluctuations to a normal state, but via an unusual quantum phase transition that is neither in the two-dimensional (2D) XY nor three-dimensional (3D) XY universality class.

A. Model

An array of Josephson junctions consists of superconducting islands arranged in a regular network. Separating the islands are tunnel junctions in which Cooper pairs are able to tunnel from one superconducting grain to the neighboring grain. The fundamental degrees of freedom are the phases of the superconducting order parameters residing on the grains. A classical two-dimensional JJA is described by the 2D XY model,

$$H = -K \sum_{\langle \mathbf{x},\mathbf{x}' \rangle} \cos(\theta_{\mathbf{x}} - \theta_{\mathbf{x}'}), \tag{1}$$

where the summation goes over nearest neighboring sites on a square lattice. $\theta_{\mathbf{x}}$ is the phase of the complex order parameter of the superconducting grain at position $\mathbf{x}$. Although the $U(1)$ symmetry of the phase variables cannot be spontaneously broken in two dimensions at any nonzero temperature (implicit in the classical description), the system nevertheless undergoes a Berezinskii-Kosterlitz-Thouless (BKT) transition in which it develops quasi-long-range order (QLRO) with power-law-decaying correlation functions in the low-temperature regime. The low-temperature phase corresponds to a dipole phase where the vortices and antivortices of the phase field are bound in pairs. At the transition the vortices proliferate and destroy the QLRO. For a given phase configuration, a single vortex is identified on a plaquette by a nontrivial line integral of the phase difference around the plaquette, taking the compactness of the phase field into account.

The quantum generalized version of the model includes two additional terms describing quantum fluctuations in imaginary time τ. The action reads[3,12,13,15,17,19,20]

$$S = \frac{1}{2E_C} \sum_{\mathbf{x}} \int_0^\beta d\tau \left(\frac{\partial \theta_{\mathbf{x},\tau}}{\partial \tau} \right)^2 - K \sum_{\langle \mathbf{x},\mathbf{x}' \rangle} \int_0^\beta d\tau \cos(\Delta\theta_{\mathbf{x},\mathbf{x}',\tau}) + \frac{\alpha}{2} \sum_{\langle \mathbf{x},\mathbf{x}' \rangle} \int_0^\beta \int_0^\beta d\tau d\tau' \left(\frac{\pi}{\beta} \right)^2 \frac{(\Delta\theta_{\mathbf{x},\mathbf{x}',\tau} - \Delta\theta_{\mathbf{x},\mathbf{x}',\tau'})^2}{\sin^2\left(\frac{\pi}{\beta}|\tau - \tau'|\right)}, \tag{2}$$

where we have defined the lattice gradient $\Delta\theta_{\mathbf{x},\mathbf{x}',\tau} = \theta_{\mathbf{x},\tau} - \theta_{\mathbf{x}',\tau}$. The first term describes the self-capacitance of a single island; the second term is the familiar Josephson interaction, coupling each superconducting island to the nearest neighbors by a periodic potential. The last term describes the Ohmic dissipation as modeled by a bath of harmonic oscillators coupling to the bond variables.[21]

A subtle consequence of the presence of this Ohmic shunt mechanism is that the phase variables become noncompact,[22] as the dissipation term in Eq. (2) breaks the 2π periodicity of the Josephson potential. Thus, the phases are no longer defined with compact support $\theta \in [-\pi,\pi\rangle$, as they would be in the nondissipative case or in a $(2+1)$D dissipative quantum rotor model. Instead, we have $\theta \in \langle -\infty,\infty\rangle$. *The impact of this decompactification on the problem is enormous*. It reflects that a sudden increase along imaginary time in the phase difference (e.g., $\Delta\theta_{\mathbf{x},\mathbf{x}',\tau} \to \Delta\theta_{\mathbf{x},\mathbf{x}',\tau} + 2\pi$) would produce a voltage imbalance over the barrier. A dissipative, measurable current would then flow through the shunting resistors until the imbalance is relaxed. Hence, the variables cannot be defined modulo 2π, since $\Delta\theta_{\mathbf{x},\mathbf{x}',\tau}$ and $\Delta\theta_{\mathbf{x},\mathbf{x}',\tau} + 2\pi$ represent distinguishable states. The noncompactness of the variables implies that we may no longer identify vortices in the same manner as described above, as a line integral around a plaquette always yields zero for a noncompact phase field. In Appendix A, we introduce a reformulation of the phase variables in terms of a compact part and an additional field describing the tunneling between wells in the extended Josephson potential. This enables us to identify vortices in the compact part of the phase. The phase transitions involving spatial ordering may therefore still be described by vortex proliferation even though the variables are of a noncompact nature.

As a description of a dissipative JJA, there are a few simplifications built into the action (2). We have only considered the effect of self-capacitance and neglected mutual capacitive coupling with neighboring grains. Also, the dissipation term only accounts for one source of dissipation, namely the flow of normal electrons through the shunting resistors. Additional dissipative effects like quasiparticle tunneling[22] and Cooper pair relaxation[4,23] have been neglected.

In order to study the behavior of a two-dimensional array of Josephson junctions at zero temperature under the influence of Ohmic dissipation, we perform large-scale Monte Carlo simulations on a discretized version of Eq. (2),

$$S = \frac{K_\tau}{2} \sum_{\mathbf{x}}^{N} \sum_{\tau}^{N_\tau} (\theta_{\mathbf{x},\tau+1} - \theta_{\mathbf{x},\tau})^2 - K \sum_{\langle \mathbf{x},\mathbf{x}' \rangle} \sum_{\tau}^{N_\tau} \cos(\Delta\theta_{\mathbf{x},\mathbf{x}',\tau}) + \frac{\alpha}{2} \sum_{\langle \mathbf{x},\mathbf{x}' \rangle} \sum_{\tau \neq \tau'}^{N_\tau} \left(\frac{\pi}{N_\tau} \right)^2 \frac{(\Delta\theta_{\mathbf{x},\mathbf{x}',\tau} - \Delta\theta_{\mathbf{x},\mathbf{x}',\tau'})^2}{\sin^2\left(\frac{\pi}{N_\tau}|\tau - \tau'|\right)}. \tag{3}$$

Here, $K_\tau = 1/E_C \Delta\tau$ and the spatial coupling has been renamed $K\Delta\tau \to K$. Our goal is to investigate the behavior of the system in the K-α-space, K_τ therefore defines the energy scale and will be kept at suitable values in the simulations.

The phase variables are defined on the vertices of a three-dimensional cubic grid. The spatial linear extent of the grid is given by N, and the number of Trotter slices used to discretize the temporal direction is given by N_τ. Thus, $\Delta\tau = \beta/N_\tau$, and the size of the space-time lattice is $N \times N \times N_\tau$. Periodic boundary conditions in imaginary time are implicit from the path integral construction, and are also applied in the spatial directions in the standard manner. The noncompactness of the variables also dictates the form of the kinetic term. Because θ is an extended variable, its derivative must be expressed by discretized differentiation. We refer to the appendix of Ref. 24 for details.

B. Outline and overview of main results

For outlining the road map to this paper, the phase diagram of the system is helpful. This is illustrated schematically in Fig. 1. *In all regions of the phase diagram, the phases θ are disordered in the imaginary-time direction.*

In Sec. II, we introduce the various observables used to identify the phases and phase transitions of the model defined in Eq. (3). In Sec. III, the details of the Monte Carlo simulations are presented in a concise form.

In Sec. IV, we take a large value of the Josephson coupling K and investigate the behavior of the system as it crosses from the CSC phase to the FSC phase in Fig. 1 upon increasing α. There is a phase transition at a critical dissipation strength, $\alpha_c^{(2)}$, above which the system is fully bond-ordered superconducting (FSC). For $\alpha < \alpha_c^{(2)}$ the system features unbounded temporal fluctuations, while at the same time featuring spatial phase coherence. Due to algebraically decaying spatial correlations in this regime, we will refer to the phase as critical superconducting (CSC). In other words, the phase configurations of the system rotate more or less as a "rigid body" in time, thus at the same time giving rise to a finite superfluid density (helicity modulus) as well as voltage fluctuations across the junctions. A detection of the CSC phase thus requires simultaneous measurements of the superfluid density of the system, as well as ac measurements of voltages across junctions.

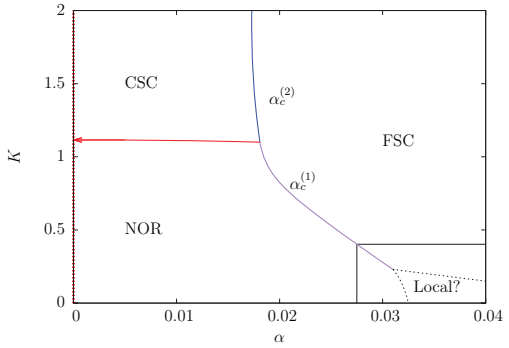

FIG. 1. (Color online) A schematic phase diagram of the system defined by Eq. (3), based on the Monte Carlo calculations presented below. Here, we have used the value $K_\tau = 0.002$, corresponding to the parameters in Sec. IV. NOR refers to the normal phase, where vortices are proliferated and the bonds $\Delta\theta$ are disordered in the τ direction. CSC refers to the critical superconducting state, where the θ variables feature power-law correlations in space, while $\Delta\theta$ remains disordered. FSC refers to the fully bond-ordered superconducting state, which features an additional ordering compared to the CSC phase, namely $\Delta\theta$ ordering in the imaginary-time direction. A hypothetical fourth, local phase has *not* been observed in our simulations, as indicated by the box in the lower right corner. See text in Sec. I B for more details.

In Sec. V, we consider the transition between the NOR phase and the CSC phase, and this is found to be a purely spatial phase transition of the BKT type.

In Sec. VI, we investigate the response of the system to increasing dissipation at low and intermediate Josephson couplings, as it crosses from the NOR phase to the FSC phase in Fig. 1. This is the most difficult case to analyze, as the system transitions from a spatio-temporally disordered phase directly to the spatio-temporally ordered state FSC upon crossing the critical line $\alpha_c^{(1)}$.

In Sec. VII, the topological defects driving the various phase transitions as well as how such a model may exhibit local quantum criticality (LQC), are discussed. This may be briefly summarized as follows.

On the line separating CSC from NOR, and on the line separating CSC from FSC, the spatial and temporal aspects of the phase transitions can be considered separately. The CSC-NOR transition is driven by point vortices and is in the 2D XY universality class. The FSC-CSC transition is driven by instantons in $\Delta\theta$ and may be characterized as a roughening transition in the space of $\Delta\theta$. On the critical line $\alpha_c^{(1)}$, there is a complicated interplay between temporal and spatial fluctuations. This critical line is neither in the 2D XY nor in the 3D XY universality class.

An additional fourth phase could conceivably have been present in the phase diagram, featuring temporal order and unbound vortices. The most likely position in the phase diagram for such a hypothetical phase would be at weak Josephson coupling and strong dissipation strength. This is shown by the dotted lines within the box in the lower right corner of Fig. 1. The local transition line would involve ordering of temporal fluctuations without onset of spatial phase coherence, and as such would describe a local quantum critical point. Our simulations, however, show no sign of such behavior in the parameter range we have considered.

The limit $\alpha = 0$ is in principle ill defined in this model since a finite dissipation is essential for the decompactification of the variables. This is indicated by drawing the $\alpha = 0$ axis as a red dotted line in Fig. 1. Thus, the value $\alpha = 0$ is also a singular endpoint of the horizontal (red) line in the phase diagram, and this is indicated by terminating this line in an arrow.

In Appendix A, we provide some more details and discussion on the fundamental implications of the noncompactness of the phase field. In Appendix B, we take a closer look at the NOR phase and investigate the description of Refs. 25, 19 of such a normal phase as a so-called floating phase.

II. OBSERVABLES

In order to describe the various phases and transitions introduced in the previous section, several quantities will be

calculated. To monitor the degree of (spatial) superconducting order, we calculate the spatial helicity modulus, or phase stiffness. This quantity measures the increase in the free energy when applying an infinitesimal twist across the system, $\theta_{\mathbf{x}} \to \theta_{\mathbf{x}} - \boldsymbol{\delta} \cdot \mathbf{x}$. It probes the degree of phase coherence in the system and thus its ability to sustain a supercurrent. The only term in the action that contributes to the helicity modulus is the Josephson interaction term. Hence, the helicity modulus Υ_x is given by

$$\Upsilon_x = \frac{1}{N^2 N_\tau}\left\langle \sum_{\langle \mathbf{x},\mathbf{x}'\rangle}\sum_{\tau}^{N_\tau} \cos(\Delta\theta_{\mathbf{x},\mathbf{x}',\tau})\right\rangle - \frac{K}{N^2 N_\tau}\left\langle \left(\sum_{\langle \mathbf{x},\mathbf{x}'\rangle}\sum_{\tau}^{N_\tau} \sin(\Delta\theta_{\mathbf{x},\mathbf{x}',\tau})\right)^2\right\rangle. \quad (4)$$

Here, the brackets indicate ensemble averaging. In the context of the classical 2D XY model, $\Upsilon_x = 0$ defines the disordered state where vortices are proliferated. In the same manner, $\Upsilon_x \neq 0$ signals the finite rigidity of the quasiordered state.

The same XY models used to describe superconducting systems also describe magnetic systems of planar spins, and the superconducting phase θ can formally be associated with the direction of the XY spins. Conventionally, the order of a superconducting system is therefore often described by a magnetization order parameter,

$$m = \frac{1}{N^2 N_\tau}\sum_{\mathbf{x},\tau} e^{i\theta_{\mathbf{x},\tau}}, \quad (5)$$

which probes the uniformity of the spin direction across the entire $(2+1)$-dimensional volume of the system.

It should be noted that these two order parameters are periodic and consequently insensitive to tunneling events where the phase difference on a single junction jumps to a neighboring potential well, $\Delta\theta \to \Delta\theta + 2\pi$. Consequently, Υ_x and m do not probe the dissipation-induced localization *per se*. In order to quantify this, we calculate the mean square displacement (MSD) of the bond variable $\Delta\theta$ along imaginary time,

$$W^2_{\Delta\theta}(N_\tau) = \frac{1}{N_\tau}\left\langle \sum_{\tau}^{N_\tau} (\Delta\theta_\tau - \overline{\Delta\theta})^2\right\rangle. \quad (6)$$

Here, we have defined $\overline{\Delta\theta} = 1/N_\tau \sum_\tau \Delta\theta_\tau$. The MSD is often used in the context of stochastically growing interfaces or diffusion processes, and it is natural to adopt some concepts from these areas for our problem. For instance, the degree to which the imaginary-time history of $\Delta\theta$ may be regarded as "rough" can be quantified by the scaling characteristics of the MSD with the length N_τ of the "interface." Normally, one finds

$$W^2_{\Delta\theta} \propto N_\tau^{2H}, \quad (7)$$

if the imaginary-time history of $\Delta\theta$ describes self-affine configurations. $H = 1/2$ corresponds to a Markovian random walk, and such linear scaling of the MSD is also referred to as normal diffusion. A deviation from linear growth of $W^2_{\Delta\theta}$ as a function of N_τ is the hallmark of *anomalous diffusion*.[26] In particular, $H < 1/2$ is referred to as subdiffusive behavior. A smooth interface is characterized by the MSD being independent of the system length.

To describe the phases and phase transitions, we will also investigate correlations of the order parameter field considered in Eq. (5). We define the spatial and temporal correlation function by

$$G_\theta(\mu; q) = \langle e^{iq(\theta_\mu - \theta_0)}\rangle, \quad (8)$$

where $\mu \in \{\mathbf{x}, \tau\}$. The extra factor q in the exponent is introduced for later reference in Appendix B, but will be set to the conventional value $q = 1$ otherwise. In Appendix B we will also consider bond correlations, defined here for convenience as

$$G_{\Delta\theta}(\mu; q) = \langle e^{iq(\Delta\theta_\mu - \Delta\theta_0)}\rangle. \quad (9)$$

For completeness we also present the susceptibility of the action,

$$\chi_S = \frac{1}{N^2 N_\tau}\langle (S - \langle S\rangle)^2\rangle, \quad (10)$$

as an additional means of locating the expected dissipation-induced phase transitions. This is the quantum mechanical equivalent of the classical heat capacity and is expected to present a nonanalyticity at a critical point.

III. DETAILS OF THE MONTE CARLO CALCULATIONS

Considerable progress has been made in constructing new, effective, nonlocal algorithms for long-range-interacting systems with extended variables.[11,27,28] However, these algorithms are presently restricted to $(0+1)$D systems, and do not seem to generalize easily to $N > 1$.[27] In the Monte Carlo simulations, we have therefore combined local updates with a parallel tempering algorithm[29,30] in which several systems are simulated simultaneously at different coupling strengths.

A Monte Carlo sweep corresponds to proposing a local update by the Metropolis-Hastings algorithm sequentially for every grid point in the system. The proposed new phases are generated by first randomly choosing to increase or decrease the value, then propagating the value by a random increment of size $2\pi n/32$, where $n \in \{1,32\}$. In other words, the continuous symmetry of the variables is emulated by 32 discrete states per 2π interval. We have confirmed that adding additional states will not change the results.

After a fixed number of Monte Carlo sweeps a parallel tempering move is made. In this move, a swap of configurations between two neighboring coupling values is proposed, and the swap is accepted with probability Ξ_{PT} given by

$$\Xi_{\mathrm{PT}} = \begin{cases} 1 & \text{if } \Delta < 0, \\ e^{-\Delta} & \text{if } \Delta \geqslant 0. \end{cases} \quad (11)$$

Here, $\Delta = \kappa'(\bar{S}[X;\kappa'] - \bar{S}[X';\kappa']) - \kappa(\bar{S}[X;\kappa] - \bar{S}[X';\kappa])$, where κ is the coupling value varied, representing in our case α or K, and X represents the phase configuration. $\bar{S}$ indicates the part of the action conjugate to the coupling parameter κ. Both the Metropolis updates and the parallel tempering swaps are ergodic and respect detailed balance.

All Monte Carlo simulations were initiated with a random configuration. Depending on system size, various numbers of sweeps were performed for each coupling value. Error bars are provided for all observables except correlation functions, but are usually smaller than the data points. Measurements on

which we perform scaling have, broadly speaking, a relative error well below 1%. The MERSENNE TWISTER[31] random number generator was used in all simulations and the random number generator on each CPU was independently seeded. It was confirmed that other random number generators yielded consistent results. In some simulations we also made use of the Ferrenberg-Swendsen reweighting technique,[32] which enables us to continuously vary the coupling parameter after the simulations have been performed.

In order to identify sharply defined nonanalyticities and observe converged scaling of $W^2_{\Delta\theta}$ at the dissipation-induced phase transitions, relatively large values of N_τ are needed. This limits the range of spatial sizes accessible in simulations with a single-site update algorithm. In the sections where we focus on the temporal scaling, we have fixed the spatial size at $N = 20$ and varied the temporal size in the range $N_\tau = 50$ to $N_\tau = 350$. In Sec. V we find that in the CSC phase the temporal size of the system is irrelevant in determining the spatial properties of the system. Consequently, the temporal size is fixed at $N_\tau = 20$ and the spatial size is varied in the range $N = 10$ to $N = 100$. To investigate the spatial correlations in θ across the NOR-FSC phase transition, we have also performed simulations on a $N_\tau = 30$ system with $N = 50$ and $N = 100$.

IV. THE CSC-FSC TRANSITION $\alpha_c^{(2)}$

In this section, we consider the behavior of the system under the influence of strong Josephson coupling K [i.e., for a value of K where the corresponding classical system would be topologically ordered even in the absence of dissipation (above the horizontal line in the phase diagram of Fig. 1)]. The coupling parameter will be fixed at $K = 1.5$ in this section, while the dissipation strength α is varied. We will use a quantum coupling $K_\tau = 0.002$. The main focus is on scaling of observables describing temporal fluctuations. Hence, the spatial system size is fixed at $N = 20$.

We start by presenting typical configurations of the bond variable $\Delta\theta$ as a function of τ. At strong coupling, the bond variables are located predominantly in the vicinity of the potential minima located at $2\pi n$, where n is an integer. Due to the noncompact nature of the variables, $\Delta\theta$ are free to tunnel between neighboring minima at weak dissipation. When considering the single-junction problem, this sudden tunneling of the bond variable from one Trotter slice to the next, $\Delta\theta_{\tau+1} - \Delta\theta_\tau \approx 2\pi n_{\rm I}$, is often referred to as instanton or anti-instanton configurations, depending on the sign of the integer-valued "instanton charge," $n_{\rm I}$. Note that the noncompactness allows for tunneling of $\Delta\theta$ also between minima of the potential located further away than nearest neighbor. This corresponds to instanton charges with values larger than unity. The tunneling behavior is easily identified in the topmost curve in Fig. 2, where frequent instantons and anti-instantons are apparent. In this temporally disordered state, the quantum paths of $\Delta\theta$ appear to be well described in terms of a gas of proliferated instantons. Beyond a threshold value of α, we observe a localization of $\Delta\theta$ in one of the minima of the Josephson potential. The imaginary-time history of a bond variable corresponding to this phase forms an essentially smooth surface and is given in the lower curve in Fig. 2. However, even though the phase gradients are localized,

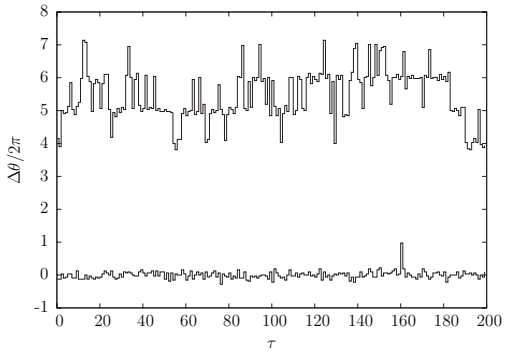

FIG. 2. The bond variable $\Delta\theta$ as a function of imaginary time τ for two different values of dissipation strength, $\alpha = 0.0102$ and $\alpha = 0.0281$, in the strong Josephson coupling regime. In the topmost curve, the bond variable clearly spends most of the time in the vicinity of the potential minima, although tunneling events between minima are frequent. The lowermost curve corresponds to the fully bond-ordered superconducting state where $\Delta\theta$ is localized and $W^2_{\Delta\theta}$ does not scale with N_τ. Note that in the CSC phase (topmost curve) the quantum paths of $\Delta\theta$ are well described in terms of instantons where the fluctuations in imaginary time are mostly given by integer multiples of 2π, in contrast to the situation for the corresponding quantum paths of $\Delta\theta$ in the NOR phase; see Fig. 8.

closely bound pairs of instantons and anti-instantons may still be present.

In Fig. 3, we show the mean square displacement as a function of dissipation strength. The temporal bond fluctuations are clearly suppressed for increasing values of α. The different curves represent different values of N_τ. Two regions of different scaling behavior of $W^2_{\Delta\theta}$ as a function of N_τ can immediately be discerned. For weak dissipation, $W^2_{\Delta\theta}$ increases with N_τ, while $W^2_{\Delta\theta}$ is independent of the temporal size at strong dissipation. Separating the two regions is a

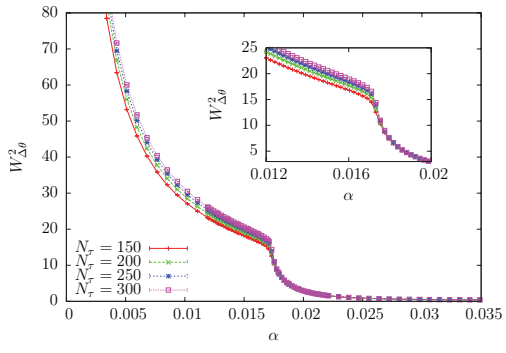

FIG. 3. (Color online) $W^2_{\Delta\theta}$, Eq. (6), as a function of dissipation strength for a system with $K_\tau = 0.002$, $K = 1.5$, $N = 20$, and various values of N_τ. Note the kink in the curves at $\alpha = \alpha_c^{(2)}$ and the saturation of $W^2_{\Delta\theta}$ at a finite value for $\alpha > \alpha_c^{(2)}$. Error bars are smaller than the data points. (Inset) A blow-up of the region around $\alpha_c^{(2)}$.

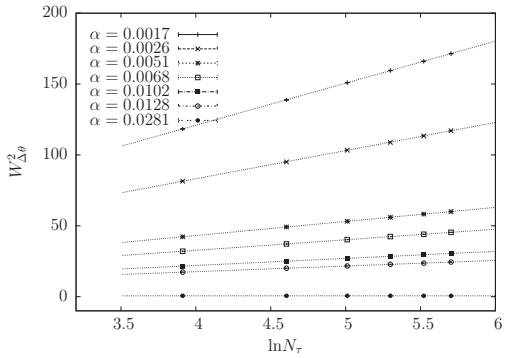

FIG. 4. $W^2_{\Delta\theta}$ as a function of $\ln N_\tau$ for various values of the dissipation strength α ranging from the weak-dissipation limit to the ordered state at the top and bottom, respectively. The dotted lines indicate the logarithmic growth of $W^2_{\Delta\theta}$. Error bars are much smaller than the data points.

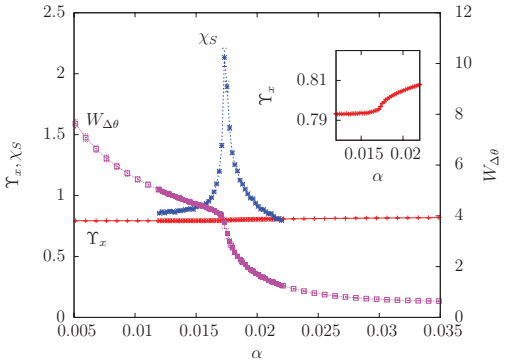

FIG. 5. (Color online) The spatial helicity modulus Υ_x, Eq. (4), action susceptibility χ_S, Eq. (10), and mean fluctuation $W_{\Delta\theta}$, Eq. (6), as a function of dissipation strength α for a system in the strong Josephson-coupling regime with $K_\tau = 0.002$, $K = 1.5$, $N = 20$, and $N_\tau = 250$. (Inset) A blow-up of the helicity modulus around the $\alpha_c^{(2)}$ transition. For $\alpha > \alpha_c^{(2)}$, the dissipation renormalizes the spatial coupling strength so that a kink in Υ_x is visible at the localization transition. However, this renormalization is miniscule. Proliferation of instantons across the line $\alpha_c^{(2)}$ in Fig. 1 does not trigger a proliferation of vortices.

precipitous drop in $W^2_{\Delta\theta}$ at a value of α that we will identify as the localization transition point $\alpha_c^{(2)}$.

Further information on the delocalized phase (CSC) can be found from investigating the dependence of $W^2_{\Delta\theta}$ on the temporal system size N_τ. Here, the MSD scales with N_τ according to

$$W^2_{\Delta\theta} = a(\alpha) \ln N_\tau, \tag{12}$$

where $a(\alpha)$ is a continuously varying proportionality constant. In Fig. 4 we have plotted $W^2_{\Delta\theta}$ as a function of $\ln N_\tau$ for various dissipation strengths. All but the lowest curve represent dissipation strengths well below $\alpha_c^{(2)}$. A clear logarithmic dependence is seen for all values of dissipation strength in the CSC phase. The lowest curve with zero slope corresponds to $\alpha > \alpha_c^{(2)}$, where temporal fluctuations are effectively quenched and $W^2_{\Delta\theta}$ does not scale with N_τ. In this way the increase of temporal fluctuations in $\Delta\theta_\tau$ as α is lowered may also be interpreted as a roughening transition at which the profile described by $\Delta\theta$ changes from smooth to rough. However, it should be noted that the logarithmic scaling presented in Fig. 4 does not conform to the scaling ansatz (7) for a self-affine interface. Instead, $\Delta\theta$ is anomalously diffusive in the sense that $H = 0$. This is sometimes referred to as *superslow diffusion*.[33] In comparison, Ref. 10 found that for the corresponding normal phase of a single resistively shunted Josephson junction, the MSD follows the power law (7) with the exponent decreasing continuously with dissipation strength (from $H = 1/2$ for $\alpha \gtrsim 0$ to $H \approx 0$ for $\alpha = \alpha_c$).

As we show in Fig. 5, $W_{\Delta\theta}$ as well as the action susceptibility χ_S and the helicity modulus Υ_x all feature nonanalytic behavior at the critical value $\alpha_c^{(2)}$. Figure 5 therefore supports the notion that the transition at $\alpha_c^{(2)}$ is indeed a genuine dissipation-induced quantum phase transition. Since we have shown that the system for $\alpha > \alpha_c^{(2)}$ has both spatial phase coherence and temporal localization of $\Delta\theta$, we can identify this region as a fully bond-ordered superconducting (FSC) phase. However, $\Upsilon_x > 0$ even for $\alpha < \alpha_c^{(2)}$, indicating that also the weak-dissipation CSC phase features spatial phase coherence. The kink in the helicity modulus shown in the inset in Fig. 5 may be attributed to the (slightly) reduced spatial rigidity as the bond variables delocalize in imaginary time when leaving the FSC phase. An important conclusion to be drawn from this is that in the regime of strong Josephson coupling, proliferation of instantons does not trigger a proliferation of vortices at $\alpha_c^{(2)}$ in Fig. 1.

A possible physical interpretation of the behavior at strong Josephson coupling and weak dissipation is a phase where there are fluctuations of voltage (and thus also of normal currents through the shunts) even though a finite superfluid density allows the system as a whole to sustain an unimpeded supercurrent. For reasons that will be apparent in the next section, we have chosen to refer to this state as a critical superconducting (CSC) phase. Similar conclusions have been made earlier for $(1+1)$D systems (e.g., in Refs. 4, 7, and 12), where the authors claimed to have found an additional superconducting state characterized by spatial coherence but large local fluctuations. An experimental signature of the FSC-CSC phase transition would be to measure an abrupt increase in voltage fluctuations across each junction while the system maintains a Josephson current across the system as the dissipation strength is reduced. The phase CSC therefore represents a locally metallic (on each junction) and globally superconducting (throughout the system) state.

V. THE NOR-CSC TRANSITION

We next consider the phase transition separating the CSC phase from the fully disordered state NOR. First, we note that the region at weak dissipation and low Josephson coupling in the phase diagram of Fig. 1 is spatially phase incoherent, $\Upsilon_x = 0$. This is therefore identified as the normal, metallic phase (NOR) of the dissipative JJA. To verify that the CSC state identified in the previous section by its finite spatial coherence

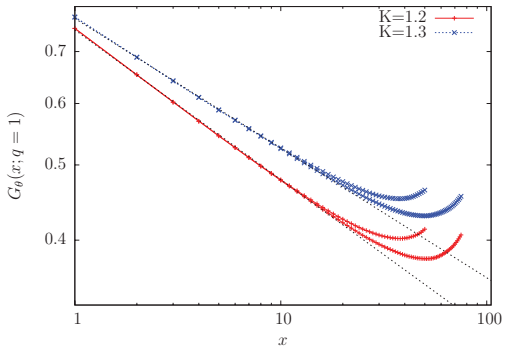

FIG. 6. (Color online) The spatial correlation functions $G_\theta(x;q=1)$, Eq. (8), calculated for $\alpha = 0.005$, $K_\tau = 0.002$, $N_\tau = 20$, and for two values of the Josephson coupling and two values of the spatial extent N. Both coupling values correspond to the CSC phase. The dotted lines show the power-law fit of the correlation functions.

is a distinct phase, we next show that it is separated from the NOR phase by a genuine phase transition and not just a crossover caused by the limited spatial extent of the systems.

In Fig. 6, we show algebraically decaying correlation functions in the spatial direction in the CSC phase, indicating QLRO within each Trotter slice. In combination with the observation of vanishing order in the temporal direction (as measured by $W^2_{\Delta\theta}$), this motivates an interpretation of the CSC phase as a dimensionally reduced critical phase in which the Trotter slices are decoupled from each other. We verified that varying N_τ had no impact on the results for any of the observables probing spatial behavior. Thus, the extent of the systems is fixed at $N_\tau = 20$ in the following.

We anticipate the phase transition separating the NOR phase from the CSC phase to be in the BKT universality class. At the transition point, the helicity modulus is expected to scale according to the finite-size scaling function[34]

$$\Upsilon_x(N) = \Upsilon_x(\infty)\left(1 + \frac{1}{2\ln N + C}\right), \qquad (13)$$

where $\Upsilon_x(\infty)$ is the value of the helicity modulus as $N \to \infty$ and C is an undetermined constant. The critical value K_c may be extracted by varying K until an optimal fit is achieved. In addition, at a BKT transition, the value of $\Upsilon_x(\infty)$ obtained at optimal fit should satisfy the universal relation $\Upsilon_x(\infty)K_c = 2/\pi$.

By treating both parameters as variables in the fitting procedure, no *a priori* assumption on the value of the jump is made. This value may consequently be used as an additional check on the validity of the conjecture of identifying the transition as a BKT transition.

In Fig. 7 we present Υ_x for various spatial system sizes and the corresponding fit with Eq. (13). Figure 7(a) shows results for the dissipationless limit, $\alpha = 0$,[35] while Fig. 7(b) gives the corresponding results for $\alpha = 0.005$. At both dissipation strengths we observe optimal fit at $K \approx 1.12$. The insets presented in both figures show $\Upsilon_x(\infty)K$, which should be compared to the broken line indicating the expected $2/\pi$ universal jump of a BKT transition. These results demonstrate

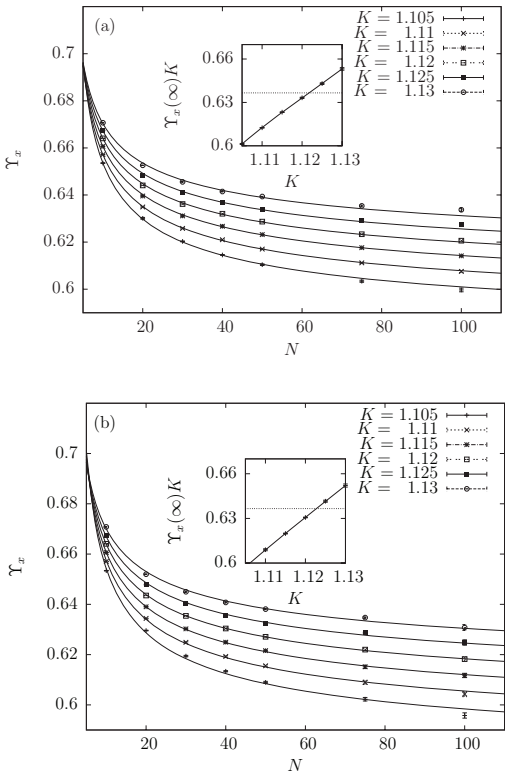

FIG. 7. Comparison of calculated values of the spatial helicity modulus Υ_x with the scaling function (13) for two different dissipation strengths. For both values of α, a good fit is observed at $K \approx 1.12$. (a) The spatial helicity modulus Υ_x as a function of spatial system sizes N for $\alpha = 0.0$, $K_\tau = 0.002$, and various Josephson coupling values. (b) Spatial helicity modulus Υ_x as a function of spatial system sizes N for $\alpha = 0.005$, $K_\tau = 0.002$, and various Josephson coupling values. (Inset) The universal jump of the helicity modulus is expected to be $2/\pi$ for a BKT transition. This value is indicated by a broken line in the insets. The universal jump as calculated from the fitting procedure is shown to be in good correspondence with the BKT scenario.

that the NOR-CSC transition is a BKT transition. The temporal interaction terms are evidently completely incapable of establishing temporal order at this transition. In particular, when comparing Figs. 7(a) and 7(b) corresponding to no dissipation and weak dissipation, respectively, no significant difference is visible. Even though the dissipation term has a major impact on the temporal fluctuations,[36] the spatial helicity modulus appears completely unaffected by the presence of dissipation in the CSC phase.

The classification of the NOR-CSC transition is important in two respects. First, the finite-size analysis shows that the existence of a finite helicity modulus in the CSC phase is not a mere finite-size effect. Secondly, the analysis places the transition in the BKT universality class. This would not have

been possible if there were a divergent correlation length in the temporal direction. Such an effect would have been likely to show up as a breakdown of the scaling procedure. In this way the analysis gives an indirect verification that the transition is of a purely spatial nature, and that the CSC phase is temporally disordered and spatially quasiordered.

VI. THE NOR-FSC TRANSITION $\alpha_c^{(1)}$

The transition line $\alpha_c^{(1)}$ is the only transition line in the phase diagram that exhibits a simultaneous temporal and spatial order-disorder transition. Hence, it involves an interplay between instantons (or instantonlike objects) and vortices, but in a complicated way that is not easy to disentangle.

In this section, the Josephson coupling strength will be fixed at an intermediate value of $K = 0.4$, for which a classical counterpart of our model would be well inside the disordered phase ($\Upsilon_x = 0$). The quantum coupling is set to $K_\tau = 0.1$. Note that this differs from the value of K_τ used to compute the phase diagram in Fig. 1.

Figure 8 shows typical configurations of the bond variable $\Delta\theta$ as a function of τ for two dissipation strengths corresponding to regimes where the model behaves quantitatively different. The topmost curve corresponds to weak dissipation, with anomalous diffusive behavior of the value of $\Delta\theta$. The lowest curve represents the regime of strong dissipation, where the imaginary-time history of $\Delta\theta$ is qualitatively less rough and where we can therefore show below that the bond variable is localized.

We see from Fig. 9 that the amplitude of the temporal bond fluctuations are rapidly decreasing with increasing α. At a critical value of the dissipation strength $\alpha = \alpha_c^{(1)}$, the MSD features a steep drop marking the localization transition where the tunneling of $\Delta\theta$ is suppressed sufficiently to give the bond variables a well-defined value in imaginary time.[37] We are once

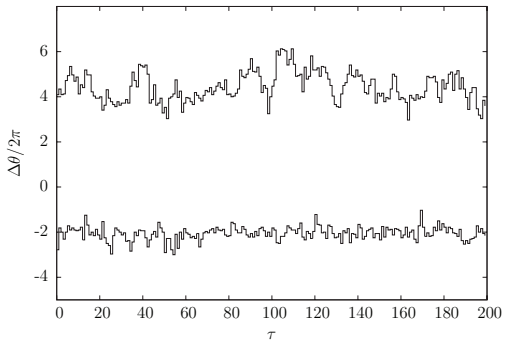

FIG. 8. The bond variable $\Delta\theta$ as a function of imaginary time τ for two different values of the dissipation strength, $\alpha = 0.011$ and $\alpha = 0.021$, in the weak and intermediate Josephson coupling regime. These values correspond to the normal phase and the ordered phase, respectively. The quantum paths of $\Delta\theta$ in the normal phase (relatively low values of K) exhibit fairly slow variations in time, and are not necessarily well described in terms of instantons. Note the contrast to the quantum paths in the topmost curve above and the topmost curve in Fig. 2.

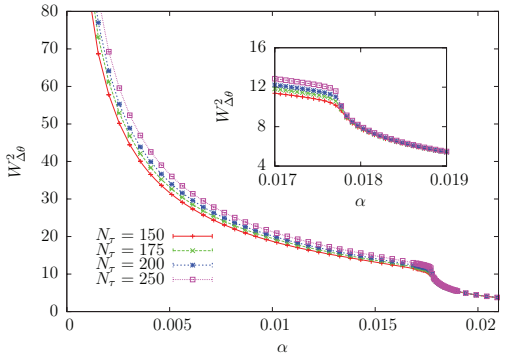

FIG. 9. (Color online) $W^2_{\Delta\theta}$, Eq. (6), as a function of dissipation strength α for a system with $K_\tau = 0.1$, $K = 0.4$, $N = 20$, and various values of N_τ. Note the kink in the curves at $\alpha = \alpha_c^{(1)}$ and the saturation of $W^2_{\Delta\theta}(N_\tau)$ at a finite value for $\alpha > \alpha_c^{(1)}$. Error bars are smaller than the data points. (Inset) Blow-up of the region around $\alpha_c^{(1)}$.

again able to distinguish between two separate states based on the scaling properties of the MSD. In Fig. 10, we present a plot of the MSD as a function of $\ln N_\tau$ for several values of α. The lowermost curve in the figure again represents the FSC phase, $\alpha > \alpha_c^{(1)}$, where the MSD is independent of N_τ. All other curves represent dissipation strengths below the localization transition, and for these a clear logarithmic scaling is observed. In this way, there are distinct delocalized and localized regimes for the bond variable also at weak Josephson coupling, and the temporal fluctuations in each of them behave in exactly the same way as for strong Josephson coupling.[38]

To confirm that the temporal transition at $\alpha = \alpha_c^{(1)}$ also marks the onset of spatial ordering, we show in Fig. 11 the helicity modulus Υ_x. Note the abrupt manner in which the phase stiffness attains a finite value at $\alpha = \alpha_c^{(1)}$. Even though the spatial extent of the system is relatively small, there is no weak-dissipation tail which would have been visible for too

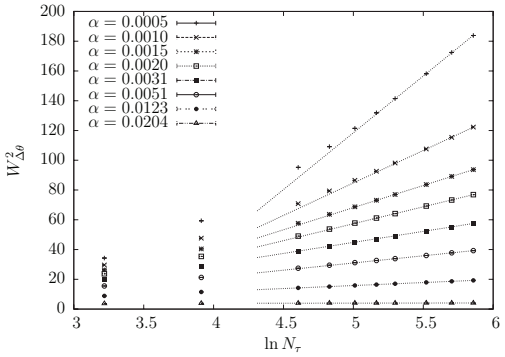

FIG. 10. $W^2_{\Delta\theta}$, Eq. (6), as a function of $\ln N_\tau$ for various values of α ranging from the weak-dissipation limit to the ordered state at the top and bottom, respectively. The logarithmic behavior found at large N_τ is indicated by dotted lines. Error bars are much smaller than the data points.

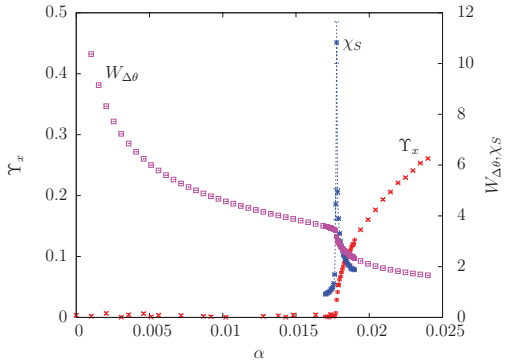

FIG. 11. (Color online) Spatial helicity modulus Υ_x, Eq. (4), action susceptibility χ_S, Eq. (10), and mean fluctuation $W_{\Delta\theta}$, Eq. (6), as a function of dissipation strengths for a system with $K_\tau = 0.1$, $K = 0.4$, $N = 20$, and $N_\tau = 250$. Note that Υ_x vanishes continuously at $\alpha_c^{(1)}$ (no jump).

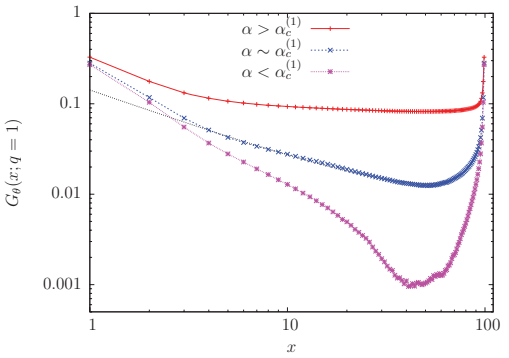

FIG. 12. (Color online) Double-logarithmic plot of the spatial correlation functions $G_\theta(x; q = 1)$ at values of α corresponding to above, close to, and below the NOR-FSC phase transition. The relevant coupling values are $K = 0.4$ and $K_\tau = 0.1$, and the system size is given by $N = 100$ and $N_\tau = 30$. At $\alpha \sim \alpha_c^{(1)}$ the correlation function appears to be linear at long distances, indicating scale-invariant spatial fluctuations. The dotted line indicates this linear behavior. Thus, $\xi \to \infty$, or at the very least $\xi > N/2$.

small system sizes. In the same figure we also show the root mean square displacement, $W_{\Delta\theta}$, and the action susceptibility, χ_S. It is clear that all observables feature a nonanalyticity at the same point. We can therefore conclude that the transition NOR-FSC is a quantum phase transition involving simultaneous onset of spatial and temporal order.

In Fig. 11, we note that the nonanalyticity in Υ_x on the line $\alpha_c^{(1)}$ is brought out very sharply at the system sizes we consider in this case, namely $20 \times 20 \times 250$. Assuming hyperscaling and two diverging length scales ξ (spatial) and ξ_τ (temporal), we may write

$$\Upsilon_x \sim \xi^{2-d-z} \sim \xi^{2-d}\xi_\tau^{-1} \sim N_\tau^{-1}. \tag{14}$$

Here we have introduced the dynamical critical exponent z defined by $\xi_\tau \sim \xi^z$. The sharpness can thus be explained by the large system size and diverging length scale in the τ direction. Very little finite-size effects may then be expected due to the limited spatial extent of the system, since $d = 2$ and the spatial correlation length drops out of the scaling.

Ordinarily, it would have been natural to attempt a scaling analysis of this phase transition based on the Binder ratio,

$$Q = \frac{\langle |m|^4 \rangle}{\langle |m|^2 \rangle^2}, \tag{15}$$

in order to extract the dynamical critical exponent of the system z. Here m is the magnetization order parameter of the superconducting phases defined in Eq. (5). An ordinary quantum critical point is characterized by diverging lengths in space and time, ξ and ξ_τ, respectively. The Binder ratio is then expected to scale according to

$$Q = Q\left(\frac{N}{\xi}, \frac{N_\tau}{\xi_\tau}\right). \tag{16}$$

The correlation lengths entering here are correlation lengths of the phase-correlation function, measuring θ correlations in the spatial and τ directions. Thus, it should be possible to collapse the Binder ratio curves, at criticality, as a function of N_τ/N^z for the correct value of z.

We have attempted such an analysis in this case, and failed. In our computations, we have been able to identify a diverging length scale ξ based on the above scaling approach, but not a diverging length scale ξ_τ. The reason is that in our model, the coupling in spatial directions is effective in ordering the phases θ, while the coupling in the τ direction is only effective in ordering bond variables $\Delta\theta$, while the θ variables never order in the τ direction. One may therefore define a diverging length ξ entering Eq. (16), but not a diverging length ξ_τ. A diverging length scale in the τ direction may very well exist for the bond variables $\Delta\theta$, but not for the phase variables θ.

The onset of long-range order in the θ variables in the spatial directions may be described by the spatial correlation function $G_\theta(x; q = 1)$, Eq. (8). In Fig. 12 we present spatial correlations corresponding to dissipation strengths slightly below the NOR-FSC transition ($\alpha < \alpha_c^{(1)}$), close to the transition ($\alpha \approx \alpha_c^{(1)}$), and slightly above the transition ($\alpha > \alpha_c^{(1)}$). The spatial correlation length appears to behave as expected for a second-order phase transition into a phase with long-range (spatial) order, implying that the NOR-FSC transition is associated with a diverging length scale in the spatial directions.

VII. DISCUSSION

Since the work of Hertz,[39] quantum critical points are commonly characterized by their dynamical critical exponent z. Underlying Hertz' scaling theory is Landau's notion that all relevant fluctuations of a system may be ascribed to fluctuations of an order parameter.[40] This is evident when considering that the exponent z is defined from a divergence of a length scale of the order parameter correlation function. Such a characterization may therefore be insufficient when the critical point cannot be well described by one single order parameter, a problem which has been pointed out in different cases in recent theoretical works.[41,42]

The model studied in this paper may be related to a problem of this kind in the sense that we are unable to find one single order parameter adequately describing the spatial, temporal, and spatio-temporal phase transitions separating the NOR, FSC, and CSC phases in Fig. 1. To substantiate this, we show in Appendix A that the noncompact θ variables may instead be formulated by a combination of a compact phase field $\tilde{\theta} \in [-\pi,\pi\rangle$ and an additional integer-valued field k containing information on what 2π interval the original variable belongs to. Using the reformulation of the θ variables described in Appendix A, it is clear that the magnetization order parameter m only probes the order of the compactified part of the phase, $\tilde{\theta}$, but is completely oblivious to the state of the integer-valued field k. Since the state of this field describes whether or not the phase differences $\Delta\theta$ are localized, m is fundamentally incapable of describing the localization transition concurring with the onset of coherence of $\tilde{\theta}$. As a result, we are unable to define a dynamical critical exponent z.

The phase transition from CSC to FSC is primarily temporal in the sense that it only involves condensation of instantons from a state where the spatial topological defects are already tightly bound. However, this localization of $\Delta\theta$ also contributes to spatial ordering by coupling the Trotter slices along imaginary time, thereby reducing spatial fluctuations sufficiently to render the system behavior 3D. Accordingly, CSC-FSC is also of a mixed character, as the transition separates a phase with spatial QLRO (CSC) from a phase where spatial long-range order is established (FSC).

The phase transition from NOR to CSC is of a purely spatial nature. As one increases the Josephson coupling for weak dissipation, this transition involves only the binding of the (spatial) vortex degrees of freedom while the (temporal) instantons remain proliferated. This conclusion is supported by the signatures of a BKT-type transition found in Sec. V. In this way, the system behaves as a stack of decoupled two-dimensional layers in the CSC phase, each exhibiting critical fluctuations in the $\tilde{\theta}$ field.

The phase transition from FSC to NOR is much more complicated than the ones from FSC to CSC and from CSC to NOR, and appears to be of a type not previously considered in connection with superconductor-metal phase transitions. Since one cannot characterize the anisotropy of the phase transitions quantitatively in terms of an exponent z, we resort to more qualitative considerations of the spatial and temporal degrees of freedom. In the case of intermediate coupling, one has a concomitant binding of vortices and localization of $\Delta\theta$ upon entering the FSC phase from the NOR phase. This corresponds to the ordering of the degrees of freedom relevant to space ($\tilde{\theta}$) and time (k), respectively. Due to this simultaneity, we characterize the NOR-FSC phase transition as a mixed spatio-temporal phase transition. It is an interplay between two distinct types of topological defects (point vortices and temporal fluctuations in $\Delta\theta$) that determines the character of the phase transition. This phase transition is therefore neither of the BKT type, nor in the 3D XY universality class. The former is characterized by proliferation of pointlike vortices in two dimensions, while the latter is characterized by the proliferation of $(2+1)$-dimensional vortex loops.[43–45] Dissipation, and the associated decompactification of the θ variables, leads to a disordering of the θ variables in the imaginary-time direction in all regions of the phase diagram. Decompactification essentially chops up the vortex loops into spatial point vortices and instantonlike objects in $\Delta\theta$, thereby destroying the Lorentz-invariant physics of vortex-loop proliferation at the quantum phase transition.

In order to exhaust all combinations of spatial and temporal order/disorder, one could also imagine a fourth phase exhibiting temporal order without accompanying spatial phase coherence. This would correspond to $W^2_{\Delta\theta} = \text{const.}$ and $\Upsilon_x = 0$ (i.e., a phase with localized bond variables and proliferated vortices). The most probable location of such a phase would be at weak spatial coupling and large dissipation strength, corresponding to the lower right corner of Fig. 1. This scenario opens the possibility of a purely temporal ordering coinciding with exponentially decaying spatial correlations upon entering this hypothetical phase from the NOR phase. Due to this locality, such a transition could be a possible realization of a local quantum critical point ("$z = \infty$") in a spatially extended system. In order to emphasize that the existence of this local phase is only a possibility that we have not actually found in our computations, we have drawn a box of solid lines around the specific region in Fig. 1 and indicated possible realizations of the phase transitions by dotted lines. Although the existence of such a phase has been conjectured by analytical work[2,5,9] and there is numerical work supporting this view,[12] we find no signatures pointing to the existence of such a local phase in any of the parameter sets considered. Rather, our results strongly indicate that a spatial coupling is always rendered relevant by a large enough dissipation parameter α.[19] In this way, the localization of $\Delta\theta$ will always induce an onset of spatial phase coherence. This is equivalent to saying that instantonlike excitations will always proliferate prior to, or simultaneously with, the unbinding of vortices as the strength of dissipation α is reduced. Local quantum criticality (in the sense of having temporal critical fluctuations coinciding with spatial disorder) would follow from vortices proliferating prior to instantons as the disordered state (NOR) is approached from the fully bond-ordered superconducting state (FSC) by reducing α.

Finally, we compare the phase diagram found in this paper with the phase diagram calculated for a model similar to Eq. (3) using compact variables.[16] Figure 13 shows two schematic phase diagrams, and the following discussion pertains to their topology. The topmost diagram summarizes the results found in this paper, while the lowermost diagram is the phase diagram for the $(2+1)$D dissipative quantum rotor model. In the latter case, the diagram features one single phase transition line separating a completely ordered state from a disordered state. The phase transition separating them is driven by a proliferation of vortex loops. This transition line is isotropic in space time ($z = 1$) meaning that the entire line is in the 3DXY universality class. From the lowermost phase diagram it is clear that if we start in the limit of no dissipation, $\alpha = 0$, and increase α for $K > K_{3DXY}$, the dissipation term only contributes to further dampening the innocuous three-dimensional spin-wave excitations. This can only increase the superfluid density in the ordered phase. However, in the noncompact model the regime $K > K_{\text{BKT}}$, and weak dissipation, represents a phase involving both two-dimensional spatial spin waves and a proliferated instanton gas. Increasing α from this regime may therefore

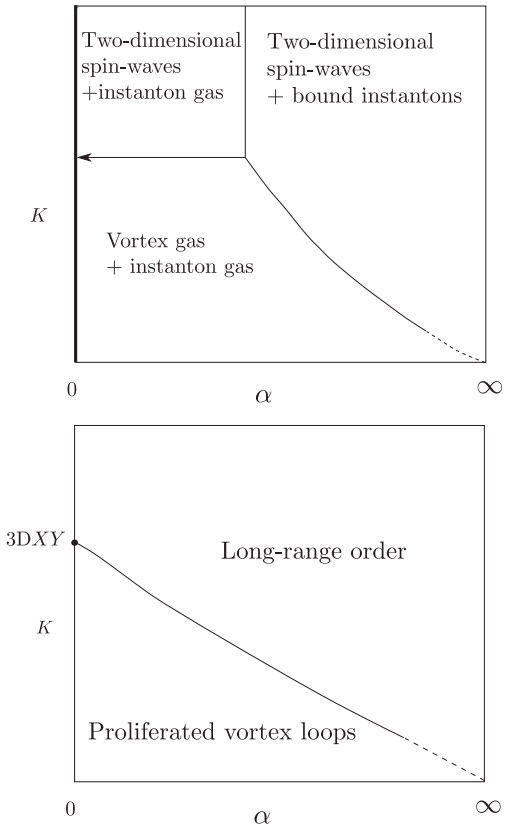

FIG. 13. Comparison of the phase diagrams of the noncompact (topmost) and compact (lowermost) models. (Topmost diagram) The phase diagram found in this work. All phases feature disordered θ variables in the imaginary-time direction. A notable feature is the phase CSC where bound vortex antivortex pairs coexist with disordered bond variables $\Delta\theta$ in the τ direction. This is a consequence of the θ variables being defined with noncompact support. This is only true for finite α as the quadratic form of the dissipation term is the origin of the decompactification. Consequently, the physics found at finite α cannot be analytically connected to the limit $\alpha = 0$. The description at $\alpha = 0$ would require compact phases and thereby a loss of the instanton degrees of freedom. For $\alpha = 0$ there is a phase transition at a critical value of K, but this phase transition is in the 3D XY universality class, as in the lowermost diagram. $\alpha = 0$ is therefore a singular endpoint of the horizontal line in the topmost diagram. (Lowermost diagram) The phase diagram found for a $(2+1)$D bond-dissipative quantum rotor model with compact variables. In this case the diagram features only a single transition line where the system undergoes a spatio-temporally isotropic ($z = 1$) phase transition in the 3D XY universality class. See Ref. 16 for details.

drive a phase transition because the dissipation term is effective in binding these temporal defects. Therefore, the feature of the phase diagram of the noncompact model that really sets it apart from the phase diagram of the dissipative 3D XY model (i.e., the compact case) is the existence of a phase at weak dissipation involving spatial ordering concomitant with temporal disorder. The resulting phase CSC has no counterpart in the dissipative 3D XY model, since in the latter model the phases θ are compact. Compact phases θ promote vortex loops as the critical fluctuations, while noncompact phases θ promote vortices and instantons as relevant fluctuations driving the phase transitions.

The phase CSC corresponds to a resistively shunted Josephson junction array which may sustain a finite Josephson current through the array, but nonetheless features finite voltage fluctuations across each junction of the junction array. This may be viewed locally (at a single junction) as a metallic state, but globally (throughout the system) as a superconductor. The most complicated aspect of the phase diagram of the noncompact model is the direct phase transition between the NOR phase and the FSC phase, which is considerably more difficult to characterize than the $z = 1$ order-disorder transition in the dissipative 3D XY model.

A $(2+1)$-dimensional model with bond dissipation has recently been considered as an effective theory of quantum criticality at optimal doping in high-T_c cuprates.[17] The claim of this work is that the phase correlators of the model at the critical point decay algebraically as $1/\tau$ while they are short ranged in space. Such a phase transition would be an example of local quantum criticality. Monte Carlo simulations on the $(2+1)$-dimensional quantum rotor model gives an order-disorder transition in the 3D XY universality class, which is quite different from local quantum criticality. From the results of the present paper, it appears to be important to specify whether the phase variables are compact or noncompact (cf. Fig. 13). The phase transitions separating the CSC phase from the FSC phase, or the CSC phase from the NOR phase, are not of the type described in Ref. 17. To verify whether or not the remaining phase transition separating the FSC phase from the NOR phase is an example of local quantum criticality one would ideally need a single order parameter measuring spatial and temporal correlations in phases, θ. Since we do not have this at our disposal, we have not been able to determine what sort of universality class the critical line separating FSC and NOR belongs to, apart form concluding that it is not in the 2D XY or 3D XY universality class. However, the spatial correlation functions presented in Fig. 12 suggest that the NOR-FSC transition line is not a line with local spatial phase correlations.

We end with an important remark on the temporal phase fluctuations we have focused on in this paper. The quantity $W^2_{\Delta\theta}$ in Eq. (6) measures temporal fluctuation in *phase gradients* $\Delta\theta$, defined on a *spatial* bond of the lattice. One could also study a corresponding measure of temporal fluctuations of the phases θ themselves. We have done this, and find the following. In all parts of the phase diagram in Fig. 1, the quantity

$$W^2_\theta(N_\tau) = \frac{1}{N_\tau}\left\langle \sum_\tau^{N_\tau} (\theta_\tau - \overline{\theta})^2 \right\rangle, \tag{17}$$

diverges with N_τ. This underlines that the instantons or instantonlike objects we have discussed in this paper are temporal fluctuations in phase gradients $\Delta\theta$, not instantons

in phases θ. On the other hand, the helicity modulus Eq. (4) measures long-range or quasi-long-range spatial ordering of phases θ, and we find such orderings in the FSC and CSC phases. Thus, the FSC phase does not exhibit 3D XY ordering. It features spatial ordering of θ and $\Delta\theta$, but temporal ordering only of $\Delta\theta$. This supports the statement made above, that the NOR-FSC transition is not in the 3D XY universality class. It is a new type of phase transition involving a complicated interplay between spatial point vortices and instantonlike excitations in $\Delta\theta$.

VIII. CONCLUSIONS

The model discussed in this paper describes a two-dimensional array of quantum dissipative Josephson junctions. By extensive Monte Carlo simulations we have shown that the model features three distinct phases (see Fig. 1) featuring different behaviors of spatio-temporal fluctuations. We have quantified these fluctuations by the mean square fluctuation $W^2_{\Delta\theta}$, Eq. (6), and the spatial helicity modulus Υ_x, Eq. (4).

The normal phase (NOR) is found at weak dissipation and weak Josephson coupling strength. In this phase, the spatial helicity modulus is zero, signaling a vanishing stiffness to infinitesimal phase twists on each Trotter slice. The phase differences of the individual junctions are highly fluctuating in imaginary time and the system therefore exhibits metallic behavior. Increasing the dissipation strength drives the system to a phase transition where the phase differences $\Delta\theta$ are localized into one of the minima of the Josephson potential. This localization of bond variables in imaginary time occurs simultaneously with an onset of rigidity towards phase twists across the spatially extended system. We identify this phase with a fully bond-ordered superconducting state (FSC).

At strong coupling and weak dissipation we identify an intriguing phase exhibiting finite phase stiffness and algebraically decaying spatial correlations. The imaginary-time direction remains disordered with wildly fluctuating bond differences. This dimensionally reduced phase is referred to as a critical superconducting (CSC) phase. The finite helicity modulus in this phase indicates that the system may sustain a dissipationless current going through the entire JJA. There are, however, voltage fluctuations present which in principle should make it experimentally distinguishable from a fully bond-ordered superconducting phase, and also distinct from the more standard 3D XY ordered fully superconducting state where even the phases θ are ordered in all directions.

We have found no signs of a phase which is temporally ordered (in the sense of having a bounded $W^2_{\Delta\theta}$) and proliferated vortices. Such a phase would naturally facilitate the observation of local quantum criticality in which a spatially disordered and temporally (quasi)ordered system disorders in the imaginary-time direction.

ACKNOWLEDGMENTS

The authors acknowledge useful discussions with E. V. Herland, A. Hansen, I. Simonsen, V. Aji, C. M. Varma, and J. Zaanen. A.S. was supported by the Norwegian Research Council under Grant No. 205591/V30 (FRINAT). E.B.S. and I.B.S thank NTNU for financial support. The work was also supported through the Norwegian consortium for high-performance computing (NOTUR). A.S. thanks the Aspen Center for Physics under NSF Grant No. 1066293, where part of this work was done, for hospitality.

APPENDIX A: REFORMULATING THE NONCOMPACT DEGREES OF FREEDOM

To gain further insight into the three phases reported in this work and the transitions between them, we consider the following decomposition of the phase degrees of freedom:

$$\theta_{\mathbf{x},\tau} \to \tilde{\theta}_{\mathbf{x},\tau} + 2\pi k_{\mathbf{x},\tau}. \tag{A1}$$

The noncompact starting point θ is thereby exchanged for a compact phase field, $\tilde{\theta} \in [-\pi,\pi\rangle$, plus an integer-valued field k, keeping track of the specific 2π interval the original variable belonged to. In the partition function, this reformulation amounts to

$$\begin{aligned} Z &= \int \mathcal{D}\theta e^{-S} = \int_{-\infty}^{\infty} \prod_{\mathbf{x},\tau} (d\theta_{\mathbf{x},\tau}) e^{-S} \\ &\to \sum_{\{k\}} \int \mathcal{D}\tilde{\theta} e^{-S} = \sum_{\{k\}} \int_{-\pi}^{\pi} \prod_{\mathbf{x},\tau} (d\tilde{\theta}_{\mathbf{x},\tau}) e^{-S}. \end{aligned} \tag{A2}$$

Note that k is defined on every point in space time and has nothing to do with the winding number found in some realizations of quantum rotor models with compact phases.

It should also be noted that the 2π-periodic spatial interaction is only sensitive to the $\tilde{\theta}$ field. Also, the compactness of $\tilde{\theta}$ enables the identification of vortices in this field in a similar way as discussed in connection with the classical 2D XY model, Eq. (1). The finite Υ_x observed in the CSC and FSC phases may thereby be attributed to phase coherence in $\tilde{\theta}$. In addition to the vortex degrees of freedom found in the classical version of the system, the noncompactness of the quantum version introduces an additional degree of freedom (k) associated with the tunneling of bond variables from one minimum of the extended Josephson potential to another.

In the NOR phase, we found $\Upsilon_x = 0$, which may be understood as a phase featuring proliferated vortices of the $\tilde{\theta}$ field, as well as proliferated instantons in $\Delta\theta$. Increasing the Josephson coupling (for small α) drives the system into the CSC phase with $\Upsilon_x \neq 0$, which corresponds to a binding of vortices into dipoles. Nonetheless, the bond variables remain anomalously diffusive, $W^2_{\Delta\theta} \propto \ln N_\tau$, in both the NOR and the CSC phase. At strong coupling, the bond variables tend to stay in the vicinity of the minima of the potential wells, $\Delta\theta \approx 2\pi\,\Delta k$. From the viewpoint of the reformulated variables, the delocalized bond variables in the CSC phase is an expression of an unbroken symmetry $\Delta k \to \Delta k + \Lambda$, where Λ is an integer. Moreover, the integer field k may be directly connected with the instanton charges in the strong-coupling limit by $\Delta k_{\tau+1} - \Delta k_\tau = n_{\mathrm{I}}$. The delocalization of $\Delta\theta$ manifests itself as proliferated instanton/anti-instanton configurations in this regime, and the CSC phase may therefore be described as an instanton gas. This is illustrated in the topmost curve of Fig. 2, illustrating the quantum paths of $\Delta\theta$ in the CSC phase of Fig. 1.

For weak Josephson coupling, the excitations in the imaginary-time path of $\Delta\theta$ are strictly speaking not well described by topological instanton defects. This is quite

evident from the topmost curve of Fig. 8, describing the quantum paths of $\Delta\theta$ in the NOR phase of Fig. 1. Nevertheless, as the quantum fluctuations still respect the same symmetry $\Delta k \to \Delta k + \Lambda$, we choose to refer to such excitations as instantons also in the NOR phase. In the FSC phase, on the other hand, localization of bond variables implies that the symmetry is broken for both weak and strong coupling. Starting at large K and large α, the picture is therefore as follows: In the FSC phase, both the defects associated with $\tilde{\theta}$ (vortices) and with k (instantons) are absent or tightly bound. Lowering α into the CSC phase, instantons are proliferated while the vortices remain bound. Lowering K from the CSC phase into the NOR phase, the vortices proliferate as well.

APPENDIX B: CORRELATION FUNCTIONS IN THE NOR PHASE

It has recently been proposed[19,25] that the metallic state of Josephson junction arrays might exhibit nontrivial behavior. Here, it was argued that the $(0+1)$-dimensional constituents of the array may slide past each other in what was denoted a "floating phase."[25] Similar dimensionally decoupled phases are also believed to be relevant to other physical systems such as layered superconductors[46] and stacks of two-dimensional arrays of membrane proteins.

These papers employed a renormalization group analysis to show that the spatial coupling between the superconducting islands is perturbatively irrelevant on the disordered side of the transition. They also calculated the correlation functions Eq. (8) and (9) in this regime and found that they had a form that indicated unconventional, purely local fluctuations. Monte Carlo studies[11] of a single resistively shunted Josephson junction also indicated that a similar form of correlation functions could be found in $(0+1)$D systems as well. The correlation functions employed in these analyses featured a noninteger parameter q that was introduced to probe fluctuations with another periodicity than the underlying Josephson potential. In the presence of a finite Josephson potential, expectation values such as $\langle \exp(\mathrm{i}\Delta\theta_{\mathbf{x},\mathbf{x}',\tau})\rangle$ will generally not be equal to zero in any phase. This is, however, due to the corresponding symmetry being explicitly—and not spontaneously—broken, and has consequently nothing to do with a phase transition. The parameter q was therefore introduced to assure correlation functions decaying to zero in the disordered phase. Similar correlation functions have also been considered before in investigations of roughening transitions of crystal surfaces with quenched bulk disorder.[47] We will refer to them as *fractional correlation functions*.

Figure 14 shows both spatial and temporal correlation functions, Eq. (8), at a dissipation strength deep in the NOR phase where the Josephson potential is expected to be irrelevant[25] and we are far away from the phase transition at $\alpha = \alpha_c^{(1)}$. The correlation functions in the bottom row include a noninteger factor $q = 1/3$; the top row shows the correlation functions without $(q = 1)$ this noninteger factor. Comparing the correlation function of the temporal direction with the spatial direction for $q = 1/3$, it is clear that the spatial and temporal behaviors of the system *appear* completely decoupled.[48] As we discuss below, this local behavior of the fractional correlation functions is misleading.

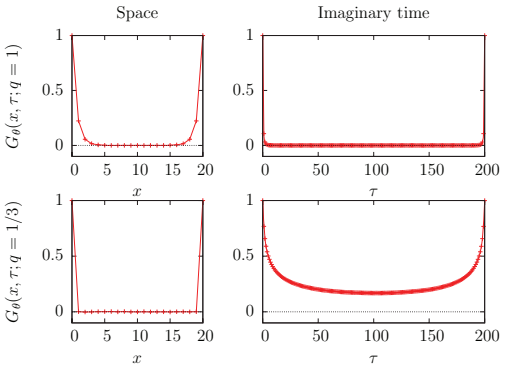

FIG. 14. (Color online) Correlation functions, Eq. (8), in both space (left column) and imaginary time (right column) in the normal phase. The relevant coupling parameters are $\alpha = 0.012$, $K = 0.4$, and $K_\tau = 0.1$. There is a pronounced difference between the correlations along the spatial and temporal directions for $q = 1/3$.

Appendix A introduced a reformulation of the phase variables that clarifies the difficulties concerning the construction of a globally defined order parameter describing our system. The reformulation of the phase variables also offers an alternative viewpoint on the fractional correlation functions. For example, imagine a 2D XY model, Eq. (1), being formulated with noncompact phase variables instead of the standard compact variables. In the partition function, the summation over k is trivial, yielding only a renormalization of the ground-state energy, because there is no coupling between different k sectors in the action. The remaining integration over $\tilde{\theta}$ is the partition function of the ordinary 2D XY model. When performing Monte Carlo simulations on the 2D XY model with a noncompact formulation of the phases, we find the usual QLRO phase at strong Josephson coupling, in which the correlation function $G_\theta(\mathbf{x}; q = 1)$ of Eq. (8) decays algebraically. However, consider probing the QLRO phase with a *fractional* correlation function, $q < 1$. This correlation function involves contributions from several k sectors, ultimately averaging the correlator to zero for all distances. The same result holds for the disordered phase, and so, although the QLRO phase is phase coherent and the disordered phase is not, the fractional correlation function essentially cannot tell them apart.

Applying exactly the same arguments as above to our CSC phase with spatial QLRO, one realizes that the spatial fractional correlation function will vanish also here. In analogy with the classical 2D XY model, we argue that this should not be regarded as a signature of completely spatial decoupling in neither the CSC phase nor the NOR phase. The apparent locality of the normal phase, and by extension the corresponding floating phase of Ref. 25, is consequently not a result of the dissipative interaction *per se*. Rather, a floating phase with such vanishing spatial fractional correlations follows as a direct result of the noncompactness of the phase variables, which in turn is caused by their coupling to a dissipative bath.

In the following we provide supplementary details regarding the fractional correlation functions. To be specific,

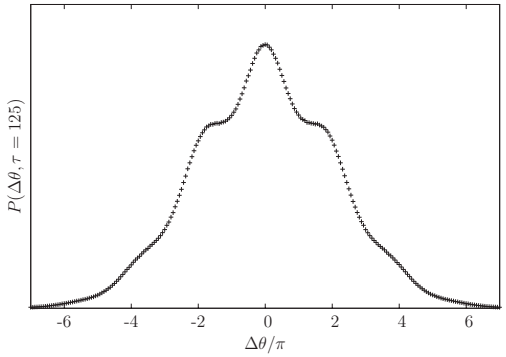

FIG. 15. The distribution of $\Delta\theta_\tau - \Delta\theta_0$, $P(\Delta\theta, \tau = 125)$, in arbitrary units for a system with $K_\tau = 0.1$, $K = 0.4$, and dissipation strength $\alpha = 0.011$. The distribution is extracted from the Monte Carlo simulations and is conjectured to follow Eq. (B1).

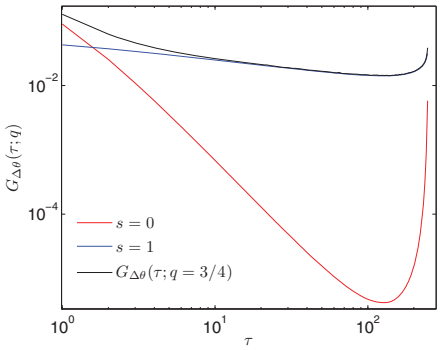

FIG. 16. (Color online) The unequal-time bond correlation function, $G_{\Delta\theta}(\tau; q = 3/4)$, for a system with $K = 0.4$, $K_\tau = 0.1$, $\alpha = 0.011$, $N = 20$, and $N_\tau = 250$. The black curve is the correlation function Eq. (9) sampled directly from the Monte Carlo simulations. The red (lowermost gray) and blue (uppermost gray) curve are the $s = 0$ and $s = 1$ terms of Eq. (B3), respectively, and are calculated as explained in the text.

we will investigate the fractional bond correlation functions $G_{\Delta\theta}(\tau; q)$ more carefully, and prove that a power-law tail is expected in the weak dissipation regime. We first consider the distribution function $P(\Delta\theta, \tau)$, as was also the starting point of Ref. 19. This function describes the diffusion of the phase difference $\Delta\theta_\tau$ with respect to its value at $\tau = 0$. The distribution broadens for increasing τ and is illustrated for a fixed imaginary-time distance in Fig. 15. We find that the distribution function can be very well fitted by the functional form,

$$P(\Delta\theta, \tau) = P_0 e^{-\frac{\Delta\theta^2}{2\sigma_G^2}} \sum_n e^{-\frac{(\Delta\theta - 2\pi n)^2}{2\sigma^2}}, \tag{B1}$$

where P_0 is a normalization constant. The distribution is made up of a sequence of sub-Gaussians with standard deviation σ centered around the minima of the Josephson potential. In addition, there is an overall Gaussian convolution characterized by a standard deviation σ_G. We find empirically that whereas σ is dependent on K, it is independent of the distance τ in imaginary time. The overall variance $\mathcal{G}(\tau)$ of the distribution, as defined by

$$\mathcal{G}(\tau) = \langle (\Delta\theta_\tau - \Delta\theta_0)^2 \rangle, \tag{B2}$$

grows logarithmically with τ. This variance can furthermore to a very good approximation be identified with the variance σ_G^2 of the convolution function.

The calculations in Ref. 19 were based on a strong-coupling limit for the distribution function, with an additional assumption that the spatial coupling will renormalize to zero regardless of its bare value. For large values of K, we have demonstrated that the system will eventually reach a superconducting state (i.e., the CSC phase or the FSC phase) for all $\alpha > 0$. It is also clear from Fig. 15 that there is an appreciable broadening of the sub-Gaussians ($\sigma > 0$) compared to the delta function distribution implicit in the strong-coupling limit ($\sigma \to 0$).

We next consider the implications of a finite σ on the correlation function $G_{\Delta\theta}(\tau; q)$. Assuming Eq. (B1), we calculate

$$\langle e^{iq(\Delta\theta_\tau - \Delta\theta_0)} \rangle = e^{-\frac{1}{2}\sigma^2\kappa q^2} \sum_{s=-\infty}^{\infty} e^{-\frac{1}{2}\sigma_G^2 (q - s/\kappa)^2}, \tag{B3}$$

where $\kappa = \sigma_G^2/(\sigma_G^2 + \sigma^2)$. The sum over n has been traded for an integral at the cost of introducing an integer Poisson summation variable s. The n variable is subsequently integrated out. Comparing with Eq. (12) in Ref. 19, the broadening of the sub-Gaussians has introduced an overall prefactor and a multiplicative adjustment of the Poisson summation variable. The strong-coupling result is easily recovered in the limit $\sigma \to 0$. In the limit $\tau \to \infty$, the term with the slowest decay is dominant, hence the sum may be substituted by the term with the smallest $(q - s/\kappa)^2$. For a logarithmically diverging σ_G, we also have $\kappa \to 1$, meaning that Eq. (B3) is a scale-free power law in this limit.

In Fig. 16, we show a plot of $G_{\Delta\theta}(\tau; q = 3/4)$ and the two terms from Eq. (B3) corresponding to $s = 0$ and $s = 1$. We have set σ_G^2 equal to $\mathcal{G}(\tau)$ as measured from the Monte Carlo simulations in order to compare the analytical result Eq. (B3) with the fractional correlation function found numerically. σ is specified from fitting Eq. (B1) to data from Monte Carlo simulations. At short distances the $s = 0$ term is still contributing, but a clear crossover to the dominant $s = 1$ term is visible for larger values of τ. The excellent fit between the curves validates the functional form of the distribution (B1).

It is interesting to compare the behavior presented above with available numerical results for a single resistively shunted Josephson junction. Ref. 11 reports temporal fractional correlation functions in a $(0+1)$D system that are power law in much the same way as those in Ref. 19. They also report a logarithmically diverging MSD, but only at the phase boundary. This is in contrast to the results presented in Secs. VI and IV, where we find logarithmic growth as a generic feature of the weak-dissipation phases. Following Ref. 11, it is natural to consider the possibility that a logarithmically diverging MSD is the signature of critical behavior for models

describing Josephson junctions. A logarithmically diverging MSD follows from a logarithmically diverging $\mathcal{G}(\tau)$, and we have shown that the latter generates fractional bond correlators that are algebraically decaying in imaginary time. A possible scenario could be that the increased dimensionality of the problem has damped the fluctuations such that, in contrast to the single junction, the entire weak-dissipation regime features critical temporal correlations of the bond variables. However, we expect such a critical phase to produce divergent susceptibilities of the action. The simulations do not support this scenario and we find nonanalytic χ_S only at the points $\alpha = \alpha_c^{(1),(2)}$. Thus, a power-law form of the temporal fractional bond correlators can not necessarily be ascribed to critical behavior of the system.

[1] A. Schmid, Phys. Rev. Lett. **51**, 1506 (1983).
[2] W. Zwerger, EPL **9**, 421 (1989).
[3] R. Fazio and H. van der Zant, Phys. Rep. **355**, 235 (2001).
[4] G. Refael, E. Demler, Y. Oreg, and D. S. Fisher, Phys. Rev. B **75**, 014522 (2007).
[5] S. E. Korshunov, Zh. Eksp. Teor. Fiz. **95**, 1058 (1989).
[6] P. Goswami and S. Chakravarty, Phys. Rev. B **73**, 094516 (2006).
[7] P. A. Bobbert, R. Fazio, G. Schön, and G. T. Zimanyi, Phys. Rev. B **41**, 4009 (1990).
[8] S. Panyukov and A. Zaikin, Phys. Lett. A **124**, 325 (1987).
[9] S. V. Panyukov and A. D. Zaikin, J. Low Temp. Phys. **75**, 361 (1989).
[10] C. P. Herrero and A. D. Zaikin, Phys. Rev. B **65**, 104516 (2002).
[11] P. Werner and M. Troyer, Phys. Rev. Lett. **95**, 060201 (2005).
[12] P. A. Bobbert, R. Fazio, G. Schön, and A. D. Zaikin, Phys. Rev. B **45**, 2294 (1992).
[13] L. Capriotti, A. Cuccoli, A. Fubini, V. Tognetti, and R. Vaia, Phys. Rev. Lett. **94**, 157001 (2005).
[14] S. Chakravarty, G.-L. Ingold, S. Kivelson, and A. Luther, Phys. Rev. Lett. **56**, 2303 (1986).
[15] S. Chakravarty, G.-L. Ingold, S. Kivelson, and G. Zimanyi, Phys. Rev. B **37**, 3283 (1988).
[16] I. B. Sperstad, E. B. Stiansen, and A. Sudbø, Phys. Rev. B **84**, 180503(R) (2011).
[17] V. Aji and C. M. Varma, Phys. Rev. Lett. **99**, 067003 (2007).
[18] A dissipation kernel differing from the Caldeira-Leggett form has been calculated for coupling of a loop-current order parameter to gapless excitations at the Fermi level of high-T_c cuprates. Namely, it was shown in Ref. 49 that the mechanism leading to dissipation is scattering of the bosonic order parameter off gapless fermionic particle-hole excitations at the Fermi level. This produces Landau damping of the form ω/q, which is a manifestly nonlocal dissipation kernel. For an alternative formulation of the coupling of the bosonic order parameter to gapless fermions on the Fermi surface, see Ref. 50.
[19] S. Tewari, J. Toner, and S. Chakravarty, Phys. Rev. B **73**, 064503 (2006).
[20] V. Aji and C. M. Varma, Phys. Rev. B **82**, 174501 (2010).
[21] A. O. Caldeira and A. J. Leggett, Ann. Phys. (NY) **149**, 374 (1983).
[22] G. Schön and A. D. Zaikin, Phys. Rep. **198**, 237 (1990).
[23] G. Refael, E. Demler, Y. Oreg, and D. S. Fisher, Phys. Rev. B **68**, 214515 (2003).
[24] E. B. Stiansen, I. B. Sperstad, and A. Sudbø, Phys. Rev. B **83**, 115134 (2011).
[25] S. Tewari, J. Toner, and S. Chakravarty, Phys. Rev. B **72**, 060505(R) (2005).
[26] R. Metzler and J. Klafter, Phys. Rep. **339**, 1 (2000).
[27] P. Werner, G. Refael, and M. Troyer, J. Stat. Mech. (2005) P12003.
[28] P. Werner and M. Troyer, Prog. Theor. Phys. Suppl. **160**, 395 (2005).
[29] K. Hukushima and K. Nemoto, J. Phys. Soc. Jpn. **65**, 1604 (1996).
[30] H. G. Katzgraber, arXiv:0905.1629.
[31] M. Matsumoto and T. Nishimura, ACM Trans. Model. Comput. Simul. **8**, 3 (1998).
[32] A. M. Ferrenberg and R. H. Swendsen, Phys. Rev. Lett. **63**, 1195 (1989).
[33] A. V. Chechkin, R. Gorenflo, and I. M. Sokolov, Phys. Rev. E **66**, 046129 (2002).
[34] H. Weber and P. Minnhagen, Phys. Rev. B **37**, 5986 (1988).
[35] As mentioned in Sec. I B, the limit $\alpha = 0$ is not physical for the model Eq. (3) with noncompact phase variables. Nevertheless, the spatial behavior of the system changes continuously as one (artificially) reduces the parameter α to zero, so the value $\alpha = 0$ of Fig. 7(a) should simply be regarded as the limit of very weak dissipation.
[36] Although not explicitly shown, we observed diffusive ($H = 1/2$) scaling of $W^2_{\Delta\theta}$ for all values of K in the artificial limit $\alpha = 0$. The diffusive behavior of $W^2_{\Delta\theta}$ found at $\alpha = 0$, is replaced by logarithmic scaling for any finite value $0 < \alpha < \alpha_c^{(1),(2)}$.
[37] As a comment relevant to both this section and Sec IV, a fluctuation measure similar to $W^2_{\Delta\theta}$ was calculated in Ref. 10 for a single dissipative Josephson junction. It was suggested that this quantity exhibited a cusp at the localization transition, but later high-quality Monte Carlo simulations revealed a smoothly changing MSD around the critical dissipation strength.[11] Apparently, the α dependence of the MSD is not suitable for locating the critical point in $(0+1)$D. From the kink shown in the inset in Figs. 9 and 3, this is not the case for the spatially extended model considered here. A similar kink in a fluctuation measure may also have been present in previous results for a related $(2+1)$D RSJJA model,[13] but this curve was based on too few points for the feature to be convincingly resolved.
[38] It should be noted that there are stronger finite-size effects in $W^2_{\Delta\theta}$ in the NOR phase than in the CSC phase.
[39] J. A. Hertz, Phys. Rev. B **14**, 1165 (1976).
[40] D. Belitz, T. R. Kirkpatrick, and T. Vojta, Phys. Rev. B **65**, 165112 (2002).
[41] Q. Si, S. Rabello, K. Ingersent, and J. L. Smith, Nature (London) **413**, 804 (2001).
[42] D. Belitz, T. R. Kirkpatrick, and T. Vojta, Rev. Mod. Phys. **77**, 579 (2005).
[43] H. Kleinert, Gauge Fields in Condensed Matter (World Scientific, Singapore, 1989).
[44] A. K. Nguyen and A. Sudbø, Phys. Rev. B **60**, 15307 (1999).

[45] Z. Tešanović, Phys. Rev. B **59**, 6449 (1999).
[46] B. Horovitz, Phys. Rev. B **45**, 12632 (1992).
[47] J. Toner and D. P. DiVincenzo, Phys. Rev. B **41**, 632 (1990).
[48] Although not explicitly shown here, the fractional bond correlators behave qualitatively similar to the site correlators. With a noninteger q, $G_{\Delta\theta}(x;q)$ is zero for all spatial distances while $G_{\Delta\theta}(\tau;q)$ is slowly decaying in imaginary time.
[49] K. Børkje and A. Sudbø, Phys. Rev. B **77**, 092404 (2008).
[50] V. Aji, A. Shekhter, and C. M. Varma, Phys. Rev. B **81**, 064515 (2010).

Paper V

Quantum criticality in spin chains with non-ohmic dissipation

Phys. Rev. B **85**, 214302 (2012).

PHYSICAL REVIEW B **85**, 214302 (2012)

Quantum criticality in spin chains with non-Ohmic dissipation

Iver Bakken Sperstad, Einar B. Stiansen, and Asle Sudbø
Department of Physics, Norwegian University of Science and Technology, N-7491 Trondheim, Norway
(Received 28 March 2012; revised manuscript received 8 May 2012; published 6 June 2012)

We investigate the critical behavior of a spin chain coupled to bosonic baths characterized by a spectral density proportional to ω^s, with $s > 1$. Varying s changes the effective dimension $d_{\text{eff}} = d + z$ of the system, where z is the dynamical critical exponent and the number of spatial dimensions d is set to one. We consider two extreme cases of clock models, namely Ising-like and U(1)-symmetric ones, and find the critical exponents using Monte Carlo methods. The dynamical critical exponent and the anomalous scaling dimension η are independent of the order parameter symmetry for all values of s. The dynamical critical exponent varies continuously from $z \approx 2$ for $s = 1$ to $z = 1$ for $s = 2$, and the anomalous scaling dimension evolves correspondingly from $\eta \gtrsim 0$ to $\eta = 1/4$. The latter exponent values are readily understood from the effective dimensionality of the system, being $d_{\text{eff}} \approx 3$ for $s = 1$, while for $s = 2$ the anomalous dimension takes the well-known exact value for the two-dimensional Ising and XY models, since then $d_{\text{eff}} = 2$. However, a noteworthy feature is that z approaches unity and η approaches $1/4$ for values of $s < 2$, while naive scaling would predict the dissipation to become irrelevant for $s = 2$. Instead, we find that $z = 1, \eta = 1/4$ for $s \approx 1.75$ for both Ising-like and U(1) order parameter symmetry. These results lead us to conjecture that for all site-dissipative Z_q chains, these two exponents are related by the scaling relation $z = \max\{(2 - \eta)/s, 1\}$. We also connect our results to quantum criticality in nondissipative spin chains with long-range spatial interactions.

DOI: 10.1103/PhysRevB.85.214302 PACS number(s): 05.30.Rt, 05.70.Jk, 75.10.Pq, 75.40.Mg

I. INTRODUCTION

The spin-boson model[1,2] (SBM) represents one of the most well-established frameworks for describing the effect of dissipation on a quantum system. In its simplest incarnation, it describes a two-level system coupled to an infinite number of harmonic oscillators with low-frequency spectral density $J(\omega) \propto \omega^s$, with ohmic damping ($s = 1$) being the most commonly studied case. Generalizations of this model include extensions to finite (spatial) dimensions $d > 0$[3,4] and models where the Z_2 (Ising) spin symmetry has been replaced by a higher symmetry.[5,6] Extended versions of such systems may also find applications in the study of quantum critical points in quantum magnets and strongly correlated systems,[6–9] and hence they are of considerable interest in contemporary condensed-matter physics.

Another generalization is to consider non-Ohmic spectral densities ($s \neq 1$), which may be relevant in the description of several different physical phenomena.[10–17] From a more fundamental physics point of view, the sub-Ohmic ($s < 1$) SBM and related models have been studied intensively in recent years[18–20] following claims that the so-called quantum-to-classical mapping may be violated in even the simplest variant of SBM for $s < 1/2$.[21] Its super-Ohmic counterpart $s > 1$ has, on the other hand, received relatively little attention. This may be due to the fact that the $(0 + 1)$-dimensional $[(0 + 1)\text{D}]$ SBM exhibits a (quantum) phase transition only for values of $s \leqslant 1$. For $d \geqslant 1$, however, the possibility of a phase transition arises for all s.

The SBM is generally described, via the quantum-to-classical mapping, by a classical $(d + 1)$D spin model with long-range interactions that decay as $1/\tau^{1+s}$ in imaginary time τ. Long-range interactions are interesting, as they allow one to increase the effective dimensionality continuously by tuning s to lower values. In classical spin glasses, for instance, low-dimensional models with long-range interactions have been studied to infer properties of higher-dimensional realizations of the same systems with purely short-range interactions.[22–24] In quantum models, the effective dimensionality is expressed by $d_{\text{eff}} = d + z$, with z being the dynamical critical exponent defined from the divergence of the correlation time $\xi_\tau \sim \xi^z$, where ξ is the spatial correlation length. At a second-order phase transition, we have in standard notation $\xi \sim |K - K_c|^{-\nu}$ as the coupling parameter K approaches its critical value K_c. The presence of dissipation in general causes z to deviate from the value $z = 1$, with a naive scaling estimate $z_0 = 2/s$.[25] Although this result is exact in mean-field theory ($d_{\text{eff}} \geqslant 4$), deviations may appear when decreasing d_{eff}. For the Ohmic case, it is known[26] that z obeys the scaling law $z = z_0 - \eta$, where η in general denotes the anomalous scaling dimension at the transition point to a disordered state. Below $d_{\text{eff}} = 4$ one has $\eta > 0$, and previous work[3] on $s = 1$ for $d = 1$ found $\eta \approx 0.015$ and $z \approx 1.985$.

One issue we address in this paper is how the exponents z and η evolve as one varies the dissipation parameter $s > 1$. For the Ohmic case considered previously, the deviations from naive scaling (i.e., from $z = z_0$) are barely significant due to the small value of η when $d_{\text{eff}} \approx 3$. This deviation should become more noticeable as the effective dimensionality decreases, although one cannot expect the relation $z = z_0 - \eta$, valid for $s = 1$, to hold also for larger s. In the limit $d + z \to 2$, the anomalous dimension might be expected to approach the relatively large value $\eta = 1/4$, which it takes for both the two-dimensional (2D) Ising and 2D XY model. A related issue is the value of s beyond which the dissipation term is irrelevant in the renormalization group sense, giving $z = 1$. Naive scaling indicates that $z = 1$ for $s \geqslant 2$, but as z is likely to decrease faster than $z_0 = 2/s$ as s increases, dissipation might turn irrelevant for a value of s smaller than 2.

Another issue which we address is how the critical exponents, in particular z and η, depend on the symmetry of the order parameter. In the limit $s = 1$, there is no significant difference between the values of η (and thereby z) for

discrete and continuous order parameter fields,[3,5] but it is not inconceivable that such a difference becomes noticeable for lower effective dimensions, that is, as s is increased.

In order to answer these questions and to study a class of dissipative models for which relatively little is known precisely, we present results from Monte Carlo simulations on both XY and Ising-like spin chains with non-Ohmic dissipation. In both cases, we consider super-Ohmic dissipation, which for the XY case allows us to interpolate between the universality class describing the three-dimensional (3D) XY model and the very different Berezinskii-Kosterlitz-Thouless (BKT) criticality of the 2D XY model. The models are presented in the next section, where we also describe the finite-size scaling procedure used to find the critical exponents. The dependence of these exponents on s are presented and discussed in Sec. III, before we give a summary of our findings in Sec. IV.

II. MODEL AND FINITE-SIZE SCALING METHODS

The starting point of the models we consider may be taken as a general $(1+1)$D ϕ^4-type quantum field theory of an $O(N)$ order parameter field ϕ. Including dissipation, the Fourier transform of its inverse bare propagator is of the form $q^2+\omega^2+|\omega|^s$, where the damping term $\propto|\omega|^s$ arises from the coupling of the field to baths of harmonic oscillators[27] with a low-frequency power-law spectral density characterized by the exponent s.

Parameterizing the order parameter field of such a $N=2$ quantum rotor model by an angle variable θ, we may formulate the discretized action as

$$\begin{aligned} S = &-K\sum_{x=1}^{L}\sum_{\tau=1}^{L_\tau}\cos(\theta_{x,\tau}-\theta_{x+1,\tau}) \\ &- K_\tau\sum_{x=1}^{L}\sum_{\tau=1}^{L_\tau}\cos(\theta_{x,\tau}-\theta_{x,\tau+1}) \\ &- \frac{\alpha}{2}\sum_{x=1}^{L}\sum_{\tau\neq\tau'}^{L_\tau}\left(\frac{\pi}{L_\tau}\right)^{1+s}\frac{\cos(\theta_{x,\tau}-\theta_{x,\tau'})}{\sin^{1+s}\left(\frac{\pi}{L_\tau}|\tau-\tau'|\right)} \end{aligned} \tag{1}$$

on a quadratic $L\times L_\tau$ lattice. Above, K is the spatial coupling constant to be varied, whereas the quantum coupling constant K_τ and the dissipation strength α are taken as fixed values during the simulations.

In order to study both continuous and discrete symmetry of the order parameter field, we consider two possible domains of the angle variables: U(1) symmetry is equivalent with $\theta\in[0,2\pi\rangle$, and for a discrete symmetry (Z_4), we choose to enforce the restriction $\theta\in\{0,\frac{\pi}{2},\pi,\frac{3\pi}{2}\}$. We refer to the former as the XY model and to the latter as the Z_4 model. Such a Z_4 model will be in the same universality class as a corresponding Z_2 (Ising) model, which is why we refer to this model as Ising-like. This equivalence is easily shown using the substitution $\cos\theta_{x,\tau}=(\sigma_{x,\tau}+\mu_{x,\tau})/2$ and $\sin\theta_{x,\tau}=(\sigma_{x,\tau}-\mu_{x,\tau})/2$ to rewrite the action as that of two Ising models in terms of decoupled Ising spins σ and μ. The order parameter for both symmetry variants is defined as $m=(LL_\tau)^{-1}\sum_{x,\tau}\exp(\mathrm{i}\theta_{x,\tau})$ in the standard manner.

When determining critical exponents of a quantum system using finite-size scaling (FSS), the system dimensions L, L_τ used have to be chosen such that they respect the system anisotropy reflected by the dynamical critical exponent, $L_\tau\propto L^z$. This is a problem when we do not know dynamical critical exponents *a priori*, and one usually has to first determine z by simulating several values of L_τ for each L, before running new simulations with L/L_τ^z fixed. We circumvent this problem by using the same data to determine z and to evaluate the FSS observables, by interpolating data for multiple L_τ values to $L_\tau=L_\tau^*(L)$. Here, L_τ^* is a characteristic temporal system size found for each spatial system size L, as explained below, and it is assumed that $L_\tau^*\propto L^z$. This has the advantage that one (along with z) can find all other critical exponents simultaneously, utilizing all (or most of) the data generated. Furthermore, we are also able to appropriately take the uncertainty in z into account when finding the uncertainty in the other exponents, by repeating the entire procedure for a number of jackknife bins based on the original data.

The procedure to find z is explained in more detail in, for example, Ref. 4, and is based on the Binder ratio

$$Q=\frac{\langle m^4\rangle}{\langle m^2\rangle^2}=\mathcal{Q}(|K-K_c|L^{1/\nu},L_\tau/L^z), \tag{2}$$

where brackets $\langle\cdots\rangle$ indicate ensemble averages and $\mathcal{Q}$ is a universal scaling function. The characteristic values $L_\tau^*(L)$ are found from the minima of Q as a function of L_τ for a given L, and the critical coupling K_c is found from the crossing points of these minima as a function of K. The correlation length exponent ν is determined through finite-size scaling of the related quantity

$$\frac{(\partial\langle m^2\rangle/\partial K)^2}{\partial\langle m^4\rangle/\partial K}\propto L^{1/\nu}, \tag{3}$$

where the derivatives are calculated by $\partial\langle m^n\rangle/\partial K=\langle E_x\rangle\langle m^n\rangle-\langle E_x m^n\rangle$, with $E_x=-\sum_{x,\tau}\cos(\theta_{x,\tau}-\theta_{x+1,\tau})$.

To extract critical exponents β and γ, we use the usual FSS forms for the magnetization

$$\langle|m|\rangle\propto L^{-\beta/\nu} \tag{4}$$

and the magnetic susceptibility

$$\chi=LL_\tau\langle m^2\rangle\propto L^{\gamma/\nu}, \tag{5}$$

respectively. The anomalous dimension η is then found from the scaling relation $\eta=2-\gamma/\nu$. We have also checked that the value of η obtained from the susceptibility data is in correspondence with that obtained (through $z+\eta$) from the critical two-point correlation function of the order parameter field, $G(L/2)\propto L^{2-d-z-\eta}$. All of the above observables are evaluated at $L_\tau=L_\tau^*$, and we are careful to only use system sizes L_τ relatively close to L_τ^* in the interpolation. Using a polynomial fit of as low order as 3 works very well in most cases, although more care must be taken when extracting ν.

The error estimates we report are jackknife estimates of statistical errors only, but include contributions from the uncertainty in L_τ^* and the critical coupling K_c. The value of K_c is in general extrapolated from the scaling form $K_c^*(L)=K_c+cL^{-\omega'}$ for the crossing points $K_c^*(L)$ of $Q(K,L_\tau=L_\tau^*)$ for adjacent system sizes L. For regions of s where the crossing

points coincide and the extrapolation procedure breaks down, we base the estimate of K_c on the largest values of L. When extracting critical exponents, we make sure to use system sizes large enough for the above mentioned FSS forms to be valid. Possible corrections to scaling are discussed below. We note in particular that we initially assume a second-order phase transition for all values of s we use, so critical exponents obtained in the case of a BKT transition should be regarded as effective exponents only. The special case of $s \approx 2$ for the XY model is therefore re-examined separately in Sec. III B. Corrections to the scaling form $L_\tau^* \propto L^z$ are discussed for a special case in Sec. III C.

The Monte Carlo simulations are performed using a Wolff cluster algorithm[28] for long-range interactions.[29] The results are obtained using an implementation of the MERSENNE TWISTER[30] random number generator, but other random number generators produce consistent results. Ferrenberg-Swendsen reweighting techniques[31] were applied to the data. For the simulations of the XY case, we use a model with Z_{32} symmetry to emulate the continuous U(1) symmetry.

III. RESULTS AND DISCUSSION

When extracting critical exponents for the model we consider in this paper, we anticipate that the only parameter in Eq. (1) relevant in determining the universality class is the interaction decay exponent s. (The values we present Monte Carlo results for are s =1, 1.25, 1.5, 1.625, 1.75, 1.875, and 2.) Nevertheless, we also find that the corrections to scaling are strongly affected by the strength of the dissipation term as quantified by α, for finite systems. In order to minimize finite-size effects and ensure a relatively fast onset of asymptotic values of the exponents, a specific value of α could in principle be tailored to each value of s.[32] Instead of adjusting α for each individual value of the decay exponent s, we have divided the span of s values into two regions where we have applied different sets of coupling constants. For $s > 1.625$, where we expect the dissipation term to be weakly relevant (in the sense of a small correction-to-scaling exponent) or even irrelevant, we set the coupling values according to $\alpha = 0.1$ and $K_\tau = -\ln(\tanh\frac{1}{2}) \approx 0.7719$. For $s \leqslant 1.5$ we find that it is more appropriate to choose a larger value of α while reducing K_τ in order to observe a rapid finite-size crossover to the asymptotic exponents. In this region we use $\alpha = 0.5$ and $K_\tau = 0.4$. For the intermediate value $s = 1.625$, we use $\alpha = 0.3$ and $K_\tau = 0.4$. We can easily confirm for the smallest values of s that the universality class does not depend on the value of α, but corrections to scaling makes this harder for larger s, as discussed in Sec. III C.

A. Results for the critical exponents

In Fig. 1 we present the dynamical critical exponent z as a function of s. A notable feature of the results is the similarity between the two order parameter symmetries. To the accuracy of our simulations, there is essentially no difference between the continuous U(1) symmetry and the discrete Z_4 symmetry. Also, the calculated z values do not conform to the scaling estimate $z_0 = 2/s$, but instead fall off faster for increasing s than expected from naive scaling.

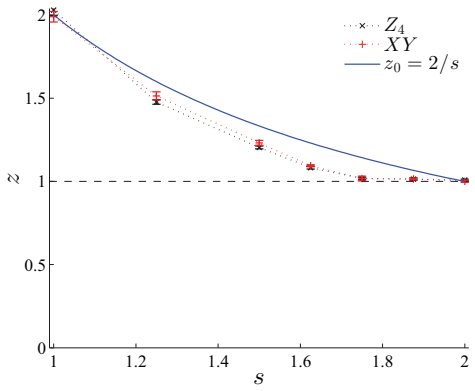

FIG. 1. (Color online) Dynamical critical exponent z as a function of s for the Z_4 and the XY model. The naive scaling estimate z_0 (the solid curve) does not coincide with the calculated z for values of s other than the integer-valued end points of our span of s values.

We present the evolution of η as a function of s in Fig. 2. Again, we find coinciding values for the two order parameter symmetries. For both Z_4 and U(1), η increases steadily with decreasing effective dimension of the system. Also shown in Fig. 2 is the quantity $\eta_0 = 2/s - z$, which quantifies the difference between the naive scaling estimate z_0 and the calculated z. For $s \leqslant 1.25$ the evolution of η_0 closely follows the calculated values of η, making the scaling relation $z = 2/s - \eta$ a fair approximation also for $s \gtrsim 1$. For larger values of s, however, this scaling relation has clearly broken down, as the values of z again approach the naive estimate as $s \to 2$. In this limit, η approaches the value $\eta = 1/4$, which is expected for both the 2D Ising model at the

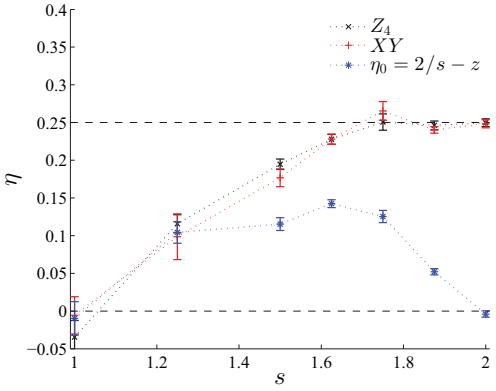

FIG. 2. (Color online) Anomalous scaling dimension η as a function of s for the Z_4 and the XY model. η_0 indicates the discrepancy between the naive scaling estimate $z_0 = 2/s$ and the actually calculated value of the dynamical critical exponent z (based on the mean for the Z_4 and XY model).

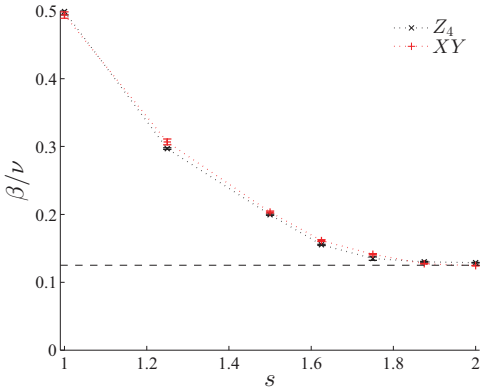

FIG. 3. (Color online) Critical exponent ratio β/ν as a function of s. This ratio appears to be independent of order parameter symmetry and is also well defined in the limit of large s. The dashed line represents $\beta/\nu = 1/8$.

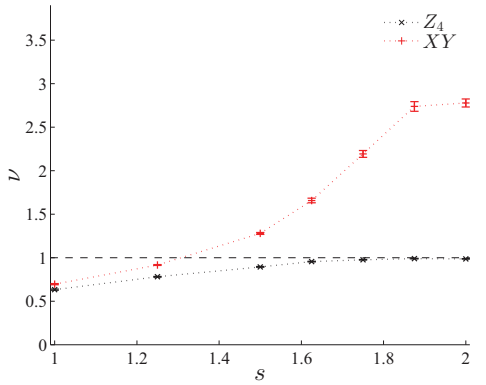

FIG. 4. (Color online) Correlation length exponent ν as a function of s. As the dissipation term becomes more short ranged with larger s, the exponent for the Z_4 model approaches the 2D Ising value $\nu = 1$. In the XY case, ν is expected to diverge in the limit $d_{\text{eff}} \to 2$. The results (obtained for finite L) presented for the largest values of s should therefore be regarded only as effective exponents.

critical point, as well as for the 2D XY model at the critical end point.

Next, we turn to the remaining critical exponents. Figure 3 shows the results for the ratio β/ν as obtained from the magnetization. We do not show the ratio γ/ν, although its behavior is easily inferred from Fig. 2 and the relation $\gamma/\nu = 2 - \eta$. Again, the FSS exponent seems to take essentially the same values for the XY model as for the Z_4 model. This is also the case for $s \to 2$, where we expect the dissipation to be irrelevant so that the effective dimensionality is reduced to $d_{\text{eff}} = 2$. For the XY model, the U(1) symmetry of the variables then cannot be spontaneously broken, and the strong-coupling phase of the model features only quasi-long-range order (QLRO). Nonetheless, the system develops a finite magnetization m as a finite-size effect, with a well-defined FSS exponent. The value $\beta/\nu \approx 0.125 = 1/8$ of this exponent when $s = 2$ (as well as the corresponding susceptibility ratio $\gamma/\nu \approx 7/4$) is also found for the classical 2D XY model and is, incidentally, the same as the corresponding ratio in the 2D Ising model. We discuss this issue in more detail in Sec. III E.

The correlation length exponent ν is shown in Fig. 4, while the critical exponent β is shown in Fig. 5. We do not show the results for the exponent γ here, but its behavior is qualitatively very similar to that of the exponent ν. In the Z_4 case, both exponents start out close to the 3D Ising limit for $s = 1$ and approach the 2D Ising limit indicated by the dashed line when $s \to 2$. Consider now the XY case. When $s = 1$, these exponents take on values close to those of the 3D XY model. However, the exponents β, ν, and γ are not well defined when $d_{\text{eff}} = d + z = 2$, as their values are formally infinite at a transition separating a disordered phase and a QLRO phase. This is the case when $s = 2$. Our FSS analysis for these exponents, which presupposes a second-order phase transition, is strictly speaking not applicable to the BKT transition. The resulting (effective) exponents β, ν, and γ appear to diverge as $L \to \infty$ close to $s = 2$. Note that although ξ is exponentially divergent at a BKT transition, we may still define z through the relation $\xi_\tau \propto \xi^z$.

Another observation in the U(1) case is that while the combination β/ν is monotonically decreasing with increasing s, β itself is exhibiting a nonmonotonic evolution as a function of s. The value of β is at first decreasing as the increasing value of s drives the system away from the 3D behavior, just as for the Z_4 case. However, as mentioned above, β is divergent in the 2D XY limit, and the reduction of β is therefore reversed at an intermediate value of s.

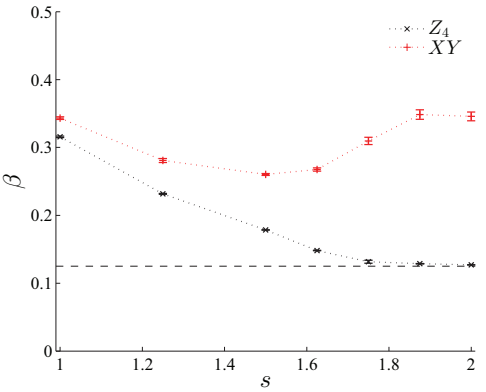

FIG. 5. (Color online) Critical exponent β as a function of s. For the Z_4 model, β evolves smoothly from the 3D Ising to the 2D Ising limit as s is increased from 1 to 2. The XY result, on the other hand, starts out near the 3D XY value for $s = 1$ and features a nonmonotic evolution of β with s, with a divergent β in the limit of large s; cf. Fig. 4.

B. Berezinskii-Kosterlitz-Thouless phase transition and the helicity modulus

The helicity modulus

$$\Upsilon = \frac{1}{LL_\tau}\left\langle \sum_{x=1}^{L}\sum_{\tau=1}^{L_\tau}\cos(\theta_{x,\tau}-\theta_{x+1,\tau})\right\rangle - \frac{K}{LL_\tau}\left\langle\left(\sum_{x=1}^{L}\sum_{\tau=1}^{L_\tau}\sin(\theta_{x,\tau}-\theta_{x+1,\tau})\right)^2\right\rangle, \quad (6)$$

is expected to scale as $\Upsilon \propto L^\kappa$ at a critical point where a U(1) symmetry is spontaneously broken, with $\kappa \equiv 2\beta/\nu - \eta$. For a 2D XY model, however, the exponent κ is exactly zero, reflecting the fact that at the BKT phase transition, the helicity modulus jumps to a finite value with logarithmic finite-size corrections. By direct comparison of the calculated values of Υ for $s = 2$ and the scaling form expected for a BKT transition,[33] unambiguous conclusions regarding the universality class of the phase transition at $s = 2$ could not be drawn. The presence of the presumably irrelevant dissipation term is still effective in driving the system away from BKT-type criticality at all but the very largest system sizes. In practice, the logarithmic scaling analysis[33] is usually best suited for small to moderate system sizes. Consequently, instead of scaling the helicity modulus directly, we resort to calculating κ via other observables and find that $2\beta/\nu - \eta = 0$ within statistical uncertainty for $s = 2$. Moreover, $2\beta/\nu - \eta$ is very close to zero for all $s \geqslant 1.75$. For even smaller values of s (where direct scaling of Υ is more reliable), we have confirmed that the scaling law $\kappa = 2\beta/\nu - \eta$ is valid also in the presence of dissipation. This scaling form is also equivalent to $\kappa = d_{\rm eff} - 2$. Thus, the helicity modulus vanishes continuously as $K \to K_c^+$, provided $d_{\rm eff} = d + z > 2$. The above equivalence assumes that hyperscaling is valid, and we have confirmed this validity for all values of s.

C. Boundary between long-range and short-range critical behavior

From Figs. 1 to 5, it is evident that all critical exponents are very close to their short-range values for $s \gtrsim 1.75$. The naive scaling estimate places the boundary at which the dissipation term becomes irrelevant at $s = 2$. For classical models with (isotropic) long-range interactions decaying with distance r as $1/r^{1+s}$, it has long been debated[34,35] whether the models feature the exponents of the corresponding short-range model already when s exceeds a value $s^* = 2 - \eta_{\rm SR}$. Here, $\eta_{\rm SR}$ denotes the anomalous dimension of the short-range model. Using large-scale Monte Carlo simulations, it has been shown[36] that for the long-range 2D Ising model, the anomalous dimension follows the conjectured exact[34] relation $\eta = 2 - s$ for $s < 1.75$, but that $\eta = 0.25 = \eta_{\rm SR}$ for $s > s^* = 1.75$. Although the long-range interaction of the dissipative quantum models we consider is highly anisotropic, in contrast to the isotropic classical long-ranged models, it is plausible that also in these models the threshold value of s beyond which dissipation is irrelevant is reduced from $s = 2$ to some lower value.

In order to establish this boundary more accurately also for the present case of anisotropic interactions, we have performed a more careful analysis of the case $s = 1.875$ for the Z_4 model. Including corrections to scaling, using the ansatz $L_\tau^* = aL^z(1 + bL^{-\omega})$, we find $z = 1.002(11)$. Hence, the decay exponent $s = 1.875$ may serve as an upper bound for the boundary value s^* necessary to render the dissipation term effectively short ranged. This, in turn, would render the system effectively Lorentz invariant with $z = 1$. To get the statistics required to include corrections to scaling in a stable manner, we included three different values of the dissipation strength α in a joint fit. This also provides an a posteriori justification of the choice of lower values of α for higher values of s.[37] Probably due to logarithmic corrections expected at the presumed boundary value $s^* = 1.75$,[36] we are not able to acquire the same level of accuracy for this value of s. Therefore we cannot rule out that the dissipation term is rendered effectively short ranged at some other value $s^* \in (1.75, 1.875)$. An exceedingly slow crossover to asymptotic critical exponents for values $s \approx s^*$ can conceivably be understood from the competition between the fixed point corresponding to short-range (Lorentz-invariant) criticality and the fixed point corresponding to long-range (dissipation-dominated) criticality.

We close this section with a remark on the evolution of the anomalous dimension. In the quantum dissipative model we have studied, the anomalous dimension increases for increasing s. This is a consequence of the effective dimensionality $d_{\rm eff} = d + z$ decreasing with increasing s. Lowering the dimensionality from the upper critical dimension, where $\eta = 0$, tends to increase η. This is quite different from the situation encountered in classical models with isotropic long-range interactions. Classical models with short-range interactions and an action of the form $S \sim q^2\phi_q\phi_{-q}$ (where ϕ_q is an appropriate order-parameter field) have propagators $G(q) \sim 1/|q|^{2-\eta}$. The corresponding long-range models with an action of the form $S \sim |q|^s\phi_q\phi_{-q}$ have propagators $G(q) \sim 1/|q|^s$, when $s < 2 - \eta_{\rm SR}$. One may now, as is customarily done in the literature on long-range classical isotropic models, define an effective anomalous scaling dimension for such systems by comparing with the corresponding expression for the short-range case, finding $\eta = 2 - s$, which decreases with increasing s. This relation is best viewed as a result of somewhat artificially imposing the standard scaling form of a propagator for short-range systems ($1/|q|^{2-\eta}$) on the form of the propagator for systems with long-range interactions, $1/|q|^s$.

D. Scaling relation between z and η

In Fig. 2, we demonstrated how the scaling relation $z = z_0 - \eta$ cannot be valid except close to the Ohmic limit $s = 1$ and that $\eta \approx 1/4$ for all $s \geqslant 1.75$. Moreover, from our numerics we think it is likely that $z(s) = 1$ for $s \geqslant 1.75$. A scaling relation between z and η which would fit well with these observations is

$$z = \max\left\{\frac{2-\eta}{s}, 1\right\}. \quad (7)$$

The scaling relation $z = (2 - \eta)/s$ has been suggested previously in Ref. 17 in the context of a damped nonlinear σ model.

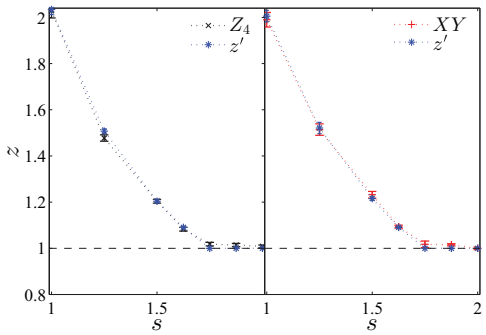

FIG. 6. (Color online) The dynamical critical exponent z as in Fig. 1, but compared with the scaling estimate $z' = (2-\eta)/s$. The values of η used in the scaling estimates are the same as reported in Fig. 2, with the left panel corresponding to the Z_4 model and the right panel to the XY model.

In Fig. 6, we show the same data for the dynamical exponent z as in Fig. 1 but compared with the ansatz (7) instead of the naive scaling estimate $z_0 = 2/s$. Although there are probably still some corrections to finite-size scaling, Eq. (7) seems to fit the data far better than the alternatives.

We next provide a heuristic argument for why the scaling relation (7) may be reasonable for $s < 2 - \eta_{\mathrm{SR}}$. Building on the arguments in Sec. III C for classical isotropic long-range-interacting systems, we take as a starting point that a dissipative quantum model with action of the form $S \sim (q^2 + |\omega|^s)\phi_{q,\omega}\phi_{-q,-\omega}$ can be viewed as an anisotropic long-range-interacting system. Introducing the suitably chosen frequency coordinate $\tilde{\omega}^s = q^2 + |\omega|^s$, the propagator takes the isotropic form $G(\tilde{\omega}) \sim 1/|\tilde{\omega}|^s$. Recall that in the quantum case, the anomalous scaling dimension η is defined from the *spatial* correlation function $G(x) \sim 1/x^{d+z-2+\eta} \equiv 1/x^{\theta_x}$. To find η, we Fourier transform the propagator to obtain the imaginary-time correlation function. In terms of the frequency coordinate $\tilde{\omega}$, the system effectively has $d'_{\mathrm{eff}} = 1 + d/z$ dimensions. Therefore, the correlation function decay exponent in terms of the isotropic space-time coordinate $\tilde{\tau} \equiv (\tau^2 + x^{2z})^{1/2}$ would be $\theta_{\tilde{\tau}} = (z+d)/z - s$. Comparing with the imaginary-time decay exponent $\theta_\tau = \theta_x/z = (d+z-2+\eta)/z$, we find $sz = 2 - \eta$, which is equivalent to Eq. (7).

Finally, we point out that our results for the scaling relation (7) for dissipative models should also have relevance for *nondissipative* quantum spin chains with long-range *spatial* interactions.[38,39] One arrives at exactly such a model by simply interchanging the x and τ coordinates of the action we have considered. The dynamical critical exponent of this model is given by $z' = 1/z = s/(2-\eta)$, with the quantity $\eta(s)$ evolving as shown in Fig. 2. This quantity will, however, not be identical to the anomalous scaling dimension of the model, η', which is given by the classical result $\eta' = 2 - s$. Hence, there exists no independent scaling relation between the dynamical critical exponent z' and the anomalous dimension η' for a nondissipative quantum spin chain with long-range interactions.

E. Dependence on symmetry

For $s = 1$, we have $z \approx 2$, $d_{\mathrm{eff}} \approx 3$, while for $s = 2$, we have $z = 1$, $d_{\mathrm{eff}} = 2$. For these two cases, it is known either analytically or numerically that the exponent η is very similar for the Ising and XY models.[40] There appears to be no particular deep reason for this. For instance, the well-known value $\eta = 1/4$ comes about for completely different reasons in the 2D Ising and 2D XY models, and their similarity thus appears to be accidental. Using the scaling relations $2\beta/\nu - \eta = d_{\mathrm{eff}} - 2$ [assuming Eq. (7)] and $\gamma/\nu = 2 - \eta$, it follows that the similarities in β/ν and γ/ν for the Ising and XY models are as coincidental as they are for η, both in 2D and 3D. It appears that these coincidences persist in all dimensions between 2 and 3. There is good reason to expect that the same also holds in the sub-Ohmic regime $s < 1$. Such values of s increase the effective dimensionality beyond 3, eventually driving all exponents to their universal mean-field values at the upper critical dimension.

We next comment on other values of q, and how our results apply to those cases. The Ising and XY models represent extreme cases of Z_q clock models, with $q = 2$, $q = \infty$, respectively. The partition function for the $q = 4$ case is simply the square of the case $q = 2$, and hence they give identical results. For larger $q > 4$, anisotropy is irrelevant,[41] and we thus expect the results of U(1) to emerge. We therefore conjecture that the results of this paper for z, η, β/ν, and γ/ν, are valid for all Z_q clock models. The only possible exception is the case $q = 3$, also equivalent to the three-state Potts model, where the anisotropy with respect to a U(1)-symmetric model is known to be relevant. Although we have not checked this, it may still be possible that Eq. (7) holds also for a dissipative Z_3 clock model, at least for $s > 1$.[42]

An alternative perspective on this, supporting the notion that the scaling relation $z = (2-\eta)/s$ is valid for all q, may be provided by the following qualitative argument. The variation of z with the parameter s determining the range of the dissipation expresses a variation in the effective space-time dimensionality of the system. This is determined by the interaction of the spins at a given site in the imaginary-time direction. Due to the long-range character of this interaction, each spin interacts with a large number of fluctuating copies of itself along a chain in the imaginary-time direction. Due to the summation over many spins at different Trotter slices, the discrete nature of the spins in a Z_q clock model is washed out, even in the case $q = 2$. Therefore, the manner in which the dissipation affects the effective dimensionality does not depend on whether the spins at each space-time lattice point take on discrete or continuous values.

IV. SUMMARY

We have performed Monte Carlo simulations on a generalized spin-boson model in one spatial dimension featuring non-Ohmic site dissipation and two variants of order parameter symmetry, namely Ising-like and U(1). By tuning the imaginary-time decay exponent of the dissipative interaction, $s \in [1,2]$, we are able to continuously vary the effective dimensionality of the system. Apparently, the order parameter symmetry has very little bearing on the evolution of the

effective dimensionality, $d_{\text{eff}} = d + z$, as a function of the decay parameter s. While naive scaling estimates a crossover from criticality dominated by the dissipation term to an irrelevant dissipation term at $s = 2$, we measure exponents in relatively good correspondence with the underlying, short-range interacting model at a somewhat lower value $s \approx 1.75$. Our results also suggest that for $1 \leqslant s \leqslant 2$, the exponents z and η to a good approximation obey the scaling relation $z = \max\{(2 - \eta)/s, 1\}$.

ACKNOWLEDGMENTS

A.S. was supported by the Norwegian Research Council under Grant No. 205591/V30 (FRINAT). I.B.S. and E.B.S. thank NTNU for financial support. The work was also supported through the Norwegian consortium for high-performance computing (NOTUR). Useful communications with E. V. Herland, D. A. Huse, F. S. Nogueira, and Z. Tešanović are acknowledged.

[1] A. J. Leggett, S. Chakravarty, A. T. Dorsey, M. P. A. Fisher, A. Garg, and W. Zwerger, Rev. Mod. Phys. **59**, 1 (1987).

[2] K. Le Hur, in *Understanding Quantum Phase Transitions*, edited by L. D. Carr (Taylor & Francis, Boca Raton, FL, 2010).

[3] P. Werner, K. Völker, M. Troyer, and S. Chakravarty, Phys. Rev. Lett. **94**, 047201 (2005).

[4] I. B. Sperstad, E. B. Stiansen, and A. Sudbø, Phys. Rev. B **81**, 104302 (2010).

[5] P. Werner, M. Troyer, and S. Sachdev, J. Phys. Soc. Jpn. **74S**, 67 (2005).

[6] M. Vojta, Phil. Mag. **86**, 1807 (2006).

[7] M. Vojta, Rep. Prog. Phys. **66**, 2069 (2003).

[8] Q. Si, in *Understanding Quantum Phase Transitions*, edited by L. D. Carr (Taylor & Francis, Boca Raton, FL, 2010).

[9] V. Aji and C. M. Varma, Phys. Rev. Lett. **99**, 067003 (2007).

[10] K.-H. Wagenblast, A. van Otterlo, G. Schön, and G. T. Zimányi, Phys. Rev. Lett. **78**, 1779 (1997).

[11] P. P. Orth, I. Stanic, and K. Le Hur, Phys. Rev. A **77**, 051601(R) (2008).

[12] T. Vojta, J. A. Hoyos, P. Mohan, and R. Narayanan, J. Phys.: Condens. Matter **23**, 094206 (2011).

[13] J. A. Hoyos, C. Kotabage, and T. Vojta, Phys. Rev. Lett. **99**, 230601 (2007).

[14] A. M. Lobos, A. Iucci, M. Müller, and T. Giamarchi, Phys. Rev. B **80**, 214515 (2009).

[15] R. M. Lutchyn, V. Galitski, G. Refael, and S. Das Sarma, Phys. Rev. Lett. **101**, 106402 (2008).

[16] M. T. Glossop and K. Ingersent, Phys. Rev. Lett. **95**, 067202 (2005).

[17] A. Gamba, M. Grilli, and C. Castellani, Nucl. Phys. B **556**, 463 (1999).

[18] A. Winter, H. Rieger, M. Vojta, and R. Bulla, Phys. Rev. Lett. **102**, 030601 (2009).

[19] S. Kirchner, Q. Si, and K. Ingersent, Phys. Rev. Lett. **102**, 166405 (2009).

[20] S. Kirchner, J. Low Temp. Phys. **161**, 282 (2010).

[21] M. Vojta, N.-H. Tong, and R. Bulla, Phys. Rev. Lett. **94**, 070604 (2005); See, however, M. Vojta, N.-H. Tong, and R. Bulla, *ibid*. **102**, 249904(E) (2009).

[22] G. Kotliar, P. W. Anderson, and D. L. Stein, Phys. Rev. B **27**, 602(R) (1983).

[23] H. G. Katzgraber, D. Larson, and A. P. Young, Phys. Rev. Lett. **102**, 177205 (2009).

[24] A. Sharma and A. P. Young, Phys. Rev. B **83**, 214405 (2011).

[25] J. A. Hertz, Phys. Rev. B **14**, 1165 (1976).

[26] S. Pankov, S. Florens, A. Georges, G. Kotliar, and S. Sachdev, Phys. Rev. B **69**, 054426 (2004).

[27] A. O. Caldeira and A. J. Leggett, Ann. Phys. (NY) **149**, 374 (1983).

[28] U. Wolff, Phys. Rev. Lett. **62**, 361 (1989).

[29] E. Luijten and H. Blöte, Int. J. Mod. Phys. C **6**, 359 (1995).

[30] M. Matsumoto and T. Nishimura, ACM Trans. Model. Comput. Simul. **8**, 3 (1998).

[31] A. M. Ferrenberg and R. H. Swendsen, Phys. Rev. Lett. **63**, 1195 (1989).

[32] M. Hasenbusch, K. Pinn, and S. Vinti, Phys. Rev. B **59**, 11471 (1999).

[33] H. Weber and P. Minnhagen, Phys. Rev. B **37**, 5986 (1988).

[34] M. E. Fisher, S.-k. Ma, and B. G. Nickel, Phys. Rev. Lett. **29**, 917 (1972).

[35] J. Sak, Phys. Rev. B **8**, 281 (1973).

[36] E. Luijten and H. W. J. Blöte, Phys. Rev. Lett. **89**, 025703 (2002).

[37] To be more specific, we carried out the joint fit for system sizes in the interval $L = 57$ to $L = 607$ for three data sets $\alpha = 0.05$, 0.1, 0.2, where only the exponents z and ω were constrained to be equal for all data sets. The value of the correction-to-scaling exponent was found to be $\omega = 0.42(25)$. The values of the correction amplitudes b were all negative within statistical uncertainty and decreasing with increasing α. This implies that α would have to be set to a vanishingly small value to reduce the corrections to scaling for $s = 1.875$, and also justifies using relatively low values of α for the largest values of s.

[38] A. Dutta and J. K. Bhattacharjee, Phys. Rev. B **64**, 184106 (2001).

[39] N. Laflorencie, I. Affleck, and M. Berciu, J. Stat. Mech.: Theory Exp. (2005) P12001.

[40] A. Pelissetto and E. Vicari, Phys. Rep. **368**, 549 (2002).

[41] S. Elitzur, R. B. Pearson, and J. Shigemitsu, Phys. Rev. D **19**, 3698 (1979).

[42] We expect that a three-state Potts model with effective dimensionality d_{eff} may have a first-order phase transition for $d_{\text{eff}} \geqslant 3$.